Kent Academic Repository

Infrared spectroscopy of eruptive variable protostars from VVV

C. Contreras Peña,[1,2,4]★ P. W. Lucas,[2]★ R. Kurtev,[3,4] D. Minniti,[1,5]
A. Caratti o Garatti,[6] F. Marocco,[2] M. A. Thompson,[2] D. Froebrich,[7]
M. S. N. Kumar,[2,8] W. Stimson,[2] C. Navarro Molina,[4,3] J. Borissova,[3,4]
T. Gledhill[2] and R. Terzi[2]

[1]*Departamento de Ciencias Fisicas, Universidad Andres Bello, Republica 220, Santiago, Chile*
[2]*Centre for Astrophysics Research, University of Hertfordshire, Hatfield AL10 9AB, UK*
[3]*Instituto de Física y Astronomía, Universidad de Valparaíso, ave. Gran Bretaña, 1111, Casilla 5030, Valparaíso, Chile*
[4]*Millennium Institute of Astrophysics, Av. Vicuna Mackenna 4860, 782-0436, Macul, Santiago, Chile*
[5]*Vatican Observatory, V-00120 Vatican City State, Italy*
[6]*Dublin Institute for Advanced Studies, School of Cosmic Physics, Astronomy and Astrophysics Section, 31 Fitzwilliam Place, Dublin 2, Ireland*
[7]*Centre for Astrophysics and Planetary Science, University of Kent, Canterbury CT2 7NH, UK*
[8]*Instituto de Astrofisica e Ciencias do Espaco, Universidade do Porto, CAUP, Rua das Estrelas, P-4150-762 Porto, Portugal*

ABSTRACT
In a companion work (Paper I), we detected a large population of highly variable Young Stellar Objects (YSOs) in the Vista Variables in the Via Lactea (VVV) survey, typically with class I or flat spectrum spectral energy distributions and diverse light-curve types. Here we present infrared spectra (0.9–2.5 μm) of 37 of these variables, many of them observed in a bright state. The spectra confirm that 15/18 sources with eruptive light curves have signatures of a high accretion rate, either showing EXor-like emission features ($\Delta v = 2$ CO, Brγ) and/or FUor-like features ($\Delta v = 2$ CO and H$_2$O strongly in absorption). Similar features were seen in some long-term periodic YSOs and faders but not in dippers or short-term variables. The sample includes some dusty Mira variables (typically distinguished by smooth Mira-like light curves), two cataclysmic variables and a carbon star. In total, we have added 19 new objects to the broad class of eruptive variable YSOs with episodic accretion. Eruptive variable YSOs in our sample that were observed at bright states show higher accretion luminosities than the rest of the sample. Most of the eruptive variables differ from the established FUor and EXor subclasses, showing intermediate outburst durations and a mixture of their spectroscopic characteristics. This is in line with a small number of other recent discoveries. Since these previously atypical objects are now the majority amongst embedded members of the class, we propose a new classification for them as MNors. This term (pronounced emnor) follows V1647 Ori, the illuminating star of McNeil's Nebula.

Key words: stars: AGB and post-AGB – stars: low-mass – stars: pre-main-sequence – stars: protostars – stars: variables: T Tauri, Herbig Ae/Be – infrared: stars.

1 INTRODUCTION

The incidence and theory of episodic accretion in young stellar objects (YSOs) and the associated eruptive variability is one of the biggest remaining gaps in our understanding of star formation. While the number of photometrically and spectroscopically verified eruptive variable YSOs remains small, the topic has attracted increasing attention from observers and theorists in recent years, alongside a more general effort to improve our understanding of lower level accretion variations and photometric variability

in YSOs at optical, near-infrared (IR) and mid-IR wavelengths (e.g. Megeath et al. 2012; Findeisen et al. 2013; Cody et al. 2014; Rebull et al. 2014; Rice et al. 2015; Wolk et al. 2015). If episodic accretion is common in normal pre-main-sequence (PMS) stars, this could solve two long-standing puzzles: the typical luminosities of YSOs are found to be lower than expected from theoretical models (the so-called luminosity problem; see e.g. Kenyon et al. 1990; Evans et al. 2009; Caratti o Garatti et al. 2012). This problem can be solved if in fact YSOs spend most of their lifetimes in quiescent states with low accretion rates and gain most of their mass in short-lived accretion bursts. The second problem relates to the wide scatter about the best-fitting isochrone seen in the Hertzsprung–Russell (HR) diagrams of PMS clusters. In this case, the final position of the star in

★ E-mail: cecontrep@gmail.com (CCP); p.w.lucas@herts.ac.uk (PWL)

HR diagrams would strongly depend on the YSO's accretion history. Moreover, the lasting effects of episodic accretion would have to be taken into account not only in stellar evolution theory (Baraffe, Chabrier & Gallardo 2009; Baraffe, Vorobyov & Chabrier 2012) but also in the theory of planet formation and planet migration.

This paper forms the second part of our investigation of eruptive variability in the VISTA Variables in the Via Lactea (VVV) survey (Minniti et al. 2010; Saito et al. 2012), the first panoramic time domain survey of the Milky Way at IR wavelengths. In the first part (Contreras Peña et al. 2016, hereafter Paper I), we described the discovery of 816 high-amplitude IR variables ($\Delta K_s > 1$ mag) in the mid-plane section of the VVV disc region, a well-studied region in the fourth Galactic quadrant (longitude $295° < l < 350°$, latitude $-1°.1 < b < 1°.1$. Most of these variables were located in star formation regions (SFRs) and have very red spectral energy distributions (SEDs), consistent with YSO classification. We estimated that about half of the 816 are YSOs and we made a preliminary classification of each into one of the following categories: eruptive, fader, dipper, short-term variable (STV), long-term periodic variable (LPV-YSO), eclipsing binary and Mira-like variable (LPV-Mira). The Mira-like variables were distinguished by their relatively smooth, approximately sinusoidal light curves, as distinct from LPV YSOs with significant lower level scatter on short time-scales, superimposed on a higher amplitude long-term periodic variation. The eruptive variables typically displayed outburst durations of 1–4 yr, but in some cases, the eruptions were much shorter or lasted for >4 yr. We posited that variables with eruptive LC were mainly YSOs undergoing episodic accretion and we further suggested that this mechanism (or variations on it) causes the variability of some of the faders and LPVs. The dippers (sources with relatively brief but deep drops in the LC) would more naturally be explained by variable extinction, although we note that the near-IR colour variability in many sources in this class does not follow the reddening path. The STVs typically had lower amplitudes and had a bluer distribution of SEDs than the rest, so the variability in most cases is more likely due to rotational modulation by bright or dark spots on the stellar photosphere or periodic extinction (e.g. by a warped inner disc), rather than episodic accretion.

Spectroscopic follow-up remains essential to test our initial conclusions, in part, because the sparsely sampled VVV LC and SEDs alone are insufficient to classify individual sources reliably. Moreover, we have only two epochs of colour variability data in the JHK_s filters (supplemented by four epoch *WISE*+NEOWISE mid-IR data in some cases), so while the evidence suggested that variable extinction is not the main cause of variability in the eruptive systems, spectroscopic confirmation is required.

Most eruptive variable YSOs have historically been classified as either FUors (after FU Orionis) or EXors (after EX Lupi). FUors have long-duration outbursts (typically decades but at least 10 yr), whereas EXors typically have outburst durations of weeks to months, with a maximum of 1.5 yr (Herbig 2008). The classical view is that FUors are at an earlier evolutionary stage and belong to the transitional phase between class I and class II objects, whilst EXors are associated with instabilities in the discs of class II objects. However, both classes of young eruptive variables were originally defined from optical detections in nearby SFRs (Herbig 1977, 1989), which tends to exclude younger YSOs which have higher accretion rates but are too deeply embedded in circum-stellar matter to be observed at visible wavelengths.

FUors display strong CO absorption in the first overtone bands at 2.3–2.4 μm and they often show broad H_2O absorption bands from 1–2.5 μm also. These absorption bands are thought to arise in the circum-stellar accretion disc (perhaps 1 au from the star; Connelley & Greene 2014). The disc is heated in the mid-plane by viscous accretion and absorption occurs in the cooler surface layers. FUors typically lack emission lines in their IR spectra. By contrast, EXors show strong H I recombination lines in emission. During outburst, the first overtone CO bands are in emission also but they are seen in absorption during quiescent periods. The H I lines are attributed to infalling matter close to the star and they often display $\sim$100 km s^{-1} linewidths. The CO emission is thought to arise in the inner part of the accretion disc which has a temperature inversion due to external heating by the star. Na I and Ca I emission lines are also sometimes seen in EXors during outburst, their behaviour correlating closely with CO (Lorenzetti et al. 2009). CO, Na I and Ca I absorption lines in classical EXors arise in the stellar photosphere. This of course requires that the stellar photosphere is not too heavily veiled by the disc or hidden by high extinction, as often occurs for normal class I YSOs, (e.g. Greene & Lada 1996). The accretion events associated with the outbursts of eruptive variables are thought to drive strong outflows (Reipurth & Aspin 1997; Magakian et al. 2013). FUors have been associated with Herbig–Haro objects (Reipurth & Aspin 1997) and drive molecular outflows (Evans et al. 1994). FU Orionis itself, although having massive winds, does not drive a molecular outflow (Evans et al. 1994), which could be explained by the lack of organization of magnetic fields required for jet launching and collimation in the binary scenario of Reipurth & Aspin (2004) or by previous outflows having cleared away the remnant envelope, leading to a lack of swept-up material which would otherwise constitute a molecular outflow (Evans et al. 1994). However, classical EXors do not show the evidence of molecular shocks or jets in the near-IR (H_2 or [Fe II] emission) at the sensitivity level of the spectra of Lorenzetti et al. (2009).[1]

The VVV candidates were initially selected from their variability over only $\sim$2 yr (2010–2012), a time-scale that favours detection of EXors over FUors. However, with VVV, we are sensitive to optically obscured YSOs with a substantial envelope, i.e. systems at an earlier evolutionary stage than most EXors. The VVV candidates are in fact almost all optically invisible at the depth of panoramic surveys such as VPHAS+ (Drew et al. 2014). This is partly because most of them have intrinsically redder SEDs than most of the classical EXors and FUors and in part because of interstellar extinction towards the relatively distant SFRs (a few kiloparsecs) in which these objects are located (see Section 2). Owing to their earlier evolutionary status, it is likely to be difficult to detect absorption features which arise in the stellar photosphere. In addition, the greater distance of the VVV YSOs biases them towards higher luminosity and mass. This may affect the relative prominence of spectroscopic features relating to the accretion luminosity of the disc and those related to the stellar photosphere (whether seen directly or in reprocessed radiation; see Calvet et al. 1991).

Prior to our work with VVV, very few deeply embedded eruptive variables were known. The known examples were OO Ser, V2775 Ori, HOPS 383, V723 Car and GM Cha (Hodapp et al. 1996; Persi et al. 2007; Caratti o Garatti et al. 2011; Safron et al. 2015; Tapia, Roth & Persi 2015), now supplemented by our two recent discoveries from the UKIDSS Galactic Plane Survey: GPSV3 in Serpens OB2 and the isolated object GPSV15 (Contreras Peña et al. 2014), as well as the recent discovery of CX330 (Britt et al. 2016). CX330

---

[1] We note that PV Cep does show H_2 emission and it is part of the EXor sample of Lorenzetti et al. (2009). However, this object has characteristics which differ from classical EXors (see e.g. Caratti o Garatti et al. 2013).

is an isolated very red source in the direction of the Galactic bulge with extreme (even unique) photometric and spectroscopic properties. As with GPSV15, an eruptive YSO interpretation appears to fit the data best, though we should consider the possibility that these unusual isolated variables are more evolved sources or previously unknown types. To this list, we might also add V1647 Ori (Aspin, Greene & Reipurth 2009) and a few other objects that are somewhat less obscured ($A_v \sim 10$). These embedded objects, along with a few other less embedded systems, show a mixture of the properties of FUors and EXors. This has given rise to the scenario where, if we think of the outburst phenomena as a continuum, these new discoveries may instead represent a 'connection' between FUors and EXors, with FUors representing one extreme (long duration) and EXors being the short-duration end of the same phenomenon. In this sense, the different types of outbursts are produced by variations of one or more of the parameters involved in the instabilities which give rise to the outburst (Gibb et al. 2006; Fedele et al. 2007; Aspin et al. 2009).

In this paper, we present the results of IR spectroscopic follow-up of a subset of the 816 high-amplitude variables. The principal aims of this work are first to validate our claim in Paper I to have discovered a large population of eruptive variables, with increasing incidence towards earlier stages of evolution, and secondly, to explore the characteristics of these embedded systems.

The paper is divided as follows: in Section 2, we describe the selection of the sample and present its photometric properties, including 70 μm data from *Herschel* Hi-Gal. We also review the near-IR colour variability using two epochs of VVV data, presented previously in Paper I for the full photometric sample. Section 3 describes the near-IR spectroscopic observations and data reduction. In Section 4, we analyse the general spectroscopic characteristics of the sample, focusing on objects which are found to be likely YSOs. We then analyse these properties according to their LC classification from Paper I and establish which objects likely belong to the eruptive variable class. In Section 5, we derive accretion luminosities and discuss the classification of our sample in the context of the established subclasses of eruptive variable YSOs (FUors, EXors) and find that most members of our sample cannot be described by the classical scheme. Finally, in Section 6, we present a summary of our analysis. Individual analyses of objects in our sample are presented in Appendices A–C. LC and spectra of the whole spectroscopic sample are presented in Appendix F.

2 THE SPECTROSCOPIC SAMPLE

We obtained near-IR spectra for 37 members of the 816 high-amplitude variables from Paper I, all taken with the Magellan Baade telescope. All of the 37 stars have red near-IR colours and SEDs and all are projected within 5 arcmin of an SFR, according to our search of the SIMBAD data base and the mid-IR *WISE* multicolour images (see Paper I). Some preference was given to sources for which a distance estimate to the associated SFR is available in the literature. We note that the VVV disc region contains no large SFRs within ∼2 kpc, so most of the targets are expected to be more distant.

We preferentially selected sources with $K_s < 14.5$ mag at the most recent available epoch in the VVV time series to the observations, in order to obtain good data in a relatively brief observation. Some preference was given to sources with signs of a recent eruption in the LC, though the most recent VVV data available were typically taken several months before the observations. For the first observing run in 2013, we had only one night at the telescope, so we observed

only the sources which either had $\Delta K_s > 2$ mag or a projected location near the massive G305 star-forming complex. In the 2014 run, we included more sources with $\Delta K_s = 1$ to 2 mag, in order to better represent the full photometric sample.

The spectroscopic sample covers a fair cross-section of the full sample of variables projected against SFRs, though it includes a high proportion of systems with eruptive LC and relatively few sources in each of the other categories. Of the 37 targets, the LC classifications were: 18 eruptive variables, 5 long-term periodic YSOs, 6 Mira-like variables, 2 faders, 3 dippers and 3 STVs. The (mean) magnitude range is approximately $11.5 < K_s < 14.5$, compared to $11.5 < K_s < 16.25$ for the full photometric sample (see Paper I). The sole exception is VVVv815 (see Appendix A), a somewhat fainter source observed as a target of opportunity.

The amplitudes of the 18 candidate eruptive variables in the spectroscopic sample are slightly higher than is typical of the 106 eruptive variables in the photometric sample but the difference is modest: the median $\Delta K_s = 1.88$ mag for the former group versus 1.61 mag for the latter group. For the full spectroscopic sample, there is a stronger bias towards higher amplitude systems: the median $\Delta K_s = 1.85$ mag, versus 1.44 mag for all the high-amplitude variables in SFRs (excluding EBs which are not included in the spectroscopic sample).

For every object, we have 2010–2014 K_s photometry from VVV, with the addition of a single 2015 data point arising from the second epoch of contemporaneous JHK_s photometry, LC classification, as well as the information collected in Paper I using SIMBAD (Wenger et al. 2000), Vizier (Ochsenbein, Bauer & Marcout 2000) and public near- and mid-IR surveys from the NASA/IPAC Infrared Science Archive. The latter includes information from 2MASS (Skrutskie et al. 2006), DENIS (Epchtein et al. 1994), *Spitzer*/GLIMPSE surveys (see e.g. Benjamin et al. 2003), *WISE* All-sky release (Wright et al. 2010), Akari (Murakami et al. 2007) and MSX6C (Price et al. 2001). In this work, we also use the information from *Herschel* Hi-Gal (Molinari et al. 2010) and the recently available data of NEOWISE (Mainzer et al. 2011) and DEEP GLIMPSE (Whitney et al. 2011). The 2010–2015 K_s LC of the 37 objects in our sample are presented in Appendix F. All VVV LC were derived from v1.3 of the VISTA pipeline developed by the Cambridge Astronomical Survey Unit, with the addition of our own saturation correction where necessary (see Paper I).

Information from the literature allows us to estimate a likely distance to our objects, based on distances to areas of star formation found within 300 arcsec in the SIMBAD data base. In general these are near-kinematic distances estimated from radial velocities of emission lines observed towards H II regions or Infrared Dark Clouds (IRDCs), such as CS (2–1) (Bronfman, Nyman & May 1996; Jackson et al. 2008), ^{13}CO(1–0) (e.g. Russeil & Castets 2004) or OH maser emission (e.g. Caswell 1998). In some other cases, distances are assumed from the location of the VVV object near-known areas of star formation, such as the G305 star-forming complex.

Table 1 shows the characteristics of the spectroscopic sample. In column 2, we show the original variable star designation from table 1 in Paper I, columns 3 and 4 show the right ascension and declination of the star, whilst columns 5–10 represent the 2010 *J*, *H* and K_s magnitude of the stars along with the respective errors. In column 11, we present $\Delta K_s = K_{s, max} - K_{s, min}$, whilst column 12 shows the slope of the SED, α, derived in Paper I via a linear fit to data points at wavelengths $2 < \lambda < 24$ μm. Column 13 shows the likely distance to our objects estimated from SIMBAD (designated as d_{SFR}), whilst column 14 shows the LC classification given in Paper I. Finally, column 15 shows the classification given to the

Table 1. Characteristics of the spectroscopic sample of VVV high-amplitude variables. In the last column, 'non-er' refers to YSOs not classified as eruptive variables.

No	Variable	α (J2000)	δ (J2000)	J (mag)	J_{err} (mag)	H (mag)	H_{err} (mag)	K_s (mag)	$K_{s, err}$ (mag)	ΔK_s (mag)	α	d_{SFR} (kpc)	Shape (Paper I)	Type (This work)
1	VVVv20	12:28:27.97	−62:57:13.97	17.38	0.04	14.10	0.01	11.70	0.01	1.71	0.6	–	Eruptive	MNor
2	VVVv25	12:35:14.37	−62:47:15.63	–	–	16.01	0.02	12.34	0.01	1.68	0.22	2.2	Eruptive	AGB
3	VVVv32	12:43:57.15	−62:54:45.09	16.07	0.01	14.07	0.01	12.45	0.01	2.49	0.32	2.7	LPV-YSO	MNor
4	VVVv42	13:09:34.64	−62:49:32.52	18.45	0.10	14.26	0.01	11.94	0.01	2.16	0.98	3.7	LPV-Mira	AGB?, YSO?
5	VVVv45	13:11:43.07	−62:48:54.77	–	–	–	–	13.33	0.01	2.31	1.27	3.7	LPV-Mira	AGB
6	VVVv63	13:46:20.48	−62:25:30.81	18.53	0.09	15.79	0.02	13.81	0.01	1.44	0.9	3.5	Eruptive	YSO, non-er?
7	VVVv65	13:47:51.09	−62:42:37.46	18.75	0.10	15.85	0.02	13.59	0.01	1.36	−0.31	3.5	STV	YSO, non-er
8	VVVv94	14:22:57.76	−61:05:47.03	–	–	16.42	0.03	13.39	0.01	1.91	0.54	2.6	Eruptive	MNor
9	VVVv118	14:51:20.97	−60:00:27.40	16.09	0.01	14.54	0.01	13.01	0.01	4.24	0.16	–	Eruptive	EXor(MNor?)
10	VVVv193	15:49:14.34	−54:34:23.66	–	–	16.59	0.04	13.90	0.01	1.26	0.86	4.2	Eruptive	MNor
11	VVVv202	15:54:26.41	−54:08:29.40	17.38	0.03	13.28	0.01	11.66	0.01	1.61	1.16	4.1	LPV-YSO	AGB
12	VVVv229	16:04:24.48	−53:01:14.01	–	–	–	–	13.01	0.01	3.7	2.41	2.3	LPV-Mira	AGB
13	VVVv235	16:09:35.53	−51:54:14.08	–	–	17.95	0.22	11.70	0.01	1.26	1.15	5.3	LPV-Mira	AGB
14	VVVv240	16:13:03.44	−51:41:51.91	–	–	16.35	0.05	12.10	0.01	1.17	0.74	3.5	LPV-Mira	Nova
15	VVVv270	16:23:27.14	−49:44:43.96	–	–	18.34	0.23	16.14	0.07	3.81	1.76	2.3	Eruptive	MNor
16	VVVv322	16:46:24.57	−45:59:21.04	18.48	0.13	16.82	0.08	15.25	0.04	2.63	0.91	3.1	Eruptive	MNor
17	VVVv374	16:58:33.99	−42:49:55.25	17.12	0.02	13.99	0.01	11.98	0.01	2.41	0.91	2.9	Eruptive	MNor
18	VVVv405	17:09:38.62	−41:38:51.81	–	–	17.50	0.13	13.50	0.01	2.00	1.77	2.3	Dipper	YSO, non-er?
19	VVVv406	17:09:57.47	−41:35:48.87	17.51	0.04	14.61	0.01	12.57	0.01	2.06	1.1	2.3	Dipper	YSO, non-er?
20	VVVv452	12:41:58.06	−62:13:42.90	18.10	0.06	15.68	0.01	13.78	0.01	2.46	0.4	–	Eruptive	MNor
21	VVVv473	13:10:57.49	−62:35:22.34	–	–	–	–	14.53	0.01	1.50	1.82	3.7	LPV-YSO	MNor
22	VVVv480	13:16:50.32	−62:23:41.61	15.81	0.01	15.08	0.01	14.58	0.01	1.70	-0.28	3.7	LPV-YSO	YSO, non-er?
23	VVVv514	14:00:45.37	−61:33:39.95	17.40	0.04	14.80	0.01	13.26	0.01	1.73	-1.46	4.3	Fader	Nova
24	VVVv562	14:53:33.59	−59:10:21.73	16.68	0.02	14.20	0.01	12.46	0.01	2.79	-0.01	2.9	Fader	MNor
25	VVVv625	15:43:17.95	−54:06:47.29	–	–	18.08	0.15	14.49	0.01	1.46	0.33	2.3	STV	YSO, non-er
26	VVVv628	15:44:49.54	−54:07:52.08	17.42	0.03	15.30	0.01	13.76	0.01	1.45	-0.51	2.2	Dipper	YSO, non-er
27	VVVv630	15:44:56.13	−54:07:03.18	–	–	18.83	0.31	15.76	0.04	1.90	2.70	2.2	Eruptive	YSO, non-er
28	VVVv631	15:45:18.36	−54:10:36.87	17.39	0.03	15.13	0.01	13.41	0.01	2.63	-0.14	2.3	Eruptive	MNor
29	VVVv632	15:44:09.80	−53:56:27.78	14.35	0.01	12.95	0.01	11.87	0.01	1.51	0.29	2.5	STV	YSO, non-er
30	VVVv662	16:10:26.82	−51:22:34.13	–	–	18.55	0.24	15.30	0.03	1.83	0.81	3.1	Eruptive	MNor
31	VVVv665	16:09:57.70	−50:48:09.42	–	–	16.57	0.04	14.09	0.01	1.63	0.95	4.3	Eruptive	MNor
32	VVVv699	16:23:44.34	−48:54:55.29	–	–	–	–	16.19	0.09	2.28	2.78	4.2	Eruptive	MNor
33	VVVv717	16:36:05.56	−46:40:40.61	–	–	–	–	14.37	0.02	2.47	0.81	–	LPV-YSO	MNor
34	VVVv721	16:39:48.77	−45:48:47.96	18.49	0.16	15.96	0.05	13.98	0.01	1.86	0.87	4.2	Eruptive	FUor
35	VVVv796	17:12:07.43	−38:41:26.86	–	–	16.87	0.09	12.45	0.01	2.94	1.1	1.4	LPV-Mira	AGB
36	VVVv800	17:12:46.04	−38:25:24.63	18.89	0.20	15.80	0.04	12.89	0.01	1.65	1.44	1.4	Eruptive	MNor
37	VVVv815	14:26:04.95	−60:41:16.81	19.17	0.16	17.90	0.13	14.94	0.02	1.71	1.58	3.1	Eruptive	MNor

objects from the results presented later in this work. Finding charts for these stars are shown in Appendix G.

Fig. 1 (top) illustrates the distributions in α and K_s magnitude of the spectroscopic sample (where K_s is taken from the first epoch of contemporaneous JHK_s data from 2010). The sample has a fairly wide range in α, though it is composed mainly of class I and flat spectrum systems. This is fairly representative of the photometric YSO sample, especially the eruptive candidates (see Paper I), though the photometric sample does include a slightly higher proportion of class II YSOs and a few class III YSO candidates. Fig. 1 also shows the VVV near-IR colour–colour diagram (based on contemporaneous data from 2010) and an $K_s - [12]$ versus $H - K_s$ diagram. Sources that we finally conclude are not YSOs and are colour coded in red (dusty asymptotic giant branch, AGB, variables) or blue (cataclysmic variables, more specifically classical novae). In the bottom panel of Fig. 1, we also show fiducial lines for the sequences of carbon and oxygen-rich AGB stars (from van Loon et al. 1998). It is interesting to see that VVV objects that are later classified as AGB stars tend to follow the fiducial line of oxygen-rich AGB stars. However, we note that not all oxygen-rich

stars in the sample of van Loon et al. (1998) are observed to follow this line.

We make use of 70 μm data from Hi-Gal in order to check whether the evolutionary classes of our sample, as defined by α, agree with the expectations for class I, flat-spectrum and class II YSOs. In Fig. 2, we show the $[24] - [70]$ versus $K_s - [24]$ and $[24] - [70]$ versus $[3.6] - [24]$ colour–colour diagrams for our sample, where we compare to the Perseus YSO sample from Young et al. (2015). The latter uses 3.6, 24 and 70 μm data from *Spitzer*, whilst K_s photometry arises from a 1 arcsec cross-match of the sample with the 2MASS catalogue. For VVV objects, we prefer the use of *WISE* $W1$ and $W4$ filters as it is nearly contemporaneous to Hi-Gal observations which were obtained in 2010. When *WISE* is not available, we make use of GLIMPSE I1 and MIPSGAL 24 μm photometry. The use of *WISE* or *Spitzer* filters can lead to small differences in the photometry. Cutri et al. (2012) shows that *WISE*/$W1$ and GLIMPSE I1 only present significant differences for objects with $W1 > 14$ mag, whilst *WISE*/$W4$ tends to be 15 per cent brighter than MIPSGAL 24 μm photometry. For objects with no 70 μm detections, we use the 90 per cent completeness limit of 1.75 Jy from Elia et al. (2013).
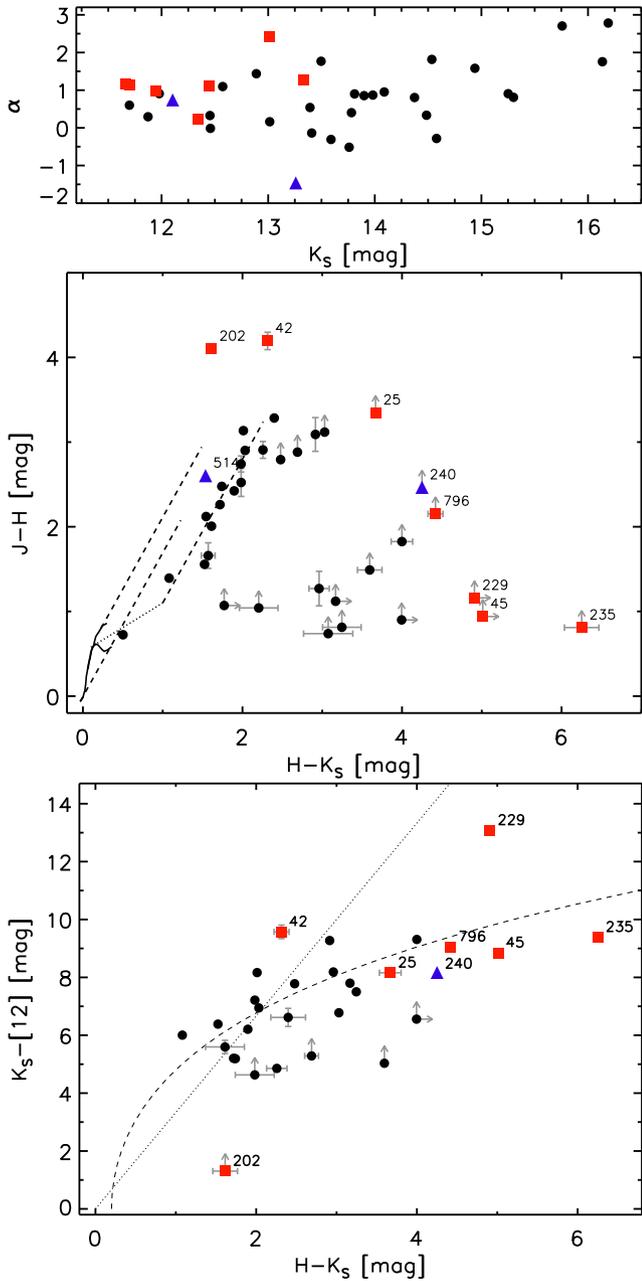
Figure 1. (top) α versus K_s for the objects of the VVV spectroscopic sample. (middle) $(H - K_s)$, $(J - H)$ colour–colour diagram. (bottom) $K_s - [12]$ versus $(H - K_s)$ for VVV objects. Magnitudes at 12 μm are from *WISE W3* filter. Error bars are only shown for objects with significant errors. In all plots, red squares mark objects that are likely asymptotic giant branch (AGB) stars, whilst blue triangles mark the two objects that are likely novae. The bottom panel shows the fiducial lines for the sequences of carbon-rich (dot–dashed line) and oxygen-rich AGB stars (dashed line, arising from van Loon et al. 1998). We note that these lines are based on the IRAS 12 μm passband (which is not identical to *W3*).

The comparison of Fig. 2 shows that our classification agrees with that of Young et al. (2015). In addition, we can see that the lack of a 70 μm detection for some VVV sources does not preclude a YSO classification. For example, for sources with 70 μm upper limits, the expected location on the [24]−[70] versus K_s −[24] diagram based on the Young et al. (2015) data typically corresponds to 70 μm fluxes that fall below the Hi-Gal completeness limit. Finally, we

can also observe that objects that are later considered to be more likely non-YSOs tend to fall in a different area than YSOs. This is especially true for VVVv42, VVVv229, VVVv235 and VVVv796. These four objects are classified as having Mira-like LC in Paper I. For further comparison with the colours of known dusty AGB stars, we refer the reader to van Loon et al. (2010a), van Loon et al. (2010b) and Boyer et al. (2011), though we note that most of the sources described therein have more modest amplitudes (but these works do include also Mira-like pulsators with $\Delta K > 1$ mag).

As we did in Paper I for the full sample, we use the two epochs of JHK_s photometry from VVV in order to study the mechanism driving variability in our sample. Once again, we stress that in most cases, the two epochs do not sample directly the large K_s magnitude changes in the systems. In addition, we note that 6 objects in our sample are undetected in the J and H passbands in at least one epoch and 20 objects are not detected in the J passband in at least one epoch. Fig. 3 shows $\Delta(H - K_s)$ versus ΔH and $\Delta(J - H)$ versus $\Delta(H - K_s)$ for objects where this is information is available. In the first plot (upper panel), we see that our sample shows an elliptical distribution with its major axis along the redder when fading/bluer when brightening quadrants, consistent with changes being cause either by variable extinction or accretion (Lorenzetti et al. 2012). The second plot shows that for sources with significant changes in colour, these changes are generally not consistent with extinction in the majority of the sample. The exception is the objects classified as dippers, for which extinction was already considered to be a more likely explanation for their variability (see Paper I).

3 OBSERVATIONS

3.1 Magellan Baade/FIRE

3.1.1 Low-resolution spectroscopy

Follow-up of one high-amplitude variable VVVv815 was performed on 2012 May 8 with the FIRE spectrograph mounted on the Magellan Baade Telescope at Las Campanas Observatory, Chile. As detailed in Paper I, VVVv815 was identified via an early search of the VVV time series, with slightly different quality criteria to the rest. The observations were carried out in the high-throughput prism mode which provides a continuous coverage from 0.8 to 2.5 μm at low resolving power of $R = \Delta\lambda/\lambda \sim 250$–350 with a 0.6 arcsec slit. Since the spectrum displayed exceptionally strong H_2 emission lines (suggesting an accretion-powered outflow), VVVv815 was observed again in echelle mode in a subsequent run allocated to the topic of this paper.

The object was observed in the usual ABBA pattern along the slit, with individual exposures of 148 s and at an airmass of 1.1. Observations of spectroscopic calibrators were carried out for purposes of telluric correction and flux calibration; the calibrators were observed at similar airmass as the objects and with the same instrumental setup. Quartz lamp images were obtained for flat fielding of the data; they consisted of high-voltage (2.2V) images which provide data for the *z/J* bands but saturate the red end of the spectrum and low voltage(1.1 V) which generate counts in H/K but are too faint for the blue end. Additionally, 'NeNeAr' arc lamp images were acquired for wavelength calibration.

The images were reduced using the longslit package of the FIREHOSE software. Using the NeNeAr lamp image FIREHOSE generates an arc solution which had typical uncertainties of 0.4 pixels or ∼2.7 Å. The second step consisted of creating a flat image; this is done by combining the 2.2 (blue) and 1.1 V (red) with a smooth
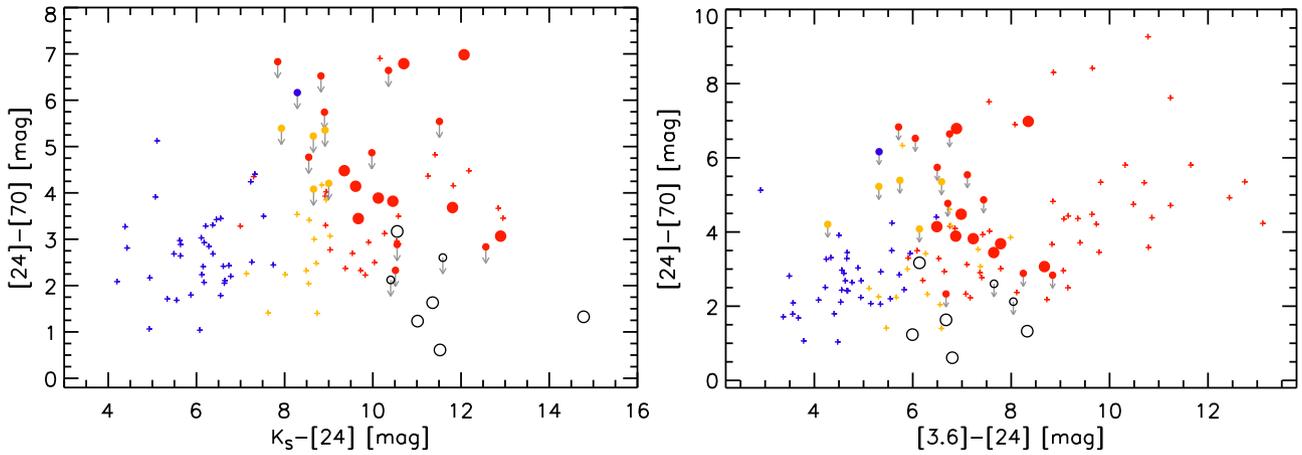
Figure 2. $[24] - [70]$ versus $K_s - [24]$ (left) and $[24] - [70]$ versus $[3.6] - [24]$ (right) colour–colour diagrams for our sample. In the plots, we show likely YSOs as filled circles and objects which were finally classified as non-YSOs as open circles. Large symbols represent objects with 70 μm detections, whilst small symbols with grey arrows represent upper limits. In the figure, we also show the Perseus YSO sample from Young et al. (2015) as plus symbols. The colours for both VVV objects and YSOs from Young et al. mark class I (red), flat-spectrum (orange) and class II (blue) YSOs.
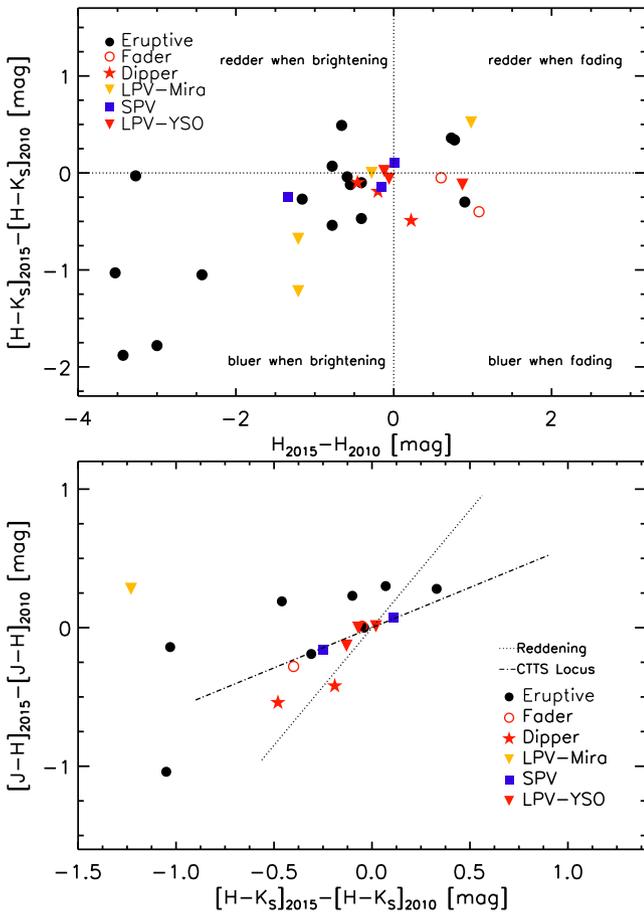

Figure 3. $\Delta(H - K_s)$ versus ΔH (top) and $\Delta(J - H)$ versus $\Delta(H - K_s)$ (bottom) for objects in the spectroscopic sample with an available second JHK_s epoch from VVV. In the plots, we mark the different classes from LC morphology. Different symbols are explained in the plots. In the bottom plot, we mark the expected changes which occur parallel to the reddening vector (dotted line) and to the classical T Tauri stars locus of Meyer, Calvet & Hillenbrand (1997) (dot–dashed line).

weighting function spread over ∼150 pixels centred on a transition pixel defined by the user. Finally, the software traces and extracts the spectrum of the object. Telluric correction and flux calibration were performed in the standard mode using NOAO/TWODSPEC package in IRAF.

3.1.2 Echelle spectroscopy

All 37 members of the sample were observed in the echellete mode with the FIRE spectrograph mounted on the Magellan Baade Telescope at Las Campanas Observatory, Chile. The echellete mode provides coverage from 0.8–2.5 μm using echelle grating orders 11–32, at a resolving power of $R \sim 6000$ with a 0.6 arcsec slit. The spatial scale is 0.18 arcsec pixel^{-1}. The bulk of the observations were carried out over a total of three nights, on 2013 April 19 and 2014 May 10 and 11. Thick cloud cover on May 10 restricted us to bright targets but did not otherwise appear to affect the results. Additional data were also taken on the nights of 2015 April 26 and 27 in order to investigate the spectroscopic variability of the sample. Data from the 2015 run are only included here for one source, VVVv25, for which the 2014 data were of insufficient quality for a clear classification. We defer further discussion of the 2015 data set to a future paper that will benefit from additional 2015 VVV time series photometry.

The majority of the variable stars were observed in the typical ABBA pattern along the slit, with individual exposure times between 158 and 260 s and a total time on source of ∼10–17 min. Airmasses were in the range 1–1.4. Immediately after observing each object, we observed ThAr lamps for wavelength calibration and F-type and A0 main-sequence stars for relative flux calibration purposes. These were also done in an AB pattern and with exposure times between 10 and 60 s. Sky and 'Qh' lamp flats were acquired at the beginning/end of each night to determine the pixel-to-pixel response calibration. Table 2 shows the date, exposure time and number of exposures for all of the VVV objects.

Data reduction was performed using the echelle mode of the FIREHOSE data reduction software. This determines the boundaries of each order in the image, constructs a master Qh flat, a slit illumination function from the sky twilight flats and determines the tilt of the slit in the detector from a wavelength calibration frame. The software then generates the wavelength solution and traces the

Table 2. Spectroscopic observations of VVV objects.

Object	R	T_{exp}(s)	Airmass	N_{exp}	Date
VVVv20	6000	253.6	1.4	4	2014 May 11
VVVv25	6000	253.6	1.2	4	2015 April 27
VVVv32	6000	253.6	1.2	8	2014 May 10
VVVv42	6000	253.6	1.4	4	2013 April 22
VVVv45	6000	253.6	1.2	4	2013 April 22
VVVv63	6000	253.6	1.4	4	2014 May 11
VVVv65	6000	158.5	1.3	4	2014 May 11
VVVv94	6000	253.6	1.2	4	2014 May 10
VVVv118	6000	253.6	1.2	4	2013 April 22
VVVv193	6000	158.5	1.1	4	2014 May 11
VVVv202	6000	158.5	1.1	2	2014 May 11
VVVv229	6000	158.5	1.1	4	2013 April 22
VVVv235	6000	158.5	1.1	2	2014 May 11
VVVv240	6000	253.6	1.2	4	2014 May 10
VVVv270	6000	158.6	1.2	4	2014 May 11
VVVv322	6000	158.5	1.3	4	2014 May 11
VVVv322	6000	253.6	1.1	4	2013 April 22
VVVv374	6000	253.6	1.1	4	2014 May 10
VVVv405	6000	158.5	1.3	4	2014 May 11
VVVv406	6000	158.5	1.4	4	2014 May 11
VVVv452	6000	253.6	1.2	8	2014 May 10
VVVv473	6000	253.6	1.2	4	2013 April 22
VVVv480	6000	253.6	1.25	12	2013 April 22
VVVv514	6000	158.5	1.2	4	2014 May 11
VVVv562	6000	253.6	1.3	4	2014 May 11
VVVv625	6000	158.5	1.2	4	2014 May 11
VVVv628	6000	253.6	1.1	4	2014 May 11
VVVv630	6000	158.5	1.2	4	2014 May 11
VVVv631	6000	253.6	1.1	4	2014 May 10
VVVv632	6000	253.6	1.2	4	2014 May 10
VVVv662	6000	158.5	1.2	4	2014 May 11
VVVv665	6000	158.5	1.1	4	2014 May 11
VVVv699	6000	158.5	1.1	4	2014 May 11
VVVv699	6000	253.6	1.1	4	2013 April 22
VVVv717	6000	253.6	1.1	4	2013 April 22
VVVv721	6000	158.6	1.2	4	2014 May 11
VVVv796	6000	253.6	1.3	4	2014 May '0
VVVv800	6000	253.6	1.2	4	2014 May 10
VVVv815	6000	253.6	1.2	4	2013 April 22
VVVv815	300	148	1.3	4	2012 May 8

object in each order. The wavelength solution has errors between 0.04 and 0.4 Å depending on the order.

The profile of the object and background sky residuals are fitted using an iterative procedure, where a non-parametric spline function is used for orders with high signal to noise, whilst a Gaussian profile is assumed for low signal-to-noise orders. It then performs an optimally weighted extraction of the object using the profile determined before.

In the case of the extraction of the telluric calibration stars, the software uses a boxcar extraction as the default, which simply sums the counts of the target within an extraction window of a pre-determined width. We found that the different extraction methods for the object and calibrator yielded odd results for the final spectrum of the object after telluric calibration, i.e. the objects had bluer spectra than expected from their near-IR colours. This problem was solved by using optimal extraction for the telluric calibration stars as well as the science targets.

The software removes intrinsic absorption features of H I from the telluric calibration stars following the methods of Vacca, Cushing & Rayner (2003). This procedure is only suitable for A0V stars and it

was used for the telluric calibration stars observed in the 2014 run. In the 2013 run, we observed F-type stars as calibrators because we were not confident that the software would remove H I features from A0V spectra with sufficient precision to allow measurement of H I emission in YSOs, such as the Brγ line. Subsequent testing showed that the pipeline does remove H I features from A0 stars very well, so we reverted to A0 stars in 2014, as recommended in the FIRE manual. For the 11 science targets observed in 2013, intrinsic features from the F-type calibrator were removed for each order by fitting and subtracting them with SPLOT in IRAF.

The final relative flux calibration and merging of individual orders were performed using the ONEDSPEC tasks, TELLURIC and SCOMBINE, respectively.

The reduced and combined FIRE spectra of 37 objects are presented in Appendix F.

4 FIRE SPECTRA

4.1 General properties

In this section and Section 4.2, we discuss the general spectroscopic characteristics of the sample which confirm most of the variables as YSOs and show that they resemble eruptive systems more than normal class I YSOs. Then, in Section 4.3, we look at how the spectroscopic characteristics of the confirmed YSOs differ between the different categories of LC, prior to a discussion on how to classify these stars in Section 5. We will present some of the individual spectra throughout the remainder of this work. However, we refer the reader to Appendix F in order to inspect the whole sample before reading through these sections.

In Table 3, we show the equivalent widths obtained from the atomic and molecular features. Equivalent widths of individual lines are measured using SPLOT in IRAF with a Gaussian line profile.

We first note that nine variable stars are found to be of a different class, based on consideration of all the data. Two objects are likely novae observed at some time after outburst and seven are likely dust-enshrouded AGB stars. The two novae, VVVv514 and VVVv240, had LC classified as a fader and Mira-like, respectively, in Paper I. We note that novae are known to have very diverse LC (e.g. Gehrz 1988). The LC of five of the seven AGB stars were classified as Mira-like in Paper I and they are listed as 'LPV-Mira' in Table 1. A sixth O-rich, VVVv202, had an 'LPV-YSO' classification in Table 1 and Paper I since its LC was not very well fit by a smooth sinusoid. A small number of such misclassifications of LPV-YSO and LPV-Mira types was to be expected, as noted in Paper I. The LC of the seventh, VVVv25, was classified as eruptive in Paper I because the sparsely sampled time series does not suggest a periodic nature, except perhaps on a time-scale substantially longer than the 4 yr baseline. However, the spectrum reveals that it is a C-rich object (which is not consistent with YSO status) and our analysis of possible periods in Paper I shows that a period of 400–500 d (typical of a carbon star) is amongst the possibilities consistent with the sparsely sampled LC, most of the troughs being missed in such a case. In Appendix C, we analyse these nine post-main-sequence objects and discuss how some of the information from the literature and their spectral characteristics can cause such objects to be misinterpreted as YSOs. These nine variable stars are not included in our discussion of YSO properties, so percentages given below for the incidence of particular features refer to the YSOs only.

We find that 28 objects display the typical characteristics of YSOs, such as Brγ or H_2 lines in emission or CO in emission or absorption. In each of these objects, the overall trend of the

Table 3. Equivalent widths of common features found in the near-IR spectra of YSOs detected in our VVV sample. The EW of CO was measured in SPLOT by visually selecting two continuum points around the CO bandhead and estimating the continuum as a linear function between the two points. The EW is estimated by summing $(1-F_i/C_i)$ over wavelength, where F_i and C_i are the flux and the continuum at pixel i. This inevitably has fairly large errors due to uncertainty in the continuum level, even though the individual transitions are often very clearly detected.

Object	$H_2(2.12\,\mu m)$ (Å)	Br $\gamma(2.16\,\mu m)$ (Å)	Na I(2.21 μm) (Å)	Ca I(2.26 μm) (Å)	$^{12}CO(2.293\,\mu m)$ (Å)	Mg I(2.28 μm) (Å)
			YSO-Eruptive			
VVVv20	-9.8 ± 0.4	-3.8 ± 0.6	-0.7 ± 0.2	–	-5.3 ± 2.5	–
VVVv32	–	-5.7 ± 2.2	–	–	-19.0 ± 10.0	–
VVVv94	-0.7 ± 0.3	-7.0 ± 1.5	–	–	-5.0 ± 7.0	–
VVVv118	–	-1.4 ± 1.0	–	–	–	–
VVVv193	-1.3 ± 0.6	-2.2 ± 0.7	–	–	-7.0 ± 4.0	–
VVVv270	-0.8 ± 0.3	-2.0 ± 0.7	-1.7 ± 0.3	–	-7.0 ± 6.0	–
VVVv322(13)	-2.0 ± 0.8	–	–	–	33.0 ± 7.0	–
VVVv322(14)	-5.5 ± 2.1	–	–	–	25.0 ± 8.0	–
VVVv374	-1.9 ± 0.2	-2.1 ± 0.3	-0.8 ± 0.2	–	-4.5 ± 1.5	–
VVVv452	-1.2 ± 0.6	-3.6 ± 1.1	–	–	-8.0 ± 4.0	–
VVVv473	-30.1 ± 3.9	-1.7 ± 1.2	–	–	-1.3 ± 12.0	–
VVVv562	-3.2 ± 0.5	-3.4 ± 1.1	2.0 ± 0.3	–	–	–
VVVv631	–	-2.4 ± 0.4	-1.4 ± 0.2	–	-1.0 ± 1.0	–
VVVv662	-0.3 ± 0.1	-4.1 ± 1.1	-1.2 ± 0.4	–	-2.0 ± 4.0	–
VVVv665	-1.9 ± 0.7	-2.4 ± 0.4	-3.4 ± 0.3	–	-52.0 ± 11.0	–
VVVv699(13)	-14.1 ± 1.3	-3.5 ± 0.5	-5.0 ± 0.4	–	-40.7 ± 11.1	-1.4 ± 0.5
VVVv699(14)	-15.5 ± 2.4	-3.1 ± 1.1	-3.1 ± 0.5	–	-21.3 ± 10.0	-0.8 ± 0.3
VVVv717	-0.8 ± 0.3	-1.1 ± 0.5	–	–	28.0 ± 4.0	-0.9 ± 0.3
VVVv721	–	–	–	–	14.0 ± 4.0	–
VVVv800	-2.0 ± 0.2	-1.2 ± 0.4	–	–	–	–
VVVv815(13)	-119.0 ± 36.0	–	–	–	–	–
VVVv815(12)	-200.0 ± 27.0	–	–	–	–	–
			YSO-Non-eruptive			
VVVv63	-4.3 ± 0.8	-2.1 ± 0.5	–	–	–	–
VVVv65	–	-1.2 ± 0.5	–	–	–	–
VVVv405	-7.5 ± 1.8	-0.9 ± 0.4	–	–	–	–
VVVv406	-0.5 ± 0.2	–	–	–	–	–
VVVv480	–	-4.4 ± 2.2	–	–	–	–
VVVv625	-0.8 ± 0.2	-3.6 ± 1.7	–	–	–	–
VVVv628	-1.7 ± 0.7	-1.4 ± 0.5	3.1 ± 0.6	3.2 ± 0.9	13.0 ± 8.0	–
VVVv630	–	0.7 ± 0.2	1.3 ± 0.2	1.8 ± 0.6	14.0 ± 5.0	–
VVVv632	-1.4 ± 0.2	-2.1 ± 0.3	1.2 ± 0.2	1.1 ± 0.2	–	–
			Non-YSOs			
VVVv25	–	–	-0.6 ± 0.3	–	16.0 ± 7.0	–
VVVv42	-0.3 ± 0.2	–	-1.0 ± 0.3	–	8.0 ± 4.0	–
VVVv45	–	–	–	–	33.0 ± 11.0	–
VVVv202	–	–	4.7 ± 0.4	5.3 ± 0.5	37.0 ± 2.0	–
VVVv229	–	–	–	–	25.0 ± 7.0	–
VVVv235	–	–	–	–	47.0 ± 12.0	–
VVVv240	–	-0.7 ± 0.3	–	–	–	–
VVVv514	–	-7.8 ± 2.3	–	–	–	–
VVVv796	–	–	–	–	27.0 ± 7.0	–

near-IR continuum is either to rise with increasing wavelength or to be approximately flat, as expected for class I and flat spectrum YSOs or other sources suffering high IR extinction. Three YSOs, VVVv322, VVVv717 and VVV721 have $\Delta v = 2$ CO absorption bands at 2.29–2.45 μm which appear to be stronger than expected from the photosphere of a K or M dwarf, and are more in line with that expected from the photosphere of late M-type giant stars. In fact, the CO absorption of these three systems is very similar to that of some of our objects which are classified as AGB stars. Such strong CO absorption is characteristic of FUors and FUor-like YSOs (Connelley & Greene 2010; Reipurth & Aspin 2010). In fact, the latter authors regard it as the defining spectroscopic characteristic,

given the inferred origin in a disc with a high accretion rate (see Section 1). Two of these three sources also display the broad H_2O absorption bands often seen in such systems.

Between 20 and 23 objects show Brγ emission (the detections being marginal in three cases). This amounts to 71–82 per cent of the 28 YSOs. This feature is noticeably broadened ($\sim$100 km s^{-1} linewidth) in most cases where it is well measured. This broadening is typical of normal YSOs where it is attributed to infalling gas near the stellar photosphere (see e.g. Muzerolle, Hartmann & Calvet 1998; Davis et al. 2001). Brγ is seen in absorption in only one YSO, VVVv630, which appears not to be an eruptive variable (see Section 4.3).

We find that 22 of the YSO spectra (79 per cent) show 2.12 μm H_2 emission. Of these, 10 objects also show additional lines from H_2. In every case, the emission from this molecule is likely arising from shock-excited emission given that higher excited transitions are usually weak or not present in the spectra. Atomic lines of Na I and Ca I are not common in our sample, with three or four objects showing absorption at these wavelengths (11–14 per cent) and emission in five–seven objects (18–25 per cent). When Na I was observed in emission, CO was usually also in emission (see Table 3) following the pattern seen in EXors (see Section 1).

CO emission is observed in 8–11 objects (27–37 per cent). We find that objects which show this characteristic can be fitted by models (see Appendix E) with temperatures between 2500 and 3500 K. This temperature range agrees with that expected to give rise to CO emission in gaseous discs of YSOs (Najita et al. 1996). We also find that some objects show the evidence of broadened CO profiles. Rotation in Keplerian discs has been shown to produce this feature (see e.g. Najita et al. 1996; Davies et al. 2010). Although this needs a more detailed investigation at higher spectral resolution, the observed broadened profile appears consistent with a similar origin in some of our systems.

Brγ is not detected in four YSOs. One of these is VVVv815, an object for which only strong H_2 emission is present (see Appendix A). In fact, the 2.12 μm line has an equivalent width of EW = −200 Å in 2012 and EW = −119 Å in 2013 which is the largest equivalent width measured for this line across the whole sample. As for VVVv815, VVVv406 also does not show any features at the wavelength of Brγ, but is also, in general, a featureless spectrum with weak H_2 2.12 μm emission. The remaining two objects, VVVv322 and VVVv721, are characterized by having CO absorption and broad H_2O absorption bands, with a lack of other photospheric absorption features such as Na I and Ca I. These two YSOs are spectroscopically similar to FUors, where CO absorption arises from the accretion disc rather than the stellar photosphere. We discuss later whether an FUor classification is appropriate in each case.

CO absorption is also observed in three objects which also show Brγ emission or absorption. The most interesting of these is VVVv717 (see Appendix A). It has the FUor-like property of very strong CO absorption: in this case, by gas at a fairly low temperature (1600 K, see Appendix E). The narrow, relatively weak Brγ emission in this object seems to be on top of a broader absorption feature. Brγ emission is not usually detected in FUors as this accretion-sensitive emission line is assumed to be quenched by the very high accretion rate in FUors. VVVv717 also shows weak H_2 2.12 μm and a marginal detection of Mg I 2.28 μm emission. No other absorption features from a stellar photosphere are observed. The two other objects that show CO absorption are VVVv628 and VVVv630. In both cases, the CO absorption seems to arise from a stellar photosphere, given that other absorption features associated with a stellar photosphere, such as Na I and Ca I, are also observed. The temperatures estimated from CO models in Appendix E (3100–3200 K) are consistent with those expected for the cool upper layers of the stellar photosphere in low-mass YSOs.

Previous spectroscopic studies of YSOs at near-IR wavelengths report the following frequencies for the atomic and molecular features. In the case of Brγ emission, Cooper et al. (2013) finds detection rates of 75 per cent for high-mass YSOs, whilst Carr (1989) and Connelley & Greene (2010) find rates of 71 per cent and 75 per cent, respectively, for low-mass YSOs. 91 per cent of intermediate-mass and Herbig Ae/Be stars in the study of Ishii et al. (2001) show this feature in emission. We note that in all of these studies, the
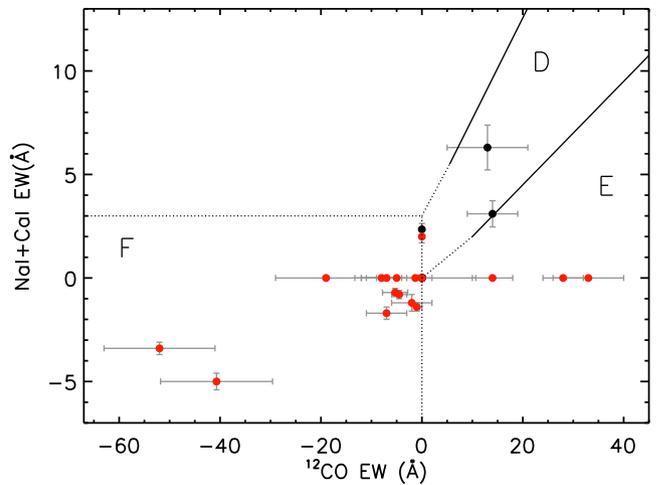

Figure 4. Comparison of the equivalent widths of Na I+Ca I versus ^{12}CO for the VVV spectroscopic sample. Regions marked on the plots are based on the work of Connelley & Greene (2010). Objects marked in red represent objects later classified as members of the eruptive variable class, whilst black symbols mark YSOs found not to be part of this variable class.

samples were composed mostly of embedded sources, though not exclusively in every case.

CO emission is observed in 17 per cent of massive YSOs (Cooper et al. 2013), 20 per cent and 22 per cent for low-mass YSOs (Carr 1989; Connelley & Greene 2010) and 22 per cent for intermediate-mass and Herbig Ae/Be stars (Ishii et al. 2001). For H_2 emission, Cooper et al. find rates of 56 per cent (high-mass YSOs), Ishii et al. report 34 per cent for intermediate YSOs, whilst low-mass YSOs are found to show this feature in 25 per cent of the objects of Carr and 42 per cent in the sample of Connelley & Greene.

The detection frequency for Brγ emission in our sample is comparable to the percentages obtained for low- and high-mass YSOs. In the case of CO emission, our numbers seem to be higher than those reported in previous studies. For H_2 emission, the detection rate in our sample appears to be significantly higher. H_2 and CO emission are commonly associated with outburst events. In addition, the absence of photospheric absorption features in most of the YSOs suggests that these are objects with high veiling from hot circum-stellar material. High veiling may be related to a high accretion state (Connelley & Greene 2010).

4.2 Eruptive YSOs versus normal YSOs: equivalent width diagrams

In Fig. 4, we plot equivalent widths of CO against those of Na I+Ca I for the VVV sample. In these plots, we mark the distinct regions defined by Connelley & Greene (2010) in their study of a large sample of class I YSOs (their fig. 5). First, we describe the results for the flux-limited sample of Connelley & Greene (2010).

(i) Region F: objects falling in this area were characterized by showing CO and Na I+Ca I emission. Brγ emission is also typical in these sources. Objects from the sample of Connelley & Greene with these characteristics had strong veiling from hot circum-stellar material which they suggested is associated with a high accretion rate.

(ii) Region D: the majority of class I YSOs in the Connelley & Greene sample fell in this region. Objects in this area had low veiling, showing CO and Na I+Ca I absorption. The EWs were

consistent with origin in the photosphere of a YSO, falling in between the loci of dwarf and giant photospheres as marked by thick lines in the upper panel of Fig. 4.

(iii) Region E: objects in this area showed CO absorption in excess of photospheric absorption, as well as a lack of photospheric absorption features. Objects in this area lack Brγ emission. The objects in the sample of Connelley & Greene falling in this region were either FUors or 'FUor-like' YSOs, a term commonly used to describe sources which have similar spectra to FUors but lack the photometric evidence for an eruption at present.

The VVV sample is clearly different from that of Connelley & Greene (2010), in that very few of the VVV sample are located in region D, where most normal class I YSOs were found. Instead, the location of the VVV YSOs is more often in the two regions of the upper panel expected for highly variable YSOs undergoing episodic accretion: (1) region F, where objects with high veiling and EXor-like active states of accretion are expected to fall. These objects display Brγ emission in addition to shock-excited emission from H$_2$. (2) Region E, where FUors are usually found.

4.3 Spectra and LC categories

We have seen that many of the 28 YSOs in the sample show characteristics that point to high states of accretion. In this section, we compare their spectroscopic characteristics to their LC classification from Paper I and analyse whether the observed variability can be explained by variable accretion or another of the known mechanisms in YSOs.

The 28 objects are divided into 4 long-period YSOs, 3 dippers, 1 fader, 3 STV stars and 17 eruptive objects. Unsurprisingly, most of the systems which we regard as bona fide examples of episodic accretion have eruptive LC classifications.

(i) Short-term: the three STV stars, VVVv65, VVVv625 and VVVv632, have lower amplitudes than most of the YSOs in the spectroscopic sample. The spectra of VVVv65 and VVVv625 lack CO emission or absorption features and show weak Brγ emission, with VVVv625 also showing weak H$_2$ emission. The spectrum of VVVv632 resembles that of classical T Tauri stars (e.g. TW Hya, see e.g. Vacca & Sandell 2011) and shows several absorption features (Na I, Ca I, Mg I, and Al I) arising from the stellar photosphere. Emission from atomic hydrogen is also present (Brγ, Pa β, Pa γ, Pa δ), as well as from some H$_2$ transitions. Finally, the He I 1.083 μm line is also observed, and it exhibits a P Cygni profile, with absorption extending to ~ -200 km s^{-1}. This feature suggests the presence of an outflow from the system. Given that clear indicators of a high accretion rate are absent and the nature of the LC is a nearly continuous short-term variability, with relatively low amplitudes ($\leq$1.5 mag) for the VVV sample, we consider that the variability in these three objects is likely caused by a different mechanism than variable accretion. We note that the VVVv65 spectrum was not taken during a bright state (and the VVVv625 spectrum may or may not have been) so we may be mistaken in this judgement). However, our main aim here is to identify the YSOs for which the evidence of episodic accretion is reasonably clear.

(ii) Dippers: VVVv628 has $\Delta K_s = 1.45$, Brγ and H$_2$ emission and absorption features of Na I, Ca I and CO with typical equivalent widths for a stellar photosphere. Given the lack of veiling despite observation in a bright state and the nature of the LC, it seems likely that another mechanism than accretion may be driving the variability in this object. VVVv405 and VVVv406 have larger amplitude ΔK_s ($\geq$2 mag), with the former showing emission from several

transitions of H$_2$, as well as Brγ emission. VVVv406, on the other hand, is faint at the epoch of observations and shows a featureless spectrum with weak H$_2$ emission. In both cases, the two epochs of near-IR variability are taken at similar K_s magnitudes so no information on colour changes could be derived. CO is not detected in these two objects. It is difficult to establish whether variable accretion is responsible for the variability in these YSOs so for the present, we classify them as non-eruptive.

(iii) Fader: VVVv562 is the only object in this category. Brγ, H$_2$ and 1.64 μm [Fe II] lines are seen in emission. No CO features are detected but we note that this object was observed when $\sim$2 mag fainter than its maximum brightness. Inspection of ancillary data from 2MASS, *WISE* and *Spitzer* supports the idea that the object went into an eruption at some time between 2004 and 2010 and has been on a fading trend since then (see Fig. 5). The colour changes seen between the two epochs of JHK_s photometry (bluer when fainter) disfavour variable extinction. We note that variations in geometry, such that absorption increases but so does scattered light, can lead to a star becoming bluer at minimum light (an effect sometimes observed in UX Ori stars deep minima due to dust clumps which screen stellar light; see e.g. Herbst & Shevchenko 1999). However, in this case, the source faded by only 1.1 mag in H between the two epochs while becoming 0.35 mag bluer in $H-K_s$, so an unusually bright source of scattered light would be required. We consider it likely that the variability in this object is due to changes in the accretion rate. Note below that this is the first of four YSOs which we classify as an eruptive variable despite the absence of the CO emission or strong CO absorption seen in EXors or FUors, respectively. These indicators are likely to be absent during quiescence and in any case, they may be veiled into invisibility in heavily embedded YSOs, as in OO Ser (Hodapp et al. 1996; Kóspál et al. 2007) or GM Cha (Gómez & Mardones 2003; Persi et al. 2007).

(iv) Long-term periodic: in Paper I, we discuss the possible mechanisms which can drive periodic variability ($P > 100$ d) in YSOs. One of these mechanisms can be variable accretion, which has been invoked to explain the variability in e.g. V371 Ser (where accretion is modulated by a binary companion, see Hodapp et al. 2012). It is very interesting to see that three-fourth YSOs with the long-term periodic classification show characteristics of objects in high states of accretion. VVVv32 and VVVv473 show Brγ and CO emission, the latter also showing several transitions of H$_2$. VVVv717 shows deep CO absorption with a lack of other absorption features and additional weak H$_2$ and Brγ emission (this object is analysed with more detail in Appendix A). It is very likely that variable accretion is the driving mechanism for these three objects, which were all observed in a bright state. Finally, VVVv480 shows only weak Brγ emission. It is difficult to establish whether this object was observed at a faint or a bright state, so the absence of the evidence for a high accretion rate might be due to observation in quiescence, but by default, we place this YSO in the non-eruptive category. The two epochs of JHK_s photometry have very similar fluxes for this source and therefore provide no information on colour changes.

(v) Eruptive: most objects with an eruptive LC classification show spectroscopic characteristics indicating a high state of accretion. From 17 YSOs, 10 show CO emission, 2 show strong CO absorption, broad H$_2$O absorption bands and a lack of other absorption features (VVVv322 and VVVv721, see Section 5.3 and Appendix A) and 3 show other characteristics that support variable accretion (VVVv118, VVVv800 and VVVv815, see Appendix A). VVVv63 has a doubtful classification given its somewhat low amplitude, $\Delta K_s = 1.44$ mag, and a spectrum with weak Brγ emission
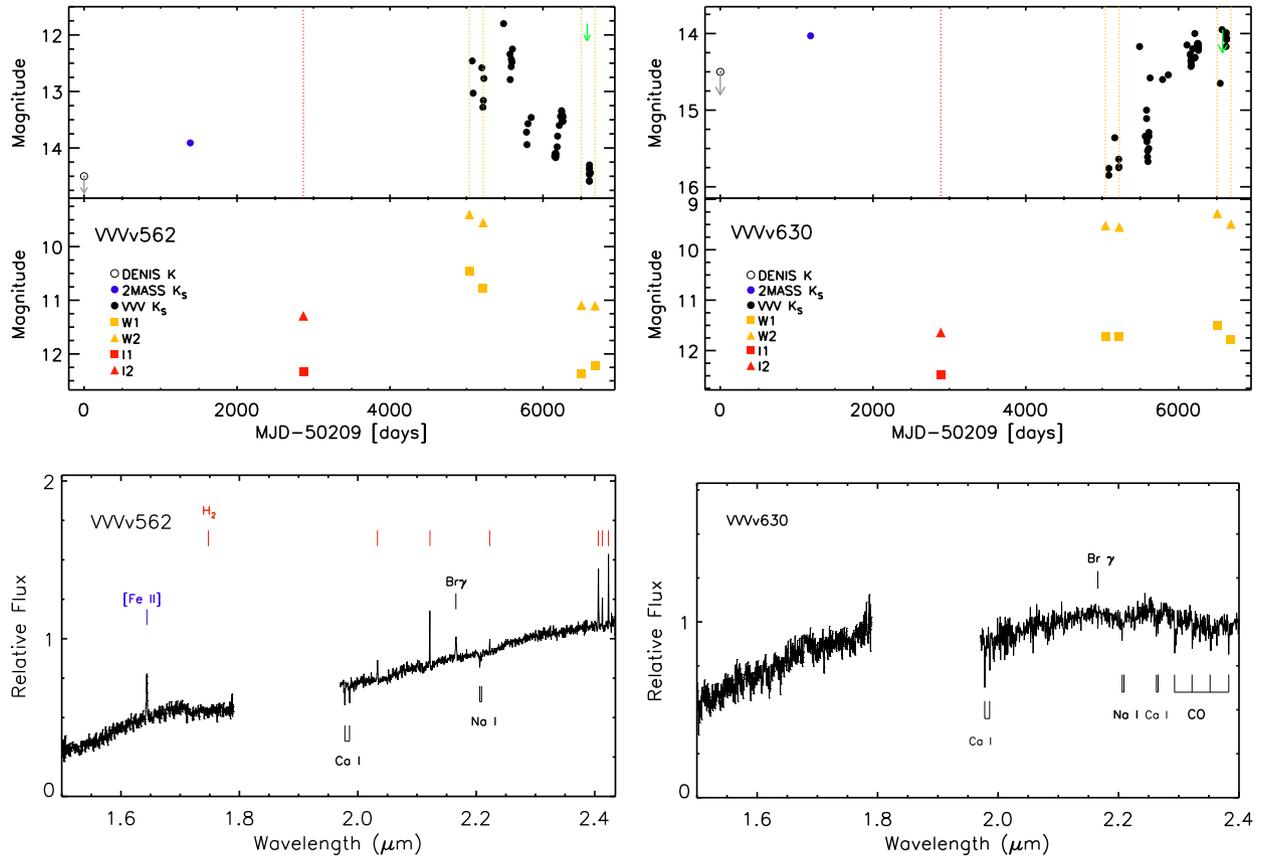
Figure 5. Near- and mid-IR photometry (top) and near-IR spectra (bottom) for objects VVVv562 (left) and VVVv630 (right). Green arrows mark the epoch of spectroscopy. The photometry from different surveys is marked by different symbols which are labelled in each plot. Different emission/absorption lines are also marked in the spectra of the objects. VVVv562 is a fader-observed 2 mag below-peak brightness which we regard as a likely eruptive variable. VVVv630 has an 'eruptive' LC and was observed in a bright state but we consider that extinction is a more likely cause of the variability given the detection of absorption lines from the stellar photosphere, coupled with colour–magnitude variations along the reddening vector in the two epochs of H and K_s photometry.

(but H_2 is clearly present). The accretion luminosity derived for this source does not support a high state of accretion (see Section 5.2) despite observation at an intermediate state. Finally, the variability in VVVv630 is more likely related to extinction events. The near-IR colour comparison shows that the object becomes bluer when brightening, following the reddening line (although this comes from the H versus ($H - K_s$) diagram only). The VVV LC resembles that of an eruptive object, with the spectrum being taken during the suspected bright state. However, the object shows photospheric absorption from CO, Na I and Ca I, with weak Brγ emission. This contradicts the expected behaviour from an eruption. 2MASS data shows that the object had a similar K_s magnitude in the bright state to that seen in 1999 (see Fig. 5). It is possible that VVVv630 went through a dust obscuration event which had cleared at the time of the observations.

5 ANALYSIS AND CLASSIFICATION

From 28 likely YSOs, we have seen that 9 are likely not part of the eruptive variable class (3 short-term, 3 dippers, 1 LPV-YSO and 2 eruptive). The remaining 19 VVV objects show characteristics of eruptive variables from their spectra and/or LC. But to which of the known subclasses of eruptive variables do these objects belong?

In the classical definition, during outburst, FUors show strong CO absorption at 2.29 μm with H_2O absorption sometimes present in their near-IR spectrum (Reipurth & Aspin 2010), whilst EXors

show strong Brγ in emission, with CO bands also in emission and veiling of photospheric features (Lorenzetti et al. 2009). By just considering spectroscopic features, we could easily classify objects in region F of the equivalent width plots discussed above as EXors, with objects falling in region E as FUors. However, the duration of the outbursts is one of the main characteristics used in the classification of eruptive variables. FU Orionis stars show outbursts lasting over >10 yr with a minimum time-scale of several thousand years for repeat eruptions (Scholz, Froebrich & Wood 2013), whilst EXors have recurrent short-lived (<1 yr) outbursts and quiescent periods of 5–10 yr (see e.g. Hartmann & Kenyon 1996; Fedele et al. 2007; Lorenzetti et al. 2009).

A second problem with the classical definition is that it was defined at optical wavelengths. This has struggled to include some intermediate objects and excludes younger protostars which have higher accretion rates but are too deeply embedded in circum-stellar matter to be observed in the optical, such as in the cases of OO Ser, V2775 Ori, HOPS 383 and GM Cha (Hodapp et al. 1996; Kóspál et al. 2007; Persi et al. 2007; Caratti o Garatti et al. 2011; Audard et al. 2014; Safron et al. 2015) or in the GPS sample of Contreras Peña et al. (2014). Thus, this definition might not apply to our VVV objects given the embedded nature of our sample.

Given the spectroscopic characteristics of the known subclasses of eruptive variables, we could assume that the from the 19 objects with characteristics of eruptive variables, those with strong CO absorption (found in region E of Fig. 4) can be classified as FUors,
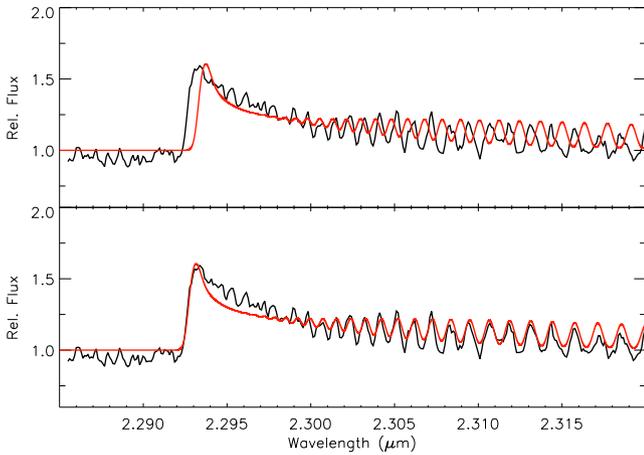
Figure 6. Comparison of the spectrum of VVVv665 (black line) with the CO emission model (red line), without any shifts (top) and after applying the shift derived by the cross-correlation function (bottom).

Table 4. Radial velocities.

Object	v_{LSR} (km s^{-1})	Δv_{LSR} (km s^{-1})	d_{near} (kpc)	d_{far} (kpc)
VVVv25	21.1	5.3	–	10.9
VVVv32	− 28.1	13.5	1.9	7.4
VVVv42	− 49.0	5.5	4.0	6.1
VVVv45	16.4	5.3	–	11.6
VVVv193	− 85.5	18.2	4.5	10.2
VVVv202	− 84.2	5.2	4.4	10.5
VVVv229	− 69.9	5.5	3.8	11.4
VVVv235	− 92.8	5.2	4.8	10.6
VVVv270	− 87.6	12.1	4.6	11.2
VVVv322	− 59.8	5.5	3.8	12.7
VVVv628	− 41.6	5.9	2.4	12.3
VVVv630	− 32.9	5.9	1.9	12.8
VVVv665	− 73.1	5.3	4.0	11.6
VVVv699	− 93.5	5.3	4.9	11.0
VVVv717	− 126.3	5.3	6.1	10.2
VVVv721	− 89.7	5.8	4.9	11.5
VVVv796	− 68.7	5.3	5.1	12.1

whilst emission-line objects (usually found in region F of Fig. 4) are more likely EXors. In the following, we will study whether emission-line objects are found at high states of accretion, as expected, by determining accretion luminosities from Brγ emission. Finally, we will discuss individual examples which demonstrate that the classical definition of eruptive variables fails to classify our VVV sample.

5.1 Radial velocities

We estimate radial velocities of objects showing CO emission/absorption by using the cross-correlation technique described in Marocco et al. (2015), taking the simple CO models which will be explained later in Appendix E, as the radial velocity templates. In every case, the velocities are corrected to take into account the Earth rotation, its motion around the Sun and the motion with respect to the local standard of rest (LSR). The errors on radial velocity are dominated, in most cases, by the error in the wavelength calibration at the order where the CO region is observed. This error is ∼0.4 Å which translates into an error of ∼5.2 km s^{-1} on radial velocity.

These estimates give us a more reliable measurement of the distance to the objects which can help us determine accretion luminosities for some of the emission-line stars. It also helps to identify likely AGB variable stars (see Appendix C).

Note that we are assuming that the CO-emitting region has a similar average velocity to the star. The measurement could be affected if the CO emission/absorption arises from an outflow or wind with a different velocity but in most YSOs, the CO arises in the rotating disc or the stellar photosphere.

In Fig. 6, we show a comparison of the observed spectrum of VVVv665 and that of the CO model before and after deriving the radial velocities for the object. In Table 4, we show the estimated values and errors for the objects where we were able to use this method. In Table 4, we also show the near- and far-kinematics distances estimated using the Galactic rotation model of Brand & Blitz (1993).

5.2 Accretion luminosities

The majority (16/19) of the eruptive VVV objects show emission-line spectra, which is one of the expected characteristics of EXors during outburst. This is not surprising given that only a 2 yr time

interval of VVV data (2010–2012) was used for our variable search (see Paper I), which would favour the detections of EXors over FUors.

From 16 objects with emission-line spectra, 15 show Brγ emission, the exception being VVVv815. This source was observed well below maximum light and the spectrum shows very strong H$_2$ emission, implying the presence of a powerful accretion-driven outflow (see Appendix A). The majority of the emission-line objects fall in region F of Fig. 4 and are thus characterized by the lack of photospheric absorption lines. CO bandhead lines in emission and/or H$_2$ lines in emission are also seen in most of these objects. The objects with Brγ emission are characterized by having broad emission profiles with full width at half-maximum >100 km s^{-1} as expected from magnetospheric accretion (see e.g. Davis et al. 2001).

In order to study whether these objects are in high states of accretion as we expect, we can try to determine the accretion luminosity, L_{acc}, of objects in our sample. The latter is obtained from the known correlation between the Brγ luminosity and the accretion luminosity in YSOs (see Muzerolle et al. 1998; Calvet et al. 2004). Then, in principle, $\dot{M}$ can be derived from

$$L_{acc} = \frac{G M_* \dot{M}}{R_*} \left(1 - \frac{R_*}{R_{in}}\right), \quad (1)$$

(see e.g. Gullbring et al. 1998). However, this last step requires knowledge of stellar (M_*, R_*) and disc parameters (inner disc radius, R_{in}). These parameters can be derived from the stellar spectral type and comparison to PMS evolutionary tracks and isochrones in HR diagrams (see e.g Calvet et al. 2004; Spezzi et al. 2008; Aspin, Beck & Reipurth 2008). This method would yield unreliable mass estimates as the majority of our sample have spectral indices of class I and flat-spectrum sources and evolutionary tracks are unreliable (and so rarely published) for ages below 10^6 yr (see e.g. Siess, Dufour & Forestini 2000). In addition to the long-standing uncertainties about the initial conditions used in such evolutionary calculations, Baraffe et al. (2009, 2012) and others have pointed out the very concept of a stellar birthline is undermined by episodic accretion because each star is likely to have a different accretion history.

Table 5. Accretion luminosity from luminosity of the Brγ line. The second column refers to the approximate state (from the LC) at which the spectrum was taken.

Object	STATE	A_{K_s} (mag)	D (kpc)	L_{acc}[a] (L$_\odot$)	L_{acc}[b] (L$_\odot$)
Eruptive					
VVVv20	bright	2.3	2.5[c]	3.8	15.1
VVVv32	mid-point	0.9	1.9[d]	0.9	2.2
VVVv94	bright	2.5	3.5[e]	11.1	68.2
VVVv118	faint	0.5	2.2[c]	0.1	0.1
VVVv193	bright	2.5	4.5[d]	3.2	11.9
VVVv270	bright	2.5	4.6[d]	7.3	38.1
VVVv374	bright	2.5	2.9[e]	5.3	24
VVVv452	bright	1.4	2.8[c]	2.5	8.4
VVVv473	mid-point?	2.5	3.7[e]	0.6	1.1
VVVv562	faint	1.4	2.9[e]	0.4	0.6
VVVv631	bright	1.2	2.3[e]	2.5	8.4
VVVv662	bright	2.5	3.1[e]	3.2	11.7
VVVv665	bright	2.5	4.3[d]	6.6	33.2
VVVv699	bright?	32[f]	4.9[d]	7.4	38.9
VVVv699	bright?	2.5	4.9[d]	3.7	14.5
VVVv800	mid-point?	2.4	1.4[e]	0.7	1.4
Non-eruptive					
VVVv63	mid-point	1.7	3.5[e]	0.6	1.1
VVVv65	faint	1.9	3.5[e]	0.8	1.8
VVVv405	faint	2.5	2.3[e]	0.2	0.2
VVVv480	faint	0	3.7[e]	0.2	0.3
VVVv625	bright?	2.5	2.3[e]	1.5	4.2
VVVv628	mid-point	1.1	2.3[d]	0.1	0.1
VVVv632	bright	0.3	2.5[e]	0.6	1.0

[a]from Calvet et al. (2004).
[b]from Muzerolle et al. (1998).
[c]Distance from SED fit.
[d]Distance from radial velocity.
[e]Distance from d_{SFR}.
[f]A_v from line ratios, see Appendix A.

Given the above, $\dot{M}$ can only be estimated by making many assumptions on the star+disc parameters, thus yielding unreliable results. We have shown in Paper I that some of our high-amplitude sample includes some PMS eclipsing binaries. Some of these have spectral indices of flat spectrum sources. Follow-up of these systems could provide information on radii and masses for these younger sources, provided the contribution of scattered light can be accounted for.

For the accretion luminosities, we first need to determine the flux of the Brγ line. We note that several assumptions are made during the derivation of this parameter. First, we do not have K_s photometry from the time of the spectroscopic observations. Thus, we assume K_s as the magnitude of the closest epoch from the VVV photometry. From this, we obtain the continuum level, F_λ, for the Brγ line at 2.1659 μm. In addition, we correct this value for the extinction along the line of sight to the source. This introduces further uncertainties given the difficulties in measuring accurate values of extinction towards class I YSOs. These objects have substantial contributions from scattered light that may cause the reddening and hence the line luminosity, to be underestimated (see e.g. Muzerolle et al. 1998; Connelley & Greene 2010). We measure A_{K_s} by dereddening the sources to the classical T Tauri locus in the $J - H$ versus $H - K$ two-colour diagram (see Fig. 1) and we present this in Table 5 as A_v using the extinction law of Rieke & Lebofsky (1985). For the

nine sources that were not detected in the J filter, we adopt a colour $J - H = 3.5$ or $A_v = 23$ and deredden them to the red end of the T Tauri locus. This is consistent with the red $H - K$ colours of these systems and the upper limits on $J - H$, which are typically between 2 and 4 mag.

The line flux, $F_{Br\gamma}$, is then estimated from

$$F_{Br\gamma} = F_\lambda \times EW \times 10^{0.4A_\lambda}, \qquad (2)$$

with A_λ from the above values. The line luminosity, $L_{Br\gamma}$, depends on the distance to the object. In our case, we have distances from (1) the distance to the nearby SFRs at the location of the VVV objects (d_{SFR}), (2) kinematic distances estimated from radial velocities and (3) results from the SED fitting tool (see Appendix D). For the calculation of $L_{Br\gamma}$, we use the best estimate available for the object: in order of preference, we use the kinematic distance (d_{near}), then d_{SFR}, then the distance from SED fits.

Finally, the accretion luminosity is calculated from the L_{acc}–$L_{Br\gamma}$ relations of Calvet et al. (2004) (their equation 3) and of Muzerolle et al. (1998) (their equation 2). Calvet et al. (2004) derive L_{acc} from UV excess for a sample of intermediate-mass T Tauri stars (1.5–4 M$_\odot$), whilst Muzerolle et al. (1998) use a similar method for a sample of lower mass classical T Tauri stars. Thus, the former relation is likely to be more suitable for objects in our sample. Table 5 shows the values for L_{acc} obtained from both relations.

We can compare our results to the published luminosities for three different sample sets of class I and class II YSOs: (A) the intermediate-mass class II sample of Calvet et al. (2004) and the low-mass class II sample of Muzerolle et al. (1998); (B) low-mass class I and class II YSOs found in the literature. These are class I objects in Muzerolle et al. (1998), class I and class II YSOs in the Chamaeleon I and Chamaeleon II clouds (Antoniucci et al. 2011) and class I YSOs HH26 IRS, HH34 IRS and HH46 IRS (Antoniucci et al. 2008); (C) finally, we compare to eruptive variables EX Lupi (2008 outburst; Aspin et al. 2010) and V1647 Ori (in quiescence and outburst, 2006–2008; Acosta-Pulido et al. 2007).

We note that we could try to compare L_{acc} for these samples directly. However, the results of this comparison would strongly depend on the relation used in estimating L_{acc}. Moreover, L_{acc} is derived independently (from UV excess) only in the class II samples of Calvet et al. (2004) and Muzerolle et al. (1998). The published accretion luminosities of objects in (B) and (C) are calculated from line luminosities using either the Calvet et al. or the Muzerolle et al. relations.

Instead, we compare Brγ luminosities which, given the correlation with L_{acc}, gives us a measure of the accretion state of our sample compared with that of typical class I and class II YSOs. The comparison is shown in Fig. 7. From the figure, we first notice that VVV objects which are classified as eruptive and observed during bright states have higher Brγ luminosities than the remainder of the sample. Brγ luminosities from bright eruptive VVV YSOs are also higher than the majority of intermediate-mass class II YSO as well as low-mass class I and class II YSOs. Unfortunately, we are not able to find published Brγ luminosities for intermediate-mass class I YSOs.

When comparing to known eruptive variables, we find that VVV objects at bright states have higher $L_{Br\gamma}$ than that of EX Lupi (the prototype of EXors) during its 2008 outburst. The $L_{Br\gamma}$ of VVV sources at bright states is comparable to that of V1647 Ori during outburst. The latter has substantial extinction ($A_v \sim 10$; Muzerolle et al. 2005) and a low to moderate accretion luminosity, L_{acc}, during outburst (12 L$_\odot$; Aspin et al. 2009, determined from the Muzerolle et al. relation), which is similar to some sources in our sample (see
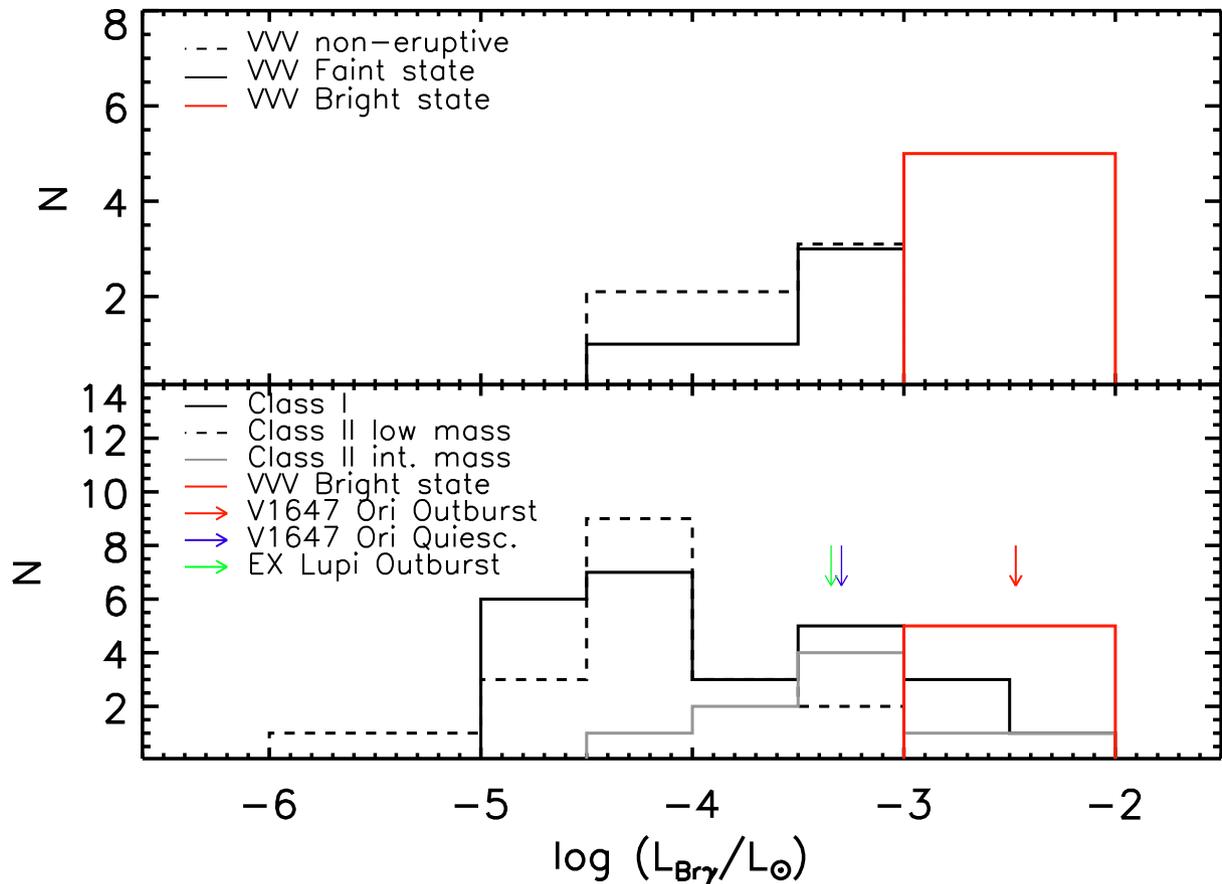
Figure 7. Histogram of Brγ luminosities for VVV objects and a sample of YSOs found in the literature (top) Comparison of eruptive VVV objects observed at bright state (red solid line) with eruptive objects observed at faint states (black solid line) and non-eruptive VVV YSOs (dashed black line). (bottom) Comparison of VVV bright objects (solid red line) with the intermediate-mass class II YSO sample of Calvet et al. (2004) (solid grey line) and the low-mass class II YSO sample of Muzerolle et al. (1998) (dashed black line), low-mass class I YSOs found in the literature (solid black line). We also compare with eruptive variables EX Lupi during outburst (green arrow) and V1647 Ori during quiescence (blue arrow) and outburst (red arrow).

Table 5). This is a further evidence to support our contention that we have identified embedded eruptive variable YSOs similar to the small number of such objects found previously, though a little more luminous on average.

We can estimate a range of values of accretion rates for eruptive objects observed at bright states (open red circles in Fig. 7), by adopting plausible values of mass and radius, $M_* = 3\ M_\odot$, $R_* = 5\ R_\odot$ and assuming $R_{in} \gg R_*$. We stress that this is done for a simple comparison with expected rates in eruptive variables and should not be considered as reliable results. Using the accretion luminosities estimated from the Calvet et al. (2004) relation yields $10^{-6.8} < \dot{M} < 10^{-6.2}\ M_\odot\ yr^{-1}$. Even allowing for a possible order of magnitude underestimate, these values would be considered at the lower end of accretion rates expected in FUor outbursts (10^{-3}–$10^{-6}\ M_\odot\ yr^{-1}$) and more in line with those seen in nearby low-mass EXor outbursts (10^{-6}–$10^{-8}\ M_\odot\ yr^{-1}$; see Audard et al. 2014). This may suggest that the Brγ emitters in our sample have lower accretion rates than FUors, which is perhaps to be expected if FUors typically quench Brγ emission above a certain accretion rate. (We note that our sample does include three sources with FUor-like spectra and no Brγ emission.) Nevertheless, the accretion rates of the Brγ emitters are higher than those estimated from SED fitting (Appendix D). This may be attributed either to the fact that SED fitting used 2010 photometry, an epoch were most of the eruptive

objects are found at quiescent states, whereas the spectra were taken at epochs close to maximum brightness, thus at higher states of accretion. Alternatively, the difference might be due to the fact that the SED fitting tool was not designed to model YSOs undergoing an eruption (see also the discussion about the reliability of the estimated parameters in Appendix D).

We note that values of L_{acc} in our sample tend to be lower than the bolometric luminosities (L_{bol}) derived from SED fits (by ~1 order of magnitude, specially when comparing the values obtained from the Muzerolle et al. relation, see Appendix D). This is somewhat surprising as we might expect that the accretion luminosity dominates the total luminosity in eruptive variables: it is often assumed that in low-mass class I objects $L_{acc} = L_{bol}$ (see e.g Enoch et al. 2009; Evans et al. 2009). However, Muzerolle et al. (1998) find that low-mass class I YSOs in their sample show $L_{acc} \sim 0.1 L_{bol}$. We also note that our sample are most likely intermediate-mass objects and the central star is expected to contribute an increasing fraction of the total luminosity of the system towards higher masses (Calvet et al. 1991); on average, $L_{acc} \propto M^2$ (Calvet et al. 2004). Although, again this comparison might be affected by the unreliability of the SED fitting tool results (as mentioned above).

In summary, the key result of the accretion luminosity estimates is that eruptive variables in a bright state have higher accretion rates than eruptive variables observed in quiescence.

5.3 The classification problem

We are confident that the 16 emission-line stars described in Section 5.2 are likely to be eruptive variables. However, all of them show a mixture of characteristics between those of EXors and FUors.

Aside from the 16 emission line stars, a further 3 stars (VVVv322, VVVv721 and VVVv717) are classified as eruptive variables. These show CO 2.29 μm absorption which appears stronger than expected from a stellar photosphere, with the additional characteristic of not displaying any other features which could be associated with a stellar photosphere. In two cases (VVVv322, VVVv717), we do in fact see emission lines of H_2 and/or Brγ (see Table 3, Fig. 10 and Appendix A) In two sources (VVVv322, VVVv721), we also observe absorption from H_2O. However, only VVVv721 shows an outburst duration that could place it under the FUor category, i.e. longer than the 5 yr time baseline of VVV. For these three objects, we cannot measure an accretion rate but we are confident that they are eruptive variables. However, two of the three show a mixture of characteristics between those of EXors and FUors.

To illustrate the difficulties found in classifying these likely eruptive variable stars, we will discuss two objects from the previous sample, one of the emission-line objects and one object showing strong CO absorption. We present similar discussions of several other objects with mixed characteristics in Appendix A. They include one source with CO in emission but H_2O in absorption (VVVv631), one with a FUor-like spectrum but a quasi-periodic LC (VVVv717), one with a somewhat EXor-like spectrum but a longer outburst duration and H_2 emission (VVVv699) and one (VVVv118) with FUor-like H_2O absorption but very brief, EXor-like outbursts. Appendix A also includes descriptions of two eruptive YSOs with neither EXor-like nor FUor-like spectra (VVVv800 and VVVv815).

5.3.1 VVVv270

This object began an outburst in late 2011 and remains bright in the most recent data from 2015. The amplitude is $\Delta K_s \sim 3.8$ mag (see Fig. 8). This star has not been detected in 2MASS nor DENIS, which is to be expected for the magnitude of the star prior to this current outburst ($K_s \sim 16$ mag). The source brightened smoothly from late 2011 to 2014, remaining at similar brightness in 2015. This slow rise resembles what has been observed in the classical FUor V1515 Cyg and the likely FUor object VVVv721 (Appendix A). However, its spectrum shows strong emission from Brγ, CO, Na I and H_2, which is more expected for EXors in outburst rather than FUors. The accretion luminosity of VVVv270 is amongst the highest in the sample (see Table 5), which supports the object being in a high state of accretion.

The object is associated with several star formation tracers within 5 arcmin, such as IR sources (Robitaille et al. 2008), intrinsically red objects and IRDCs identified with *Spitzer* from Peretto & Fuller (2009). The only distance information from SIMBAD sources within 5 arcmin arises from the methanol maser Caswell CH3OH 333.931−00.135, with a radial velocity of $v_{LSR} = -36.8$ km s^{-1} (Ellingsen et al. 1996). However, this object is located 222 arcsec from VVVv270 and the radial velocity of VVVv270 (-87.6 ± 10.9 km s^{-1}) is too different for there to be a physical association. Our estimate from the VVV radial velocity places the object at $d \sim 4.6$ kpc.

5.3.2 VVVv322

The projected location of this object is found close to several indicators of star formation as revealed by SIMBAD (see Fig. 9). These include molecular clouds, IRDCs, likely YSOs (as determined by their mid-IR colours by Robitaille et al. 2008) and most interestingly, several X-ray sources which could be associated with the young massive cluster Westerlund 1, which is located at $d = 3.55 \pm 0.17$ kpc and has an age of 4–5 Myr (Clark et al. 2005). The projected location of VVVv322 is 651 arcsec from the centre of the massive cluster. The object is classified as being associated with SFRs in Paper I, although whether this association is with Westerlund 1 is not clear, owing to the separation on the sky. However, we note that the near kinematic distance to the object ($d = 3.8$ kpc, see Table 4), is remarkably similar to the distance of the cluster. Therefore, the association seems likely.

The near-IR colours of the star show an $(H - K)$ excess which can be attributed to warm circum-stellar material, placing it to the right of the reddened T Tauri locus in Fig. 1. The SED of the star is constructed using *Spitzer* photometry (due to non-detection in *WISE*) and the spectral index is $\alpha = 0.92$, corresponding to a class I YSO. The *Spitzer* and VVV measurements are not contemporaneous, but the star appears to have been at quiescence prior to the 2011 outburst, giving some confidence that α is estimated correctly.

The LC of VVVv322 (Fig. 9) shows the object was in a quiescent state at $K_s \sim 15.5$ mag before going into outburst between the end of the 2011 coverage and the beginning of the 2012 campaign. The object had apparently been at this faint state for >10 yr given that it is not detected by DENIS nor 2MASS. The brightness of the object is already declining by 2013. Due to the lack of complete coverage, we cannot be certain of the amplitude of the outburst but it is likely to be $\Delta K_s > 2.5$ mag. Mid-IR photometry from the GLIMPSE I (Benjamin et al. 2003) and DEEP GLIMPSE (Churchwell et al. 2009) surveys also shows a large change with 1.8 and 1.4 mag at 3.6 and 4.5 μm, respectively. The DEEP GLIMPSE data was taken on 2012 October, which would place it close to the maximum brightness of VVVv322. Given that the object appears to have been at a quiescent state for a long time prior to 2011, we can then consider the GLIMPSE I measurements as being pre-outburst data. The mid-IR change is in agreement with the expected change from variable accretion in protostars (see e.g. Fischer et al. 2012; Scholz et al. 2013).

The observed K_s LC during 2013 implies a decline rate of ~1.57 mag yr^{-1}. This rate implies that the duration of the outburst would not be longer than approximately 3 yr. VVV photometry from 2014 July/August shows that this trend continued, returning the object to a brightness close to the quiescent state of 2010. However, the 2015 photometry shows that the rate of decline has slowed in the most recent data.

The spectrum for this object was obtained in 2013 April when it was slightly below maximum brightness, based on inspection of the LC. The spectrum shows the presence of strong H_2O absorption bands at 1.3–1.4, 1.7–2, 2.3–2.5 μm and CO absorption at 2.29 μm. In addition, the 1–0 $S(1)$ H_2 line at 2.12 μm is seen weakly in emission. The spectrum lacks any other absorption features that could be associated with a stellar photosphere (see Fig. 10).

The evidence presented above supports the scenario of VVVv322 being an eruptive YSO. However, the classification of this object within the known classes of eruptive variables seems to be uncertain. The 2013 spectrum resembles that of FU Orionis stars during periods of high accretion, (see e.g. V900 Mon; Reipurth, Aspin &
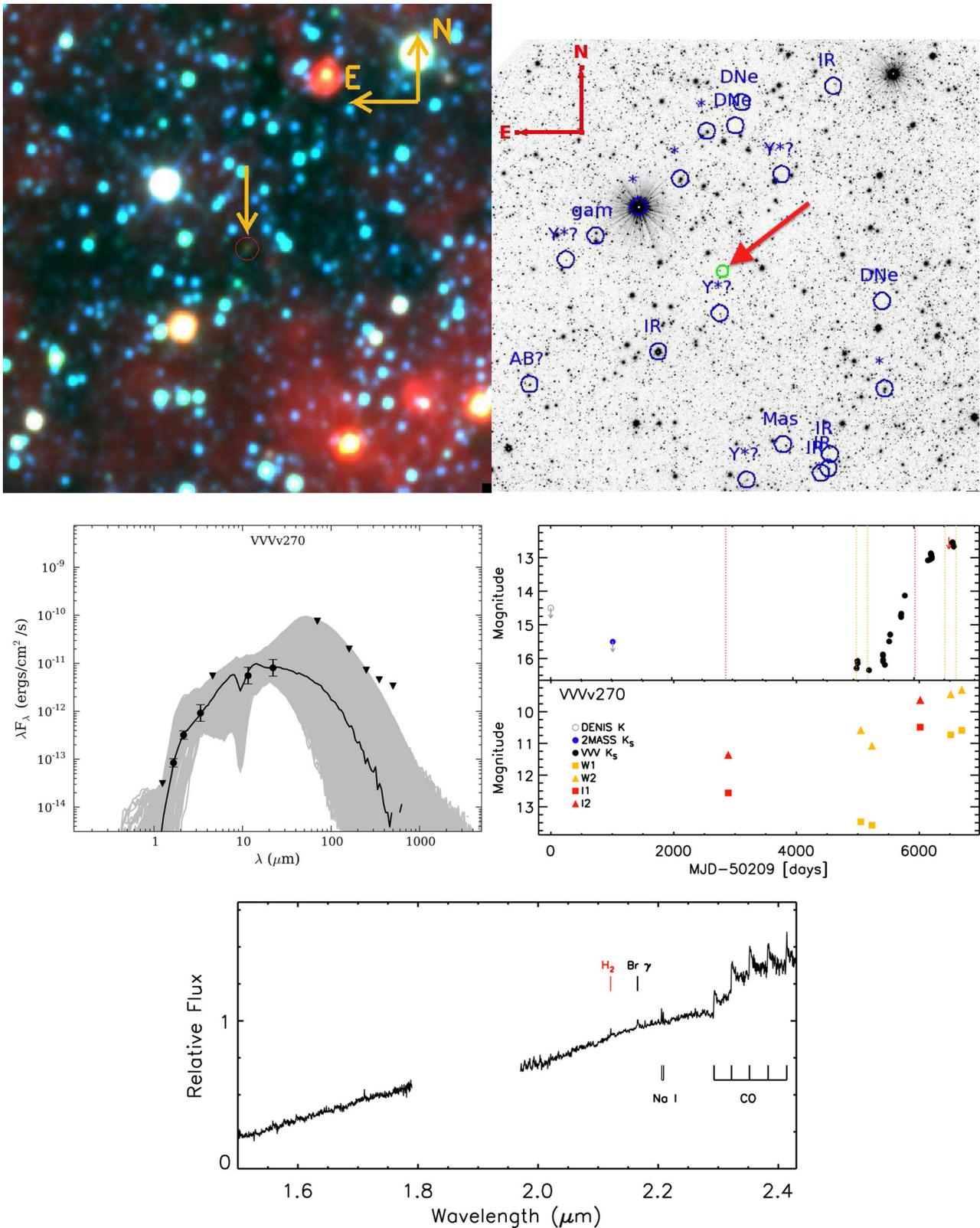
**Figure 8.** (top left) False colour *WISE* image (blue = 3.5 μm, green = 4.6 μm, red = 12 μm) of a 10 arcmin× 10 arcmin area centred on VVVv270. The location of the object is marked by the arrow. (top right) K_s image of a 10 arcmin×10 arcmin area centred on VVVv270. The location of the object is marked by the red arrow and green circle. In addition, blue circles and labels mark objects found in a SIMBAD query with a 5 arcmin radius. (medium left) SED of VVVv270 along with Robitaille et al. (2007) YSO models that fulfil the criteria of $\chi^2 - \chi^2_{\rm best} < 3N$, with N the number of data points used to generate the fits. This image is generated by the fitting tool. (medium right) Near- and mid-IR photometry of VVVv270. Data arising from different surveys are marked by different symbols which are labelled in the figure. The red arrow marks the approximate date of the spectroscopic follow-up. (bottom) FIRE spectrum of VVV270. The spectroscopic features found for this object are marked in the graph.
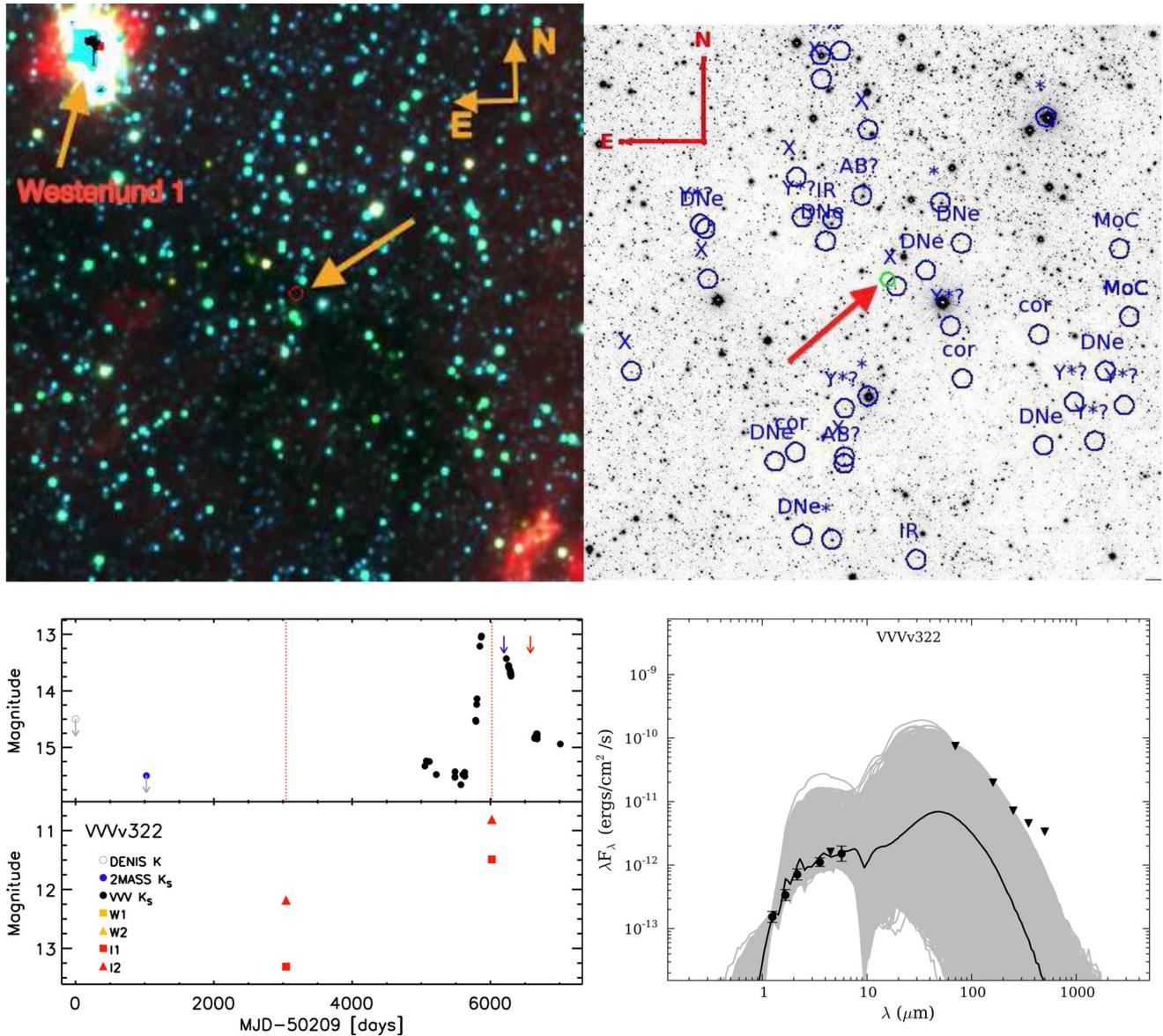
Figure 9. (top left) False colour *WISE* image (blue = 3.5 µm, green = 4.6 µm, red = 12 µm) of a 20 arcmin×20 arcmin area centred on VVVv322. The location of the object is marked by the arrow. The SFR Westerlund 1 is also shown in the image. (top right) K_s image of a 10 arcmin×10 arcmin area centred on VVVv322. The location of the object is marked by the red arrow and the green circle. In addition, blue circles and labels mark objects found in a SIMBAD query with a 5 arcmin radius. (botton, left) Near- and mid-IR photometry of VVVv322. The approximate dates of spectroscopic follow-up are marked by blue (2013) and red(2014) arrows. (bottom, right) SED of VVVv322 along with Robitaille et al. (2007) YSO models that fulfil the criteria of $\chi^2 - \chi^2_{best} < 3N$, with N the number of data points used to generate the fits. This image is generated by the fitting tool.

Herbig 2012) and it would agree with the fact that the star was observed at a point close to maximum brightness. However, the duration of the outburst would seem to be much shorter than expected for FU Orionis stars, but longer than for EXors. In this sense, this object resembles more recently discovered objects which display mixed characteristics of eruptive variable classes (see e.g. V1647 Ori, V2775 Ori; Fedele et al. 2007; Caratti o Garatti et al. 2011).

A second spectrum was taken in 2014,[2] which allows us to note some interesting points about this source. The 2014 May spectrum was taken at a time where the object has apparently faded by about

1.3 mag. By this time the H_2O and CO features seem to have weakened (see Fig. 10) but the H_2 line at 2.12 µm has become stronger. The spectrum, as in 2013, does not show any apparent photospheric features

We note that the weakening of the H_2O and CO features by 2014 agrees with the fact that the luminosity of the star had faded by this epoch. The lack of Brγ emission in FU Orionis objects has been attributed to the fact that for high accretion rates ($\dot{M} > 10^{-5}$ $M_\odot$ yr^{-1}), there is a breakdown in the magnetospheric accretion model (see e.g. Fischer et al. 2012). It would be very interesting to see that with VVVv322 returning to a quiescent state, the star would show absorption features arising from a stellar photosphere rather than the disc and Brγ returning to emission in the spectrum of the object.

---

[2] Two other objects, VVVv815 and VVVv699, have repeated spectroscopy. Their characteristics are presented in Appendix A.
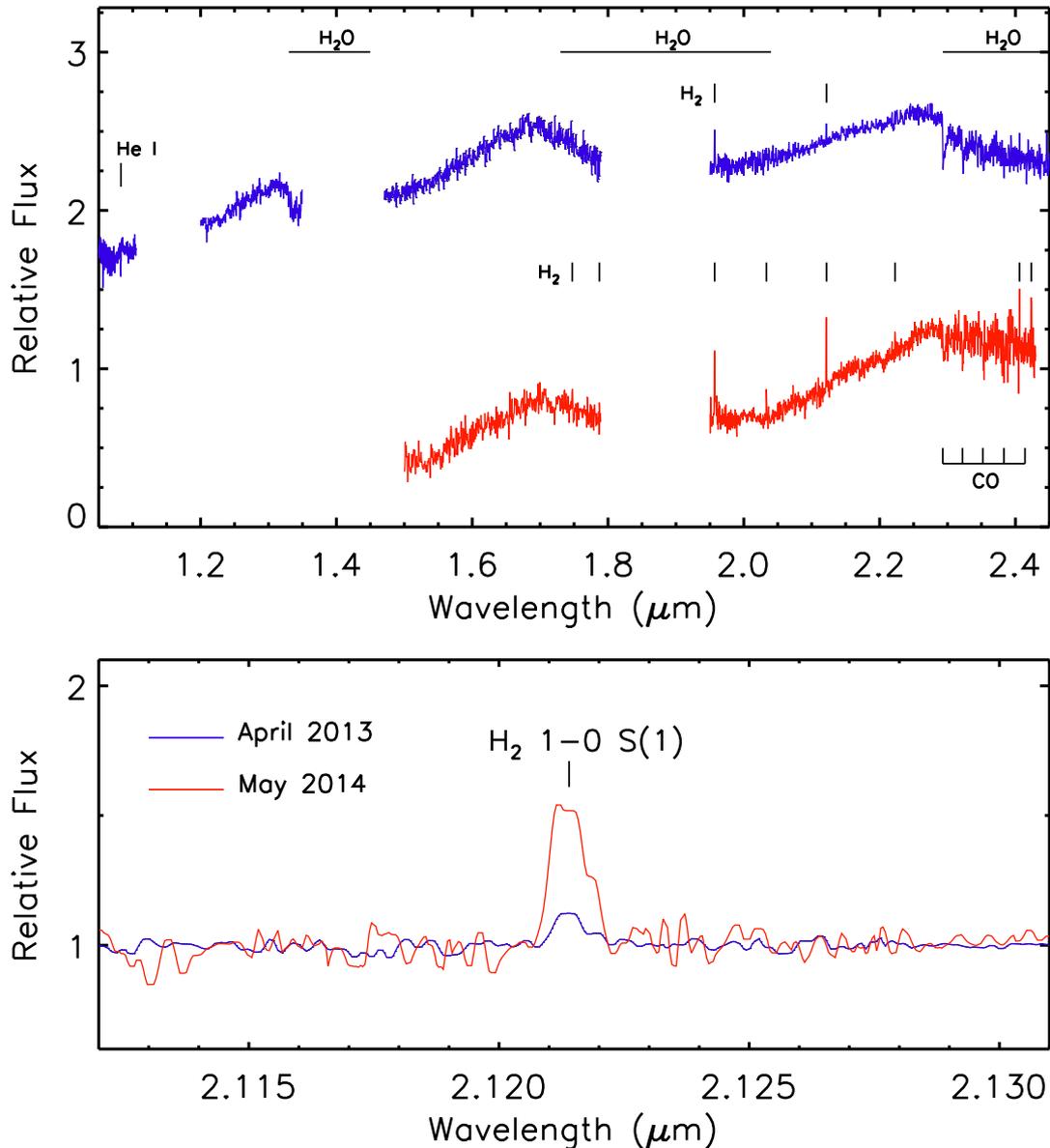
Figure 10. (top) Graph comparing the 2013 (blue) and 2014 (red) FIRE spectra of VVVv322, where we mark the observed absorption features of H_2O and CO, along with emission lines from H_2. (bottom) 2013 and 2014 observations in the region 2.10–2.13 μm comparing the 2.12 μm 1–0 $S(1)$ H_2 emission line.

The H_2 2.12 μm emission feature has become stronger between 2013 and 2014 (see Fig. 10), with the equivalent width increasing by a factor of 3 to 4. The emission does not appear to be spatially extended at either epoch. The presence of this feature could be associated with shocks from molecular outflows linked to this particular outburst event. While this is not certain, continuous monitoring and high-resolution imaging could help clarify this picture. A direct link between an outburst and an outflow has been observed in V2494 Cyg (Magakian et al. 2013).

5.4 Final remarks on classification

In the previous sections, we have shown that most spectra of our young eruptive variables fail the classical FUor/EXor classification. In fact, only one object in our sample would fall into the classical FUor definition, VVVv721, which shows the characteristic CO ab-

sorption as well as a long-lasting outburst, at least extending beyond the coverage from VVV, of these objects.

The majority of the remaining YSOs show characteristics which are more commonly found in EXors, such as an emission-line spectrum. However, H_2 emission is common in our objects, and in some cases, [Fe II] emission is also present in their spectra. These features were not observed in the sample of EXors studied by Lorenzetti et al. (2009). In addition, the duration of the outburst is longer than expected from this subclass, but also shorter than the long-lasting outburst of classical FUors. Both VVVv322 and VVVv717, two of the three objects that show strong, FUor-like, CO absorption, have LC properties which are different to classical FUors.

The different characteristics of our sample to that of the known classes of eruptive variables could be explained by the fact that the majority of our sample is optically invisible and found at early evolutionary stages. This is certainly true when we compare to classical

EXor events (usually associated with instabilities in discs of class II YSOs). In addition, the classical FUors are often described as being at the boundary between T Tauri stars and protostars with an envelope (see e.g. Audard et al. 2014), comparable to flat-spectrum YSOs. Inspection of their SEDs reveals that none of the classical, optically visible FUors have steeply rising class I SEDs (see Gramajo, Rodón & Gómez 2014).

Considering the arguments presented above, we are confident that these 19 objects are new additions to the eruptive variable class, with four more objects where it is unclear if variable accretion is responsible for the observed variability. Of the 19 eruptive sources, 16 are classified as class I and 3 as flat spectrum sources, from their value of α. 17/19 are optically very faint, defined here by non-detection in the VVV Z-band images.

The characteristics of our sample are in line with what has been observed in a small but increasing number of new members of the eruptive variable subclass. For example, V1647 Ori went into outburst in 2003 and showed a near-IR spectrum with strong Brγ and CO emission (see e.g. Ninan et al. 2013). This object returned to quiescence after 2 yr and then underwent a second outburst in 2008 (Aspin et al. 2009), but now showing CO weakly in absorption at 2.29 μm. OO ser (Hodapp et al. 2012) is a deeply embedded object which shows a featureless near-IR spectrum and an outburst duration of less than 10 yr. V2775 Ori (Caratti o Garatti et al. 2011) went into outburst in 2011 and its near-IR spectrum shows the characteristic H_2O and CO absorption of FUors, but it is unclear if the outburst duration is comparable to that for FUor objects. V723 Car is a highly embedded class I object which went into outburst between 1999 and 2003 reaching peak magnitude of $K = 12.9$ mag. The LC of the object after the outburst shows an erratic behaviour with $\Delta K = 2$ mag. The near-IR spectrum of V723 Car shows H_2, Brγ and CO emission. Tapia et al. (2015) argue that these characteristics make V723 Car different from EXors and FUors. V1180 Cas is a flat-spectrum YSO which shows an outburst duration that is between that of both EXors and FUors (Kun et al. 2011) and shows an emission-line spectrum during outburst (Antoniucci et al. 2014). V512 Per is a class I object which went into outburst in 1990 (Eislöffel et al. 1991) and has remained close to the maximum brightness ever since (Hodapp & Chini 2014), resembling the duration of FUor outbursts. However, the object shows strong CO emission during outburst (Eislöffel et al. 1991) and drives an H_2 molecular outflow (Hodapp & Chini 2014). V2492 Cyg is a class I YSO which went into outburst in 2010 and shows an emission-line spectrum with an outburst duration of >3 yr (Covey et al. 2011; Kóspál et al. 2013). Covey et al. (2011) point out that this object differs from FUors and EXors and resembles the characteristics of V1647 Ori.

A label of some sort is likely to be useful to categorize these eruptive YSOs which show a mixture of characteristics of FUors and EXors. We propose 'MNors' (pronounced 'emnors') given the resemblance with V1647 Ori, the illuminating star of the McNeil's Nebula (McNeil's Nebular Object). Given the characteristics of our sample and their similarities with some of the recent discoveries from the literature, MNors could be considered as objects which: (1) have SEDs of class I or flat-spectrum sources, (2) show outburst durations >1.5 yr but shorter than those usually associated with FUors, (3) show spectroscopic characteristics of eruptive variables, i.e. CO emission, absorption and (4) usually have 2.12 μm H_2 emission, most likely due to a molecular outflow. As exceptions to item (3), sources lacking CO emission or absorption may still be MNors, e.g. if the spectrum is taken in quiescence or there is strong veiling of the photosphere and the innermost parts of the disc

(e.g. see the individual discussions of VVVv800 and VVVv815 in Appendix A).

Our definition of the MNor subclass includes sources with diverse spectroscopic properties. The classification is therefore provisional, pending further study. The most likely scenario is one in which the known FUor, EXor and MNor subclasses are not different types of objects but are instead different representations of the same phenomena, i.e. episodic accretion. For example, Vorobyov & Basu (2015) show that their disc fragmentation models, one of the mechanisms which is invoked to explain episodic accretion, can produce isolated luminosity bursts, similar to FUors, or clustered bursts, i.e. a succession of closely packed bursts, similar to EXors and the majority of the objects in our sample.

The 19 new episodic variables approximately double the number of the spectroscopically verified eruptive variable YSOs known so far. These new additions increase the number of embedded members of the class by a large factor.

Table 6 shows the classification of the objects according to their LC, as well as their spectroscopic characteristics.

6 SUMMARY AND CONCLUSIONS

We have presented intermediate resolution IR spectra of 37 VVV high-amplitude variable stars, 18 of which have eruptive LC classification from Paper I. The observed systems generally have class I or flat spectrum SEDs, typical of the full VVV photometric sample of YSOs. In the following, we summarize the main points of our work.

(i) From the sample, nine stars show characteristics which indicate that they are AGB stars or novae rather than YSOs (see Appendix C). Amongst the 28 YSOs, the incidence of Brγ emission is high, as in normal YSOs, but the incidences of CO emission and especially H_2 are higher than in normal embedded YSOs. The locations of the YSOs in the equivalent width diagrams of Connelley & Greene (2010) are, in general, very different from those of normal YSOs, especially for VVV sources followed up during a bright state.

(ii) Three YSOs show the characteristic strong CO absorption and lack of photospheric features which are associated with FUors, though only one of these has an outburst of sufficient duration to be considered a likely classical FUor.

(iii) Of the 25 other YSOs, we classify 16 as likely eruptive variables. These show emission-line spectra with Brγ, CO and/or H_2 almost always present. The H_2 emission-line ratios are consistent with shock-excited emission from molecular outflows. The latter is not observed in classical EXors (see e.g. Lorenzetti et al. 2009). They have LC which are characterized by large variations ($\Delta K_s > 1.5$ mag), with apparent durations of the bright state of 1–5 yr, which is longer than the characteristic time-scale of EXors (Lorenzetti et al. 2012). Of the 16 systems, 12 have eruptive LC classifications, 1 is a fader, and 3 are LPVs. We note that the periodicity in these three is not perfect: such objects show short-term scatter and the sparse sampling of the LC prevents precise period determination. As noted in Paper I, some of the eruptive variables show repetitive bursts (a quasi-periodic behaviour), so the distinction between these provisional LC classifications is not clear cut.

(iv) Three objects show outburst durations that extend over the 5 yr period covered by VVV, which would be expected if these are FUor-like outbursts. However, for two of these, the near-IR spectra do not show the usual CO and H_2O absorption characteristic of the

Table 6. ΔK_s, time-scale of the variability and main features observed in the spectra of VVV objects from our sample. The last column provides a likely classification as eruptive, non-eruptive or non-YSO. For eruptive YSOs the time-scale relates to the approximate duration of the outburst (marked as Δt_{out}). In non-eruptive YSOs, the time-scale corresponds to the duration of the observed large amplitude changes; in some cases, these could correspond to outburst durations such as in objects marked as non-eruptive?. Finally, for non-YSOs, we provide the periods for AGB stars and the approximate duration of what could be eruptions in novae.

Object	ΔK_s	Variability	Spectrum	Classification
		YSO-eruptive		
VVVv20	1.71	$\Delta t_{out} \sim 2.5$ yr	Brγ, CO, Na I, H$_2$ emission	Eruptive, MNor
VVVv32	2.50	$\Delta t_{out} \sim 3.3$ yr, periodic?	Brγ, CO emission	Eruptive, MNor
VVVv94	1.91	$\Delta t_{out} > 3$ yr	Brγ, CO, H$_2$ emission	Eruptive, MNor
VVVv118	4.24	$\Delta t_{out} < 150$ d, repetitive	Brγ emission, H$_2$O absorption(?)	Eruptive, EXor(MNor?)
VVVv193	1.26	$\Delta t_{out} > 2$ yr?	Brγ, CO, H$_2$ emission	Eruptive, MNor
VVVv270	3.81	$\Delta t_{out} > 3.5$ yr, ongoing	Brγ, CO, Na I, H$_2$ emission	Eruptive, MNor
VVVv322	2.63	$\Delta t_{out} \sim 3.5$ yr	CO, H$_2$O absorption	Eruptive, MNor
VVVv374	2.41	$\Delta t_{out} > 3.5$ yr, ongoing?	Brγ, CO, Na I, H$_2$ emission	Eruptive, MNor
VVVv452	2.46	$\Delta t_{out} \sim 2.2$ yr	Brγ, CO, H$_2$ emission	Eruptive, MNor
VVVv473	1.50	$\Delta t_{out} \sim 275$ d, periodic	Brγ, CO, H$_2$ emission	Eruptive, MNor
VVVv562	2.79	$\Delta t_{out} > 2$ yr?	Brγ, H$_2$ emission. Na I absorption	Eruptive, MNor
VVVv631	2.64	$\Delta t_{out} > 4$ yr, ongoing?	Brγ, CO, Na I emission. H$_2$O absorption	Eruptive, MNor
VVVv662	1.83	$\Delta t_{out} > 2$ yr	Brγ, CO, Na I, H$_2$ emission	Eruptive, MNor
VVVv665	1.63	$\Delta t_{out} > 2$ yr	Brγ, CO, Na I, H$_2$ emission	Eruptive, MNor
VVVv699	2.28	$\Delta t_{out} > 4$ yr, ongoing	Brγ, CO, Na I, H$_2$ emission	Eruptive, MNor
VVVv717	2.47	$\Delta t_{out} > 2$ yr, periodic?	CO absorption	Eruptive, MNor
VVVv721	1.86	$\Delta t_{out} > 5$ yr, ongoing	CO absorption	Eruptive, FUor
VVVv800	1.65	$\Delta t_{out} > 3$ yr	Brγ, H$_2$ emission	Eruptive, MNor
VVVv815	1.71	$\Delta t_{out} \sim 1.8$ yr	H$_2$ emission	Eruptive, MNor
		YSO-Non Eruptive		
VVVv63	1.44	$\Delta t \sim 1$ yr?	Brγ, H$_2$ emission	non-eruptive?
VVVv405	2.00	$\Delta t > 1$ yr	Brγ, H$_2$ emission	non-eruptive?
VVVv406	2.06	$\Delta t > 1$ yr	H$_2$ emission	non-eruptive?
VVVv480	1.70	$\Delta t \sim 1$ yr	Brγ, H$_2$ emission	non-eruptive?
VVVv630	1.90	$\Delta t > 1$ yr	Brγ, H$_2$, CO, Na I, Ca I absorption	non-eruptive
VVVv625	1.46	$\Delta t < 100$ d	Brγ, H$_2$ emission	non-eruptive
VVVv628	1.45	$\Delta t < 1$ yr	Brγ (?), CO, Na I, Ca I absorption	non-eruptive
VVVv632	1.51	$\Delta t < 100$ d	Brγ, H$_2$ emission. Na I, Ca I absorption	non-eruptive
VVVv65	1.36	$\Delta t < 100$ d	Brγ emission	non-eruptive.
		Non-YSOs		
VVVv25	1.68	$P \sim 2000$ d?	CO absorption	Evolved star
VVVv42	2.16	$P \sim 812$ d, periodic	cold CO absorption	Evolved star? YSO?
VVVv45	2.32	$P \sim 560$ d, periodic	CO absorption	Evolved star
VVVv229	3.70	$P \sim 978$ d, periodic	CO absorption	Evolved star
VVVv235	1.26	$P \sim 769$ d, periodic	CO absorption	Evolved star
VVVv796	2.94	$P \sim 796$ d, periodic	CO absorption	Evolved star
VVVv202	1.61	$P > 1000$ d, periodic	^{12}CO, ^{13}CO, Na I, Ca I absorption	Evolved star
VVVv514	1.73	$\Delta t > 500$ d?	Brγ, He I (?) emission	Nova
VVVv240	1.17	$\Delta t > 500$ d?	Brγ, CI emission	Nova

FUor class (Hartmann & Kenyon 1996). Instead, they are dominated by emission from CO, H$_2$ and Brγ, which is typical in EXors.

(v) The predominance of outburst durations longer than EXors but shorter than FUors, coupled with a mixture of EXor and FUor spectroscopic characteristics, leads us to propose a new classification, MNors, for these embedded eruptive variable YSOs. The name follows V1647 Ori, the illuminating source of the McNeil nebula, which is one of a small but growing number of such eruptive variables discovered in recent years (see e.g. Fedele et al. 2007; Aspin et al. 2009). While these might have been considered rare exceptions in the past, they now appear to represent the majority of eruptive YSOs at earlier evolutionary stages. This designation is of course provisional, given that these objects are heterogeneous and so further distinctions and subclasses might be needed in future. The paucity of EXor-like systems with short-duration outbursts ap-

pears to be a genuine difference between optically visible class II eruptive YSOs and their embedded counterparts. The small number of FUor candidates is likely a selection effect given the short (2 yr) duration of the data set used for the initial search. The fact that FUor outbursts are seen in nearby SFRs amongst optically visible YSOs with flat spectrum SEDs but MNor outbursts were not until recently may simply be due to small number statistics.

(vi) Overall, we have classified 19/28 YSOs as eruptive variables. Two or three of the remainder might also be eruptive systems observed in quiescence. The results validate our contention in Paper I that members of the VVV photometric sample with eruptive LC are mainly bona fide YSOs undergoing episodic accretion, along with some of the LPV-YSOs and faders also. The STVs and dippers generally show weaker evidence for episodic accretion, as was expected. The classification of one or two of the eruptive systems

could be disputed but that would not affect our broader conclusion about the properties of the eruptive population. The 18 spectroscopically observed candidates with eruptive LC are fairly representative of the 106 systems with this classification in the full photometric sample, with only a moderate bias towards higher amplitude (and brighter mean magnitude). Much work remains to be done to explore the full VVV sample of high-amplitude variables, particularly sources in the other LC categories.

(vii) The accretion luminosities of YSOs estimated from Brγ emission show that those objects classified as eruptive and observed at a bright state have higher $L_{\rm acc}$ than the remainder of the YSO sample. These also show higher accretion luminosities than normal low-mass class I YSOs and low- and intermediate-mass class II YSOs, comparable to those of known Brγ-emitting eruptive variables. The accretion rates of the Brγ emitters are found to be lower than those of FUors, which is unsurprising if we expect this emission line to be quenched at the high accretion rates of FUors (Audard et al. 2014). The variability amplitudes are also slightly lower on average than those of classical FUors; the data none the less support the view that episodic accretion events lasting a few years are common amongst class I and flat spectrum YSOs. In this context, FUors may represent the more extreme examples of a common phenomenon and there may be no clear distinction between YSOs with relatively small ($\sim$1 mag) eruptions and the lower level accretion variability commonly observed in long-duration studies of normal YSOs. A variability-based census of normal YSOs in VVV will be invaluable to quantify the incidence of episodic accretion.

(viii) For three objects, we have repeat observations which allows us to study the spectroscopic variability of eruptive variables. Object VVVv322 is of special interest. The LC of the object shows a large outburst and its near-IR spectrum closely resembles those of classical FUors. However, the duration of the outburst appears to be $\sim$3 yr, much shorter than expected for classical FUors. The spectrum of the object also shows variations as absorption features from CO and H_2O become weaker as the star goes back into quiescence.

ACKNOWLEDGEMENTS

REFERENCES

Acosta-Pulido J. A. et al., 2007, AJ, 133, 2020
Antoniucci S., Nisini B., Giannini T., Lorenzetti D., 2008, A&A, 479, 503
Antoniucci S. et al., 2011, A&A, 534, A32
Antoniucci S. et al., 2014, A&A, 565, L7
Aspin C., Sandell G., 2001, MNRAS, 328, 751
Aspin C., Beck T. L., Reipurth B., 2008, AJ, 135, 423
Aspin C., Greene T. P., Reipurth B., 2009, AJ, 137, 2968
Aspin C. et al., 2009, ApJ, 692, L67
Aspin C., Reipurth B., Herczeg G. J., Capak P., 2010, ApJ, 719, L50
Audard M. et al., 2014, in Beuther H., Klessen R. S., Dullemond C. P., Henning T., eds, Protostars and Planets VI. Arizona Univ. Press, Tucson, AZ, p. 387
Baraffe I., Chabrier G., Gallardo J., 2009, ApJ, 702, L27
Baraffe I., Vorobyov E., Chabrier G., 2012, ApJ, 756, 118
Baume G., Carraro G., Momany Y., 2009, MNRAS, 398, 221
Beck T. L., 2007, AJ, 133, 1673
Benjamin R. A. et al., 2003, PASP, 115, 953
Boyer M. L. et al., 2011, AJ, 142, 103
Brand J., Blitz L., 1993, A&A, 275, 67
Britt C. T. et al., 2016, MNRAS, 460, 2822
Bronfman L., Nyman L.-A., May J., 1996, A&AS, 115, 81
Brown C., Dickey J. M., Dawson J. R., McClure-Griffiths N. M., 2014, ApJS, 211, 29
Calvet N., Patino A., Magris G. C., D'Alessio P., 1991, ApJ, 380, 617
Calvet N., Muzerolle J., Briceño C., Hernández J., Hartmann L., Saucedo J. L., Gordon K. D., 2004, AJ, 128, 1294
Caratti o Garatti A. et al., 2011, A&A, 526, L1
Caratti o Garatti A. et al., 2012, A&A, 538, A64
Caratti o Garatti A., Garcia Lopez R., Weigelt G., Tambovtseva L. V., Grinin V. P., Wheelwright H., Ilee J. D., 2013, A&A, 554, A66
Cardelli J. A., Clayton G. C., Mathis J. S., 1989, ApJ, 345, 245
Carey S. J. et al., 2009, PASP, 121, 76
Carr J. S., 1989, ApJ, 345, 522
Caswell J. L., 1998, MNRAS, 297, 215
Caswell J. L., Kramer B. H., Sukom A., Reynolds J. E., 2010, MNRAS, 402, 2649
Chandra S., Maheshwari V. U., Sharma A. K., 1996, A&AS, 117, 557
Churchwell E. et al., 2006, ApJ, 649, 759
Churchwell E. et al., 2009, PASP, 121, 213
Clark J. S., Negueruela I., Crowther P. A., Goodwin S. P., 2005, A&A, 434, 949
Cody A. M. et al., 2014, AJ, 147, 82
Connelley M. S., Greene T. P., 2010, AJ, 140, 1214
Connelley M. S., Greene T. P., 2014, AJ, 147, 125
Contreras Peña C. et al., 2014, MNRAS, 439, 1829
Contreras Peña C. et al., 2016, MNRAS, in press (Paper I)
Cooper H. D. B. et al., 2013, MNRAS, 430, 1125
Covey K. R. et al., 2011, AJ, 141, 40
Cutri R. M. et al., 2012, Explanatory Supplement to the WISE All-Sky Data Release Products. Tech. rep.
Das R. K., Banerjee D. P. K., Ashok N. M., Mondal S., 2013, Bull. Astron. Soc. India, 41, 195
Davies B., Lumsden S. L., Hoare M. G., Oudmaijer R. D., de Wit W.-J., 2010, MNRAS, 402, 1504
Davis C. J., Ray T. P., Desroches L., Aspin C., 2001, MNRAS, 326, 524
Deharveng L., Zavagno A., Schuller F., Caplan J., Pomarès M., De Breuck C., 2009, A&A, 496, 177
Drew J. E. et al., 2014, MNRAS, 440, 2036
Dunham J. L., 1932, Phys. Rev., 41, 721
Eislöffel J., Günther E., Hessman F. V., Mundt R., Poetzel R., Carr J. S., Beckwith S., Ray T. P., 1991, ApJ, 383, L19
Elia D. et al., 2013, ApJ, 772, 45
Ellingsen S. P., von Bibra M. L., McCulloch P. M., Norris R. P., Deshpande A. A., Phillips C. J., 1996, MNRAS, 280, 378
Enoch M. L., Evans N. J., II, Sargent A. I., Glenn J., 2009, ApJ, 692, 973

Epchtein N. et al., 1994, A&SS, 217, 3

Evans N. J., II, Balkum S., Levreault R. M., Hartmann L., Kenyon S., 1994, ApJ, 424, 793

Evans N. J., II et al., 2009, ApJS, 181, 321

Faimali A. et al., 2012, MNRAS, 426, 402

Farrenq R., Guelachvili G., Sauval A. J., Grevesse N., Farmer C. B., 1991, J. Mol. Spectrosc., 149, 375

Fedele D., van den Ancker M. E., Petr-Gotzens M. G., Rafanelli P., 2007, A&A, 472, 207

Findeisen K., Hillenbrand L., Ofek E., Levitan D., Sesar B., Laher R., Surace J., 2013, ApJ, 768, 93

Fischer W. J. et al., 2012, ApJ, 756, 99

Gibb E. L., Rettig T. W., Brittain S. D., Wasikowski D., Simon T., Vacca W. D., Cushing M. C., Kulesa C., 2006, ApJ, 641, 383

Gómez M., Mardones D., 2003, AJ, 125, 2134

Gramajo L. V., Rodón J. A., Gómez M., 2014, AJ, 147, 140

Greene T. P., Lada C. J., 1996, AJ, 112, 2184

Gullbring E., Hartmann L., Briceño C., Calvet N., 1998, ApJ, 492, 323

Guzmán A. E., Garay G., Brooks K. J., Voronkov M. A., 2012, ApJ, 753, 51

Hartmann L., Kenyon S. J., 1996, ARA&A, 34, 207

Herbig G. H., 1977, ApJ, 217, 693

Herbig G. H., 1989, in Reipurth B., ed., ESO Workshop on Low-Mass Star Formation and Pre-Main-Sequence Object. ESO, Garching, p. 233

Herbst W., Shevchenko V. S., 1999, AJ, 118, 1043

Hodapp K. W., Chini R., 2014, ApJ, 794, 169

Hodapp K. W., Chini R., Watermann R., Lemke R., 2012, ApJ, 744, 56

Hodapp K.-W., Hora J. L., Rayner J. T., Pickles A. J., Ladd E. F., 1996, ApJ, 468, 861

Ishihara D., Kaneda H., Onaka T., Ita Y., Matsuura M., Matsunaga N., 2011, A&A, 534, A79

Ishii M., Nagata T., Sato S., Yao Y., Jiang Z., Nakaya H., 2001, AJ, 121, 3191

Jackson J. M., Finn S. C., Rathborne J. M., Chambers E. T., Simon R., 2008, ApJ, 680, 349

Kenyon S. J., Hartmann L. W., Strom K. M., Strom S. E., 1990, AJ, 99, 869

Kenyon S. J., Hartmann L. W., Kolotilov E. A., 1991, PASP, 103, 1069

Kóspál Á., Ábrahám P., Prusti T., Acosta-Pulido J., Hony S., Moór A., Siebenmorgen R., 2007, A&A, 470, 211

Kóspál Á. et al., 2013, A&A, 551, A62

Kraus M., 2009, A&A, 494, 253

Kraus M., Krügel E., Thum C., Geballe T. R., 2000, A&A, 362, 158

Kumar M. S. N., Contreras Peña C., Lucas P. W., Thompson M. A., 2016, preprint (arXiv:1609.08711)

Kun M. et al., 2011, ApJ, 733, L8

Lorenzetti D., Larionov V. M., Giannini T., Arkharov A. A., Antoniucci S., Nisini B., Di Paola A., 2009, ApJ, 693, 1056

Lorenzetti D. et al., 2012, ApJ, 749, 188

Magakian T. Y. et al., 2013, MNRAS, 432, 2685

Mainzer A. et al., 2011, ApJ, 731, 53

Marocco F. et al., 2015, MNRAS, 449, 3651

Martins F., Pomarès M., Deharveng L., Zavagno A., Bouret J. C., 2010, A&A, 510, A32

Megeath S. T. et al., 2012, AJ, 144, 192

Meyer M. R., Calvet N., Hillenbrand L. A., 1997, AJ, 114, 288

Minniti D. et al., 2010, NewA, 15, 433

Molinari S. et al., 2010, PASP, 122, 314

Murakami H. et al., 2007, PASJ, 59, 369

Muzerolle J., Hartmann L., Calvet N., 1998, AJ, 116, 2965

Muzerolle J., Megeath S. T., Flaherty K. M., Gordon K. D., Rieke G. H., Young E. T., Lada C. J., 2005, ApJ, 620, L107

Najita J., Carr J. S., Glassgold A. E., Shu F. H., Tokunaga A. T., 1996, ApJ, 462, 919

Ninan J. P., Ojha D. K., Bhatt B. C., Ghosh S. K., Mohan V., Mallick K. K., Tamura M., Henning T., 2013, ApJ, 778, 116

Ochsenbein F., Bauer P., Marcout J., 2000, A&AS, 143, 23

Peretto N., Fuller G. A., 2009, A&A, 505, 405

Persi P., Tapia M., Gòmez M., Whitney B. A., Marenzi A. R., Roth M., 2007, AJ, 133, 1690

Price S. D., Egan M. P., Carey S. J., Mizuno D. R., Kuchar T. A., 2001, AJ, 121, 2819

Purcell C. R. et al., 2012, MNRAS, 426, 1972

Rebull L. M. et al., 2014, AJ, 148, 92

Reipurth B., Aspin C., 1997, AJ, 114, 2700

Reipurth B., Aspin C., 2004, ApJ, 606, L119

Reipurth B., Aspin C., 2010, in Harutyunian H. A., Mickaelian A. M., Terzian Y., eds, Proc. Conf. Evolution of Cosmic Objects through their Physical Activity. Gitutyun Publ. House, Yerevan, p. 19

Reipurth B., Aspin C., Herbig G. H., 2012, ApJ, 748, L5

Rice T. S., Reipurth B., Wolk S. J., Vaz L. P., Cross N. J. G., 2015, AJ, 150, 132

Rieke G. H., Lebofsky M. J., 1985, ApJ, 288, 618

Robitaille T. P., Whitney B. A., Indebetouw R., Wood K., 2007, ApJS, 169, 328

Robitaille T. P. et al., 2008, AJ, 136, 2413

Russeil D., Castets A., 2004, A&A, 417, 107

Safron E. J. et al., 2015, ApJ, 800, L5

Saito R. K. et al., 2012, A&A, 537, A107

Schlafly E. F., Finkbeiner D. P., 2011, ApJ, 737, 103

Schlegel D. J., Finkbeiner D. P., Davis M., 1998, ApJ, 500, 525

Scholz A., Froebrich D., Wood K., 2013, MNRAS, 430, 2910

Sevenster M. N., Chapman J. M., Habing H. J., Killeen N. E. B., Lindqvist M., 1997, A&AS, 124, 509

Siess L., Dufour E., Forestini M., 2000, A&A, 358, 593

Simpson R. J. et al., 2012, MNRAS, 424, 2442

Skrutskie M. F. et al., 2006, AJ, 131, 1163

Smith M. D., 1995, A&A, 296, 789

Spezzi L. et al., 2008, ApJ, 680, 1295

Stellingwerf R. F., 1978, ApJ, 224, 953

Tapia M., Roth M., Persi P., 2015, MNRAS, 446, 4088

Vacca W. D., Sandell G., 2011, ApJ, 732, 8

Vacca W. D., Cushing M. C., Rayner J. T., 2003, PASP, 115, 389

van Loon J. T. et al., 1998, A&A, 329, 169

van Loon J. T., Cohen M., Oliveira J. M., Matsuura M., McDonald I., Sloan G. C., Wood P. R., Zijlstra A. A., 2008, A&A, 487, 1055

van Loon J. T. et al., 2010a, AJ, 139, 68

van Loon J. T., Oliveira J. M., Gordon K. D., Sloan G. C., Engelbracht C. W., 2010b, AJ, 139, 1553

Venturini C. C., Rudy R. J., Lynch D. K., Mazuk S., Puetter R. C., 2004, AJ, 128, 405

Vorobyov E. I., Basu S., 2015, ApJ, 805, 115

Wallace L., Hinkle K., 1997, ApJS, 111, 445

Walsh A. J., Hyland A. R., Robinson G., Burton M. G., 1997, MNRAS, 291, 261

Wenger M. et al., 2000, A&AS, 143, 9

Whitelock P. A., Feast M. W., van Leeuwen F., 2008, MNRAS, 386, 313

Whitney B. et al., 2011, Deep GLIMPSE: Exploring the Far Side of the Galaxy. Spitzer Proposal

Wolk S. J. et al., 2015, AJ, 150, 145

Wright E. L. et al., 2010, AJ, 140, 1868

Young K. E., Young C. H., Lai S.-P., Dunham M. M., Evans II N. J., 2015, AJ, 150, 40

Zavagno A., Pomarès M., Deharveng L., Hosokawa T., Russeil D., Caplan J., 2007, A&A, 472, 835

APPENDIX A: INDIVIDUAL OBJECTS

(i) VVVv721: previously identified as a likely YSO in the Robitaille et al. (2008) catalogue of intrinsic red objects, the SED and near-IR colours of the star are consistent with a class I object. The star is found within 244 arcsec of the dark cloud SDC G338.734+0.584 (Peretto & Fuller 2009), molecular clouds [RC2004] G338.7+0.6−72.1 and [RC2004] G338.7+0.6−62.2 (Russeil & Castets 2004) and H II region GAL 338.74+00.64 (Brown et al. 2014), which measured radial velocities between −62 and −72.1 km s^{-1}. The use of CO model templates yield

$v_{LSR} = -89.7 \pm 2.6 \, \text{km s}^{-1}$ for VVVv721. Other star formation tracers are found within 300 arcsec of the source (H II region, YSOs) and the *WISE* false colour image reveals the evidence of active star formation in the area (Fig. B1).

The LC shows a slow rise with $\Delta K_s = 1.9$ mag between 2010 and 2014. The classical FUor V1515 Cyg is known for displaying a slow rise in its LC and taking approximately 25 yr to reach its maximum brightness (Kenyon, Hartmann & Kolotilov 1991). This slow rise has been explained as arising from thermal instabilities that spread from the inner regions towards the outer parts of the accretion disc (see e.g Audard et al. 2014). However, VVVv721 is detected in 2MASS with $K_s = 13.23 \pm 0.03$ mag, thus being at least 0.7 mag brighter than the first VVV epoch. The LC in Fig. B1 also shows the variability observed at 3.4 and 4.6 μm using the photometry from the *WISE* (Wright et al. 2010) and NEOWISE (Mainzer et al. 2011) surveys. The mid-IR data points also show large variability with $\Delta W1 = 1.53$ and $\Delta W2 = 1.02$ mag, values which agree with the expected change from variable accretion in YSOs (Scholz et al. 2013). These changes do not appear to be related to variable extinction along the line of sight.

VVVv721 is an optically invisible star, as it is not detected in *Z* nor *Y* bands in VVV. The spectrum of the star (Fig. B1) rises longwards of 1.3 μm and it is nearly featureless, apart from the deep CO feature characteristic of FUors. Absorption from H_2O is also present in the spectrum.

Some doubt will remain as to whether the duration of the outburst is in line with the expected duration in FUor objects. Nevertheless, this variable star is very likely a new addition to the FUor eruptive variable class.

(ii) VVVv717: this object has been previously classified as a likely YSO by Robitaille et al. (2008), based on *Spitzer* and MIPS photometry. The SED and near-IR colours are those of a class I object. It is found within 5 arcmin of six IRDCs from Peretto & Fuller (2009), whilst two other likely YSOs from the Robitaille et al. catalogue are found within 30 arcsec from this object (see Fig. B2). There are no distance estimates to objects around this source.

VVVv717 is an optically invisible star, not being detected in *J* nor *H* bands in VVV. Fig. B2 shows a red rising, nearly featureless spectrum, with no flux at wavelengths shorter than 1.4 μm. The object shows strong and broad CO absorption and although it does not show any absorption from H_2O, we note that other deeply embedded FUor objects have been classified as such even when lacking this feature (e.g. OO Ser, PP13S; Hodapp et al. 1996; Aspin & Sandell 2001). Brγ is also apparent in this object, with relatively weak emission that seems to be on top of a broader absorption feature. This emission line is usually not observed in FUors as this accretion-sensitive emission line is assumed to be quenched by the very high accretion rate of these systems. VVVv717 also shows weak H_2 2.12 μm and a marginal detection of Mg I 2.28 μm emission. Further follow-up of the system (Contreras Peña et al., in preparation) shows that the H_2 2.12 μm has become much more evident.

The LC shows some possible periodicity with $P > 400$ d. It was classified as a YSO with a long-term period in Paper I. It rose in brightness during 2010, remained bright in 2011, showed a drop in brightness in 2012, recovered in 2013 and then showed a deeper drop in 2014. The object shows $K_{s, \, max} - K_{s, \, min} = 2.47$ mag. The 2013 data points reveal that this object was probably close to maximum brightness at the time of the spectroscopic follow-up. The mid-IR data points from *WISE* and NEOWISE seem to follow the behaviour of the VVV photometry. The change in *W1* of ~1.1 mag agrees with that expected from large changes in the accretion rate

of a YSO (Scholz et al. 2013). The changes in colour from *WISE* and NEOWISE are also not consistent with variable extinction. The fact that the object is highly variable over a somewhat short period time (that could point to periodicity) is confirmed by the GLIMPSE I detection of the object. The star shows [3.6] = 10.12 and [4.5] = 8.81, which are close to the maximum brightness observed during the 2010–2014 period. In addition VVVv717 is not detected in 2MASS nor DENIS, which makes the object fainter than at least *K* = 15.3 at the epoch of the surveys (~1999). This is fainter than any of the data points measured during the coverage of VVV.

While the observed emission lines should be sufficient to rule out an AGB star classification, we also test that possibility by estimating the distance to such an object using the Akari method, which is further explained in Appendix C. VVVv717 was not detected at 9 μm by the Akari survey, so we use the 8 μm measurement from *Spitzer*/GLIMPSE I instead. This should give similar results because the two passbands are fairly similar (6.0–11.0 μm for Akari versus 6.5–9.3 μm for *Spitzer*). VVVv717 shows [8.0]=6.8 mag or 0.12 Jy. We use the $K_s - [8]$ colour in equation A4 of Ishihara et al. (2011) to derive the mass-loss rate of an OH/IR or carbon star with similar colours to VVVv717.

This yields $\dot{M} = 10^{-4.9}$ M$_\odot$ yr^{-1}. According to equation A3 of Ishihara et al. (2011), an OH/IR or carbon star with this mass-loss rate and 8 μm flux would be located at 70^{+41}_{-27} kpc from the Sun, where the large uncertainties reflect the large uncertainty in the $K_s - [8]$ colour based on non-contemporaneous data as well as the scatter in the distance versus colour relation. This distance would place VVVv717 well outside the Galactic disc. We have checked if extinction could explain the red colour of VVVv717; Schlegel, Finkbeiner & Davis (1998) maps give $A_{Ks} = 2.16$ mag at the coordinates of the object, which implies $E(K_s - [9]) \sim 1$ mag. This value is within the uncertainties assumed in the $K_s - [8]$ colour and it is not large enough to put the object within the Galactic disc. We conclude that an AGB star interpretation is very unlikely.

The near kinematic distance derived from the radial velocity of VVVv717, of $d = 6.1$ kpc, also contradicts the large distances derived from the AGB scenario.

We conclude that this star is very likely an eruptive YSO. However, it is also impossible to place it within the original classification for this type of stars.

(iii) VVVv631: also in an area rich in star formation, went into outburst during 2010 and 2011 and has remained in outburst since that time, though perhaps beginning to fade in 2015. It has $\Delta K_s \sim 2.5$ mag (Fig. B3). This star was detected in 2MASS with $K_s = 14.11 \pm 0.12$, suggesting that the object had been in a quiescent state prior to the VVV coverage. The 2014 data show that the object was at a bright state during our follow-up. The spectrum shows Brγ (2.16 μm) and Pa β (1.28 μm) emission as well as Na I, CO and possible Mg I (1.502 μm) emission. The $\Delta v = 3$–1 CO bandhead is more prominent than the $\Delta v = 2$–0 bandhead (this is confirmed in the recent spectrum from the 2015 run; Contreras Peña et al., in preparation). This object also shows blueshifted 1.08 μm He I absorption, probably from a wind. This feature is blueshifted by ~2.5 Å (-70 km s^{-1}), but with a velocity profile extending to ~ -220 km s^{-1}. This feature has been observed in FUors and EXors but, on its own, is not a discriminant of FUor-like activity (Fischer et al. 2012).

It is very interesting to see that the object displays absorption from H_2O. The object IRAS 06297+1021(W) in the sample of Connelley & Greene (2010) shows a remarkably similar spectrum. In that case, the authors had mixed feelings about classifying it as an FUor-like object due to its rich emission spectrum. However,

the observed photometric behaviour of our object makes it a very strong candidate for being part of the eruptive variable class.

The fact that we are seeing both CO emission (assumed to arise from the innermost parts of the disc) and H_2O absorption would suggest that two separate regions are contributing to the near-IR spectrum. H_2O is never seen in emission in the near-IR spectra of YSOs, presumably because the innermost part of the disc is too hot for the molecule to remain bound.

(iv) VVVv118: classified as a likely YSO by Robitaille et al. (2008), VVVv118 is found 124 arcsec from IRAS 14477−5947, a high-mass YSO candidate (see e.g. Guzmán et al. 2012) and 94 arc-sec from IR bubble [SPK2012] MWP1G317420−005582 (Simpson et al. 2012). The star is detected in 2MASS with $K_s = 12.49 \pm 0.04$. Fig. B4 shows that the object displays large variations (>2 mag) over short time-scales (with changes occurring on time-scales less than 100 d). This short time-scale resembles that of objects in the STV category of Paper I. However, both the short-term changes and the total amplitude ($\Delta K_s = 4$ mag) are much larger than those of all other objects in that category, allowing us to definitely discard rotational modulation from hot/cold spots as the driving physical mechanism for the variability of VVVv118. In addition, colour changes (bluer when fainter) seen in the two epochs of near-IR photometry disfavour the possibility of variable extinction, so the LC was classified as eruptive in Paper I. This large ΔK_s over short time-scales is consistent with an eruptive variable of the EXor type. However, the spectrum (Fig. B4) displays not only weak Brγ emission but also a probable detection of weak H_2O absorption, the latter being commonly found in FUor variables rather than EXors. The presence of CO absorption at 2.29 μm cannot be confirmed. Assuming that water absorption is present, this represents yet another example of eruptive variables in our sample showing a mixture of characteristics between those of EXors and FUors.

(v) VVVv800 is located in the vicinity of H II region RCW120 ($d \sim 1.4$ kpc; Deharveng et al. 2009) and has already been classified as a YSO by Martins et al. (2010) (source 76 of YSOs around RCW120). The latter have obtained a near-IR spectrum of the object, which shows a lack of absorption features and only has H_2 emission at 2.03, 2.12, 2.22 μm. Our observation of this object (Fig. B5) shows a similar behaviour, with several transitions from molecular hydrogen present, as well as Brγ emission. This object also shows strong emission at 1.64 μm from [Fe II]. The variable star seems to be driving a powerful outflow. VVV 2014 photometry shows that our observations were taken close to the maximum brightness of the object (see Fig. B5). We note also that this object is detected in both 2MASS and DENIS with $K_s = 10.82 \pm 0.03$ and $K = 11.02 \pm 0.08$ respectively, suggesting that this object had gone into a bright state prior to our VVV coverage. The accretion luminosity for this object is at the low end of L_{acc} for eruptive VVV objects (see Table 5), which is not expected given that this object was observed close to the brightest point in the LC. The absence of CO emission may cast some doubt on its eruptive nature but this could be explained by high extinction towards the inner disc region, e.g. due to an edge-on disc. Such a geometry would also be expected to veil the Brγ emission line: as noted earlier, we should not expect the individual estimates from this line to be accurate in every case. We note that the spectrum of VVVv800 resembles that of the eruptive variable GM Cha, an object with a red-rising featureless continuum dominated by H_2 emission (see e.g. Persi et al. 2007). The long duration of the bright state appears to rule out rotational modulation by bright or dark spots and the colour changes (bluer when fainter) seen in the two epochs of JHK_s colour data disfavour extinction as the cause of variability,

leaving only accretion as the likely cause of variability. Given that the LC is well described as an ∼1 mag outburst with additional short time-scale scatter, this object may be regarded at the low end of what might be termed an eruptive variable. Rice et al. (2015) observed lower level accretion variations in some YSOs on time-scales of years, as well as shorter time-scales. Detection of objects such as VVVv800 perhaps indicates that there is no clear distinction in amplitude between normal low-level variations in accretion rate and episodic accretion. The other eruptive variables in our sample that were observed in a bright state have higher derived accretion luminosities and amplitudes.

(vi) VVVv815: this object was discovered as a high-amplitude variable in an early data release of VVV 2010 data and is not selected in the 2010–2012 analysis (see Paper I). It was found to be an intrinsically red object from mid-IR colours and classified as a likely YSO by Robitaille et al. (2008). The star is likely associated with an SFR (see Fig. B6) and its projected location is 79 arcsec from H II region [WHR97] 14222−6026 ($v_{LSR} = -44$ km s^{-1}, $d \sim 2.5$ kpc; Walsh et al. 1997). Its SED is consistent with a class I object ($\alpha = 1.58$).

VVVv815 was observed in low resolution with FIRE on 2012 May. The spectrum shows no flux in the J or H bands and is dominated by strong emission of $v = 1$–$0\Delta J = -2$ rovibrational transitions from molecular hydrogen, with the 1–0 S(1) 2.12 μm being the most prominent feature (EW $= -200$ Å). The lack of higher excited lines in the spectrum of this object points to the emission arising from molecular shocks.

The 2013 medium resolution echelle spectrum from FIRE shows very similar characteristics (see Fig. A1), although the equivalent width of the 1–0 S(1) 2.12 μm decreased to -119 Å. The higher quality of this spectrum allows us to derive a ratio 1–0 S(1)/2–1 S(1) of ∼6 which agrees with models of emission arising from molecular shocks (see e.g. Smith 1995).

(vii) VVVv699: Robitaille et al. (2008) finds the *Spitzer* IRAC colours of this object to be consistent with those of a YSO and it is thus classified as such in their study. The automatic search for mid-IR detections within 1 arcsec of the source only yields a GLIMPSE I (Benjamin et al. 2003) detection. Inspection of the images arising from *WISE* show the possible presence of VVVv699 (Fig. B7) and there is one detection at 1.3 arcsec from the VVV source. Comparison of the magnitudes from *WISE W*1, *W*2 with *Spitzer* I1,I2 shows an agreement between the two measurements, which suggests that VVVv699 had been in quiescence previous to the 2011 outburst. This is also supported by the fact that the source falls below the detection limit in both 2MASS and DENIS surveys (see Fig. B7). Thus, use of *Spitzer* photometry to build the SED of VVVv699 is preferred given that the centroid of the detection is closer to the VVV position. Our analysis shows the object as a class I YSO, with $\alpha = 2.08$.

The LC (Fig. A2) shows an outburst between the 2010 and 2011 campaigns of VVV, with $\Delta K \sim 2.2$ mag. The fact that the object had been on a quiescent state prior to 2010 seems to be supported by mid-IR information. In addition, the object seems to be displaying some shorter term, lower amplitude variability ($\Delta K < 1$ mag) during 2012 and 2013.

Fig. A2 shows that VVVv699 is located within 300 arcsec of several indicators of active star formation, such as likely YSOs from Robitaille et al. (2008), six IRDCs, and is within the broken GLIMPSE IR bubble [CPA2006] S43 (Churchwell et al. 2006). These IR bubbles are expected to be formed around hot young stars in massive SFRs (Churchwell et al. 2006). Unfortunately, none of the indicators have available distance information. The radial
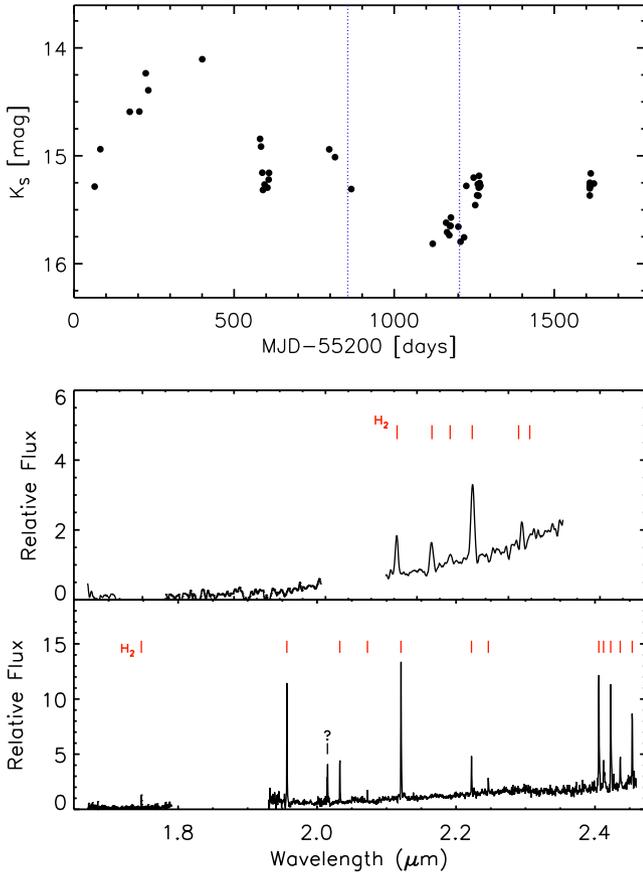
Figure A1. (top) K_s LC of VVVv815, where the arrows mark the dates of the 2012 and 2013 spectroscopic follow-up. (middle) 2012 FIRE low-resolution spectrum of VVVv815. (bottom) 2013 FIRE high-resolution spectrum of VVVv815. In both spectra, the observed rovibrational transitions of H_2 are marked at the top of each graph.

Figure A2. (top) K_s LC of VVVv699. The dashed lines in the graph mark the dates of the 2013 April 2013 (blue) and 2014 May(red) FIRE observations. (middle) Graph comparing the 2013 (red) and 2014 (blue) FIRE spectra of VVVv699 in the region 2.1–2.25 μm. Emission lines observed in this object are marked in the graph. (bottom) Similar comparison to the previous graph, but in the region 2.29–2.42 μm.
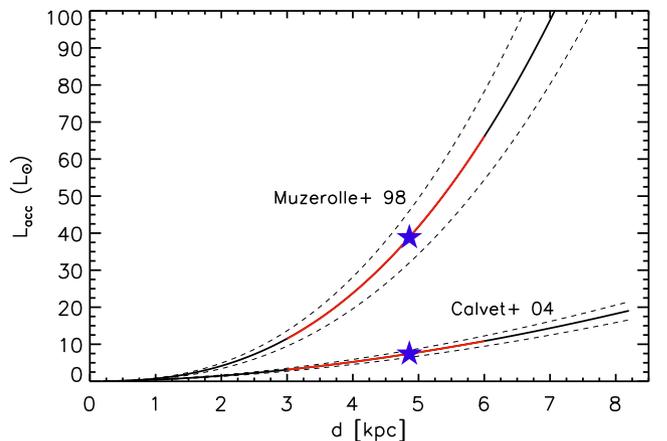
Figure A3. Accretion luminosity of VVVv699, estimated from the observed flux of the Brγ line in the 2013 observations and for the distance range of IR bubbles from Churchwell et al. (2006). L_{acc} is derived from the Calvet et al. (2004) and the Muzerolle et al. (1998) relations. The red line marks the estimated L_{acc} for $3 < d < 6$ kpc. Errors on L_{acc} are shown as dashed lines. The accretion luminosity estimated using the distance from radial velocities is marked by a blue star.

velocity of the object (see Table 4) suggests that VVVv699 is located at a heliocentric distance of 4.9 kpc.

The 2013 follow-up (Fig. B7) reveals a rich emission line spectrum, with strong H_2 lines from several transitions and Brγ emission. CO and Na I are also in emission. CO and Na I emission are usually attributed to a hot inner disc at a distance of a few astronomical units from the central star. The observations from 2014 (Fig. A2) show a decrease in the strength of several lines, most noticeable in the CO and Na I lines, with also an apparent decrease in the intensity of the Brγ emission. The H_2 emission on the other hand seems to increase, an effect that is apparent in all of the observed transitions. We do note that the changes in Brγ and H_2 are within the measurement errors and do not appear to be larger than 10 per cent.

Connelley & Greene (2014) have studied the spectroscopic variability of a sample of class I YSOs. They have found that tracers of mass accretion, Brγ and CO emission, are variable at all time-scales, with CO being most variable (up to a factor of 3) on a time-scale of 1–3 yr which corresponds to a spatial scale of within 1–2 au in a Keplerian disc (Connelley & Greene 2014). These authors also find that changes in mass flow on to the central star, as traced by Brγ, are coupled to changes in the disc surface temperature (which gives rise to the CO emission), whenever there is a large change in the CO emission and on long time-scales. The observed variability in VVVv699 over a period of 1 yr seems to support the latter. We observed a large variation of up to a factor of 2 in CO emission,

accompanied by an apparent change in Brγ emission. However, we cannot rule out the possibility that changes in EWs are affected by changes in veiling.

Unfortunately, we are not able to estimate whether this relates to a change in the accretion rate between the two epochs. We do not have contemporaneous photometry to the spectroscopic measurements and as we saw before, there seems to be a short-term variability with $\Delta K \sim 0.5$ magnitudes. Thus, trying to assign a K-band brightness to the dates of the spectroscopic observations from the LC of VVVv699 would yield unreliable results. Most importantly, we have already stated the difficulties in deriving this parameter in Section 5.2.

We can estimate a range of values for the accretion luminosity from the 2013 observations. Following Section 5.2, we can derive the flux of the Brγ emission, $F_{\text{br}\gamma}$, using the measured equivalent widths, the extinction A_v to the system and the continuum flux from K-band photometry.

In Section 5.2, we estimated the visual extinction to the source by adopting a colour $J - H = 3.5$, which yields $A_v = 23$. This can be considered as a lower limit of A_v. In this section, we attempt to derive this parameter with a different method.

The visual extinction to the source can be estimated using the H$_2$ 1–0 $Q(3)/S(1)$ ratio, r_{obs}, since these lines originate in the same upper state. We compare the observed ratio to the intrinsic one (0.7; see Beck 2007, and references therein) and derive A_v assuming the Cardelli, Clayton & Mathis (1989) extinction law. Then,

$$0.404 A_V \left[\left(\frac{1}{\lambda_{Q(3)}} \right)^{1.61} - \left(\frac{1}{\lambda_{S(1)}} \right)^{1.61} \right] = \log \left(\frac{0.7}{r_{\text{obs}}} \right), \qquad \text{(A1)}$$

where we estimate $A_v = 42$ and 23 mag for 2013 and 2014, respectively. This change in A_v would imply $\Delta K_s \sim 2.2$ mag, which seems highly unlikely from the LC of this object. We note that Connelley & Greene (2010) argue against this ratio as a reliable measurement of the visual extinction, given the large discrepancies that they found between the values using this method and those found through either photometry or modelling of the continuum. They suspect that

the closeness of the $Q(3)$ line to a telluric absorption feature is likely to affect the observed ratio. A_v is also found to be variable in their sample. The Schlegel et al. (1998) maps yield an upper limit of the visual extinction of $A_v = 35.3$ mag (30.8 mag in the revised values of Schlafly & Finkbeiner 2011).

We then assume $K = 14.1$, which corresponds to the approximate mean brightness in the 2013 epochs from VVV. From this, we obtain the continuum level, F_λ for the Brγ line at 2.1659 μm. In addition, we correct this value for the extinction along the line of sight to the source, assuming $A_v = 32$ (a simple mean of the values obtained using line ratios). The line flux is then estimated following Section 5.2. We finally obtain $F_{\text{Br}\gamma} = (7.54 \pm 1.08) \times 10^{-15}$ erg s^{-1} cm^{-2}.

In order to estimate the line luminosity, we take a range of values for the distance of VVVv699 between 0.2 and 8.2 kpc, which corresponds to the distribution of near kinematic distances of Galactic bubbles in Churchwell et al. (2006). The accretion luminosity is derived from the Calvet et al. (2004) and Muzerolle et al. (1998) relations. We obtain a large range in L_{acc}, up to 20 and >100 L$_\odot$ from the Calvet et al. and Muzerolle et al. relations, respectively. The peak distribution of the Churchwell et al. sample with known distances is found to be at $d = 4.2$ kpc, a similar distance to that estimated from the radial velocity of the object, with the majority of the sample being located between 3 and 6 kpc. If we assume the latter range for the distance of [CPA2006] S43, then the maximum luminosities derived from the two relations reduce to 10 and 60 L$_\odot$, respectively. Using the near kinematic distance from radial velocities yields $L_{\text{acc, Calvet}} = 7.4$ L$_\odot$ and $L_{\text{acc, Muzerolle}} = 38.9$ L$_\odot$. These values are also higher than the ones obtained in Section 5.2. This is due to the lower value of A_v estimated from dereddening the $J - H$ colour of VVVv699 to the T Tauri locus in Section 5.2. However, this particular value might not represent the true A_v to the system as VVVv699 is not detected in J nor H. Nevertheless, these values of L_{acc} support the object being in a high state of accretion.

APPENDIX B: PLOTS FOR INDIVIDUAL OBJECTS
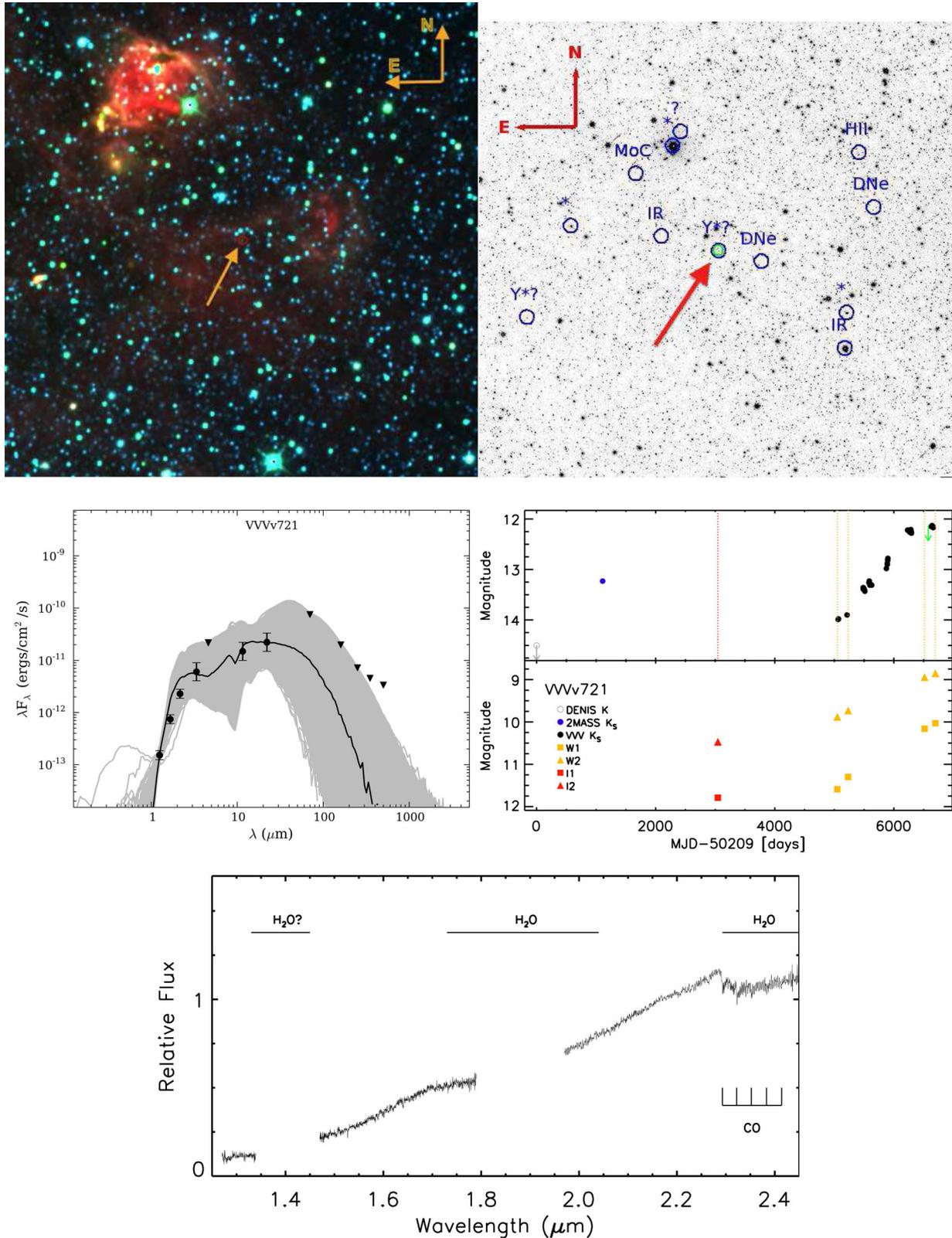
Figure B1. (top left) False colour *WISE* image (blue = 3.5 μm, green = 4.6 μm, red = 12 μm) of a 0°.44 × 0°.44 area centred on VVVv721. The location of the object is marked by the arrow. (top right) K_s image of a 10 arcmin × 10 arcmin area centred on VVVv721. The location of the object is marked by the red arrow and the green circle. In addition, blue circles and labels mark objects found in a SIMBAD query with a 5 arcmin radius. (middle left) SED of VVVv721 along with Robitaille et al. (2007) YSO models that fulfil the criteria of $\chi^2 - \chi^2_{best} < 3N$, with N the number of data points used to generate the fits. This image is generated by the fitting tool. (middle right) Near-IR (K_s) and mid-IR photometry of VVVv721. Data arising from different surveys are marked by different symbols which are labelled in the figure. The green arrow marks the time when the spectrum was taken. (bottom) FIRE spectrum of VVVv721. The spectroscopic features found for this object are marked in the graph.
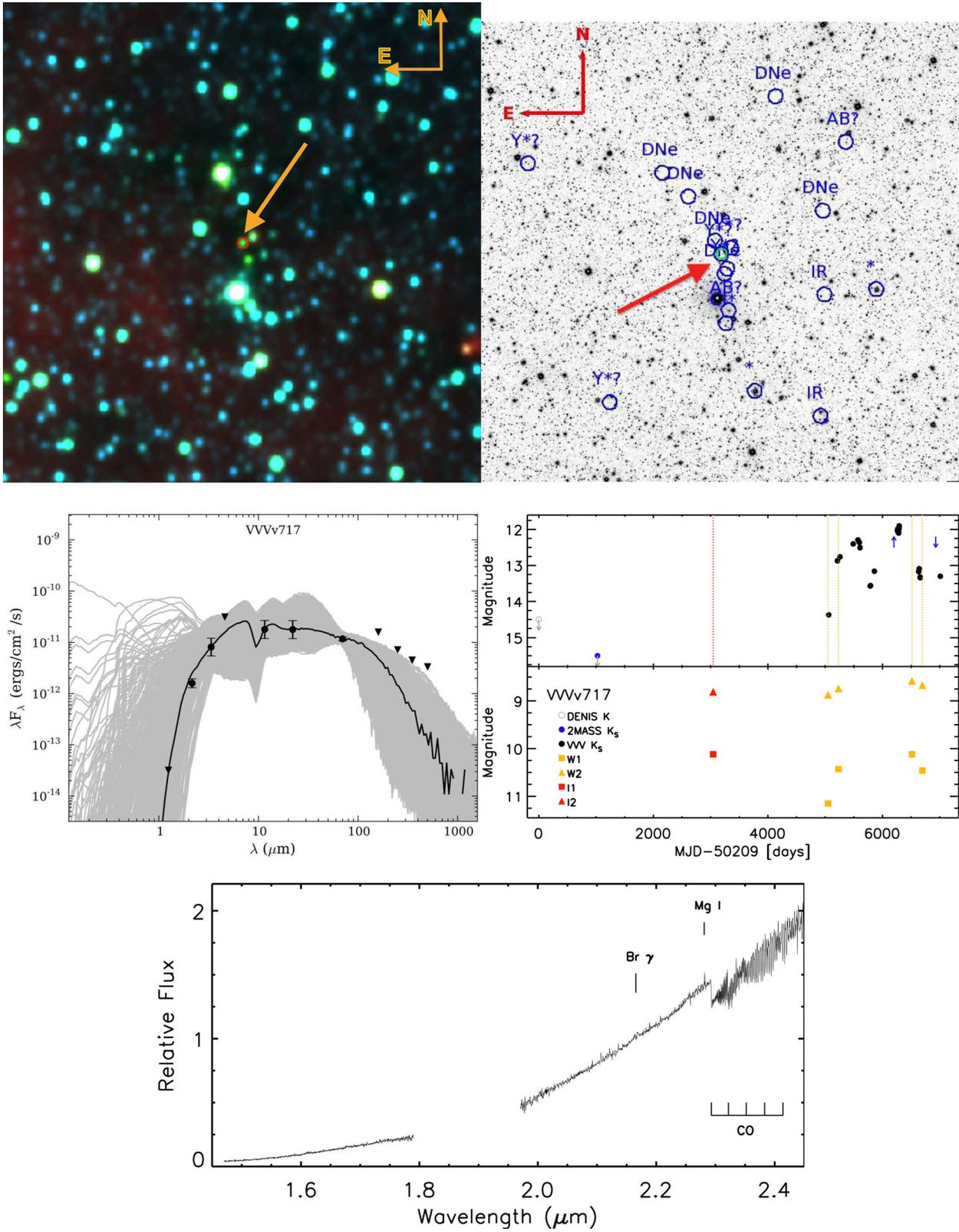
Figure B2. Same as Fig. B1. In the top left, we present a 10 arcmin×10 arcmin *WISE* false colour image of the area near VVVv717.
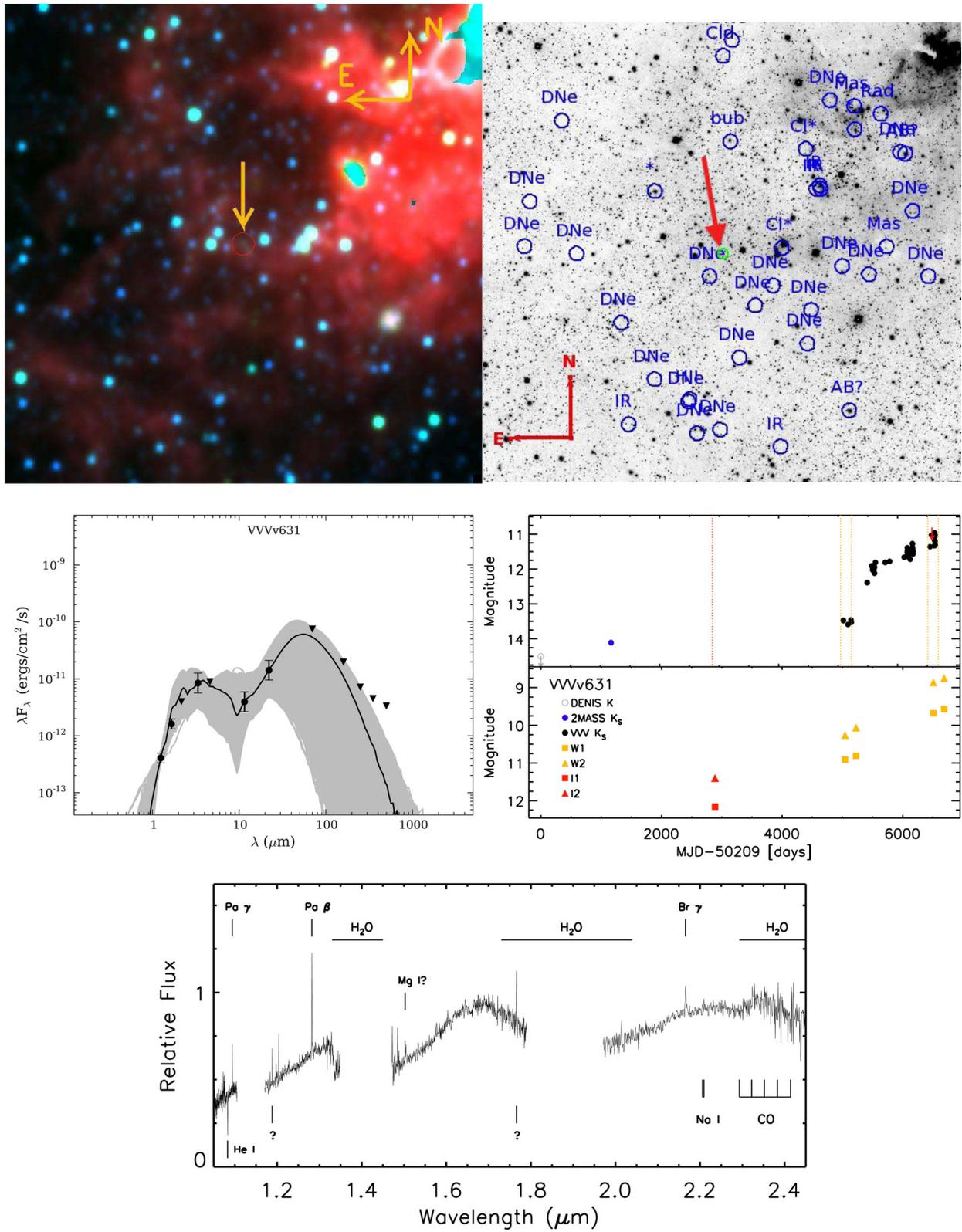
Figure B3. Same as Fig. B1. In the top left, we present a 10 arcmin×10 arcmin *WISE* false colour image of the area near VVVv631.
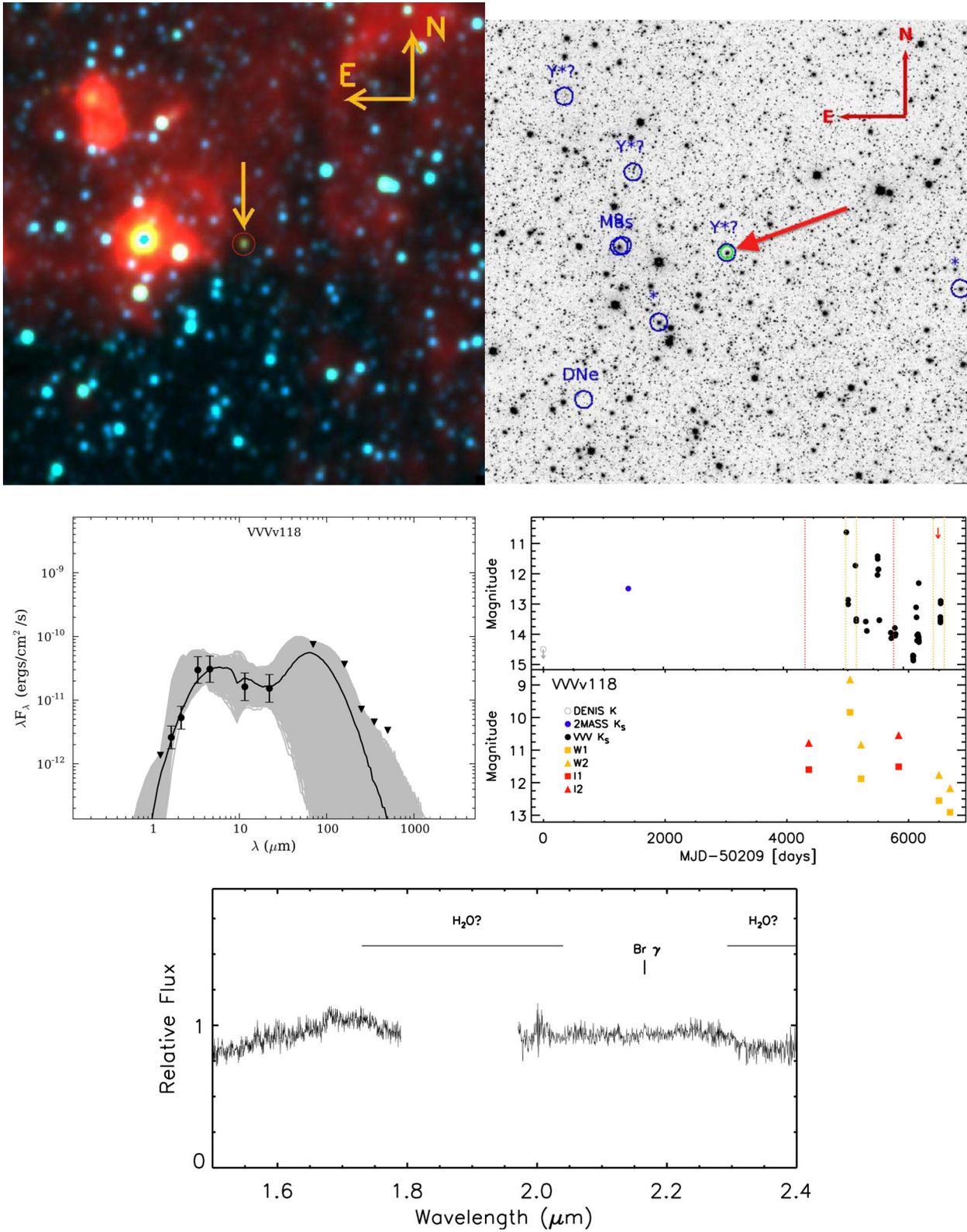
Figure B4. Same as Fig. B1. In the top left, we present a 10 arcmin×10 arcmin *WISE* false colour image of the area near VVVv118.
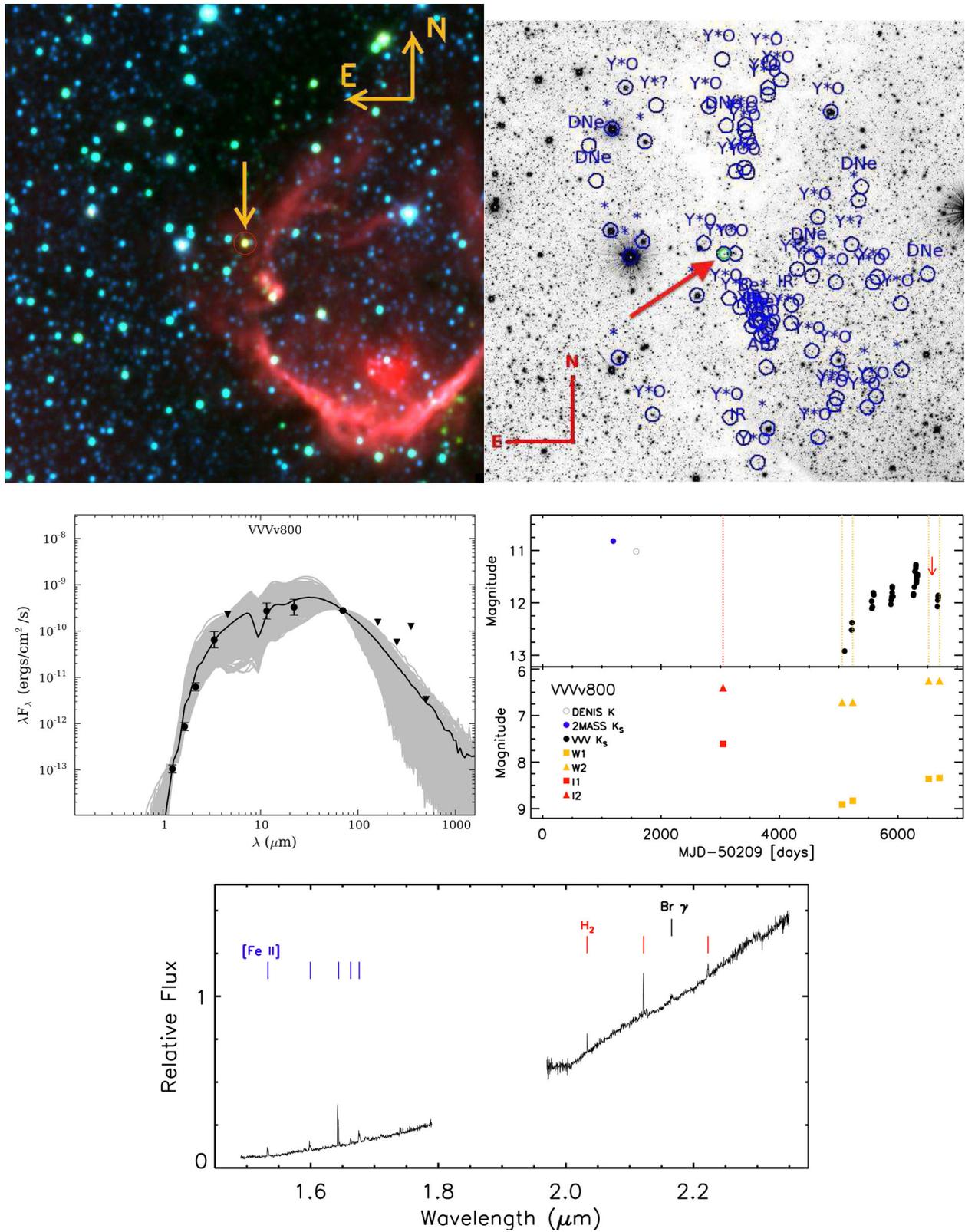
Figure B5. Same as Fig. B1. In the top left, we present a 10 arcmin×10 arcmin *WISE* false colour image of the area near VVVv800.
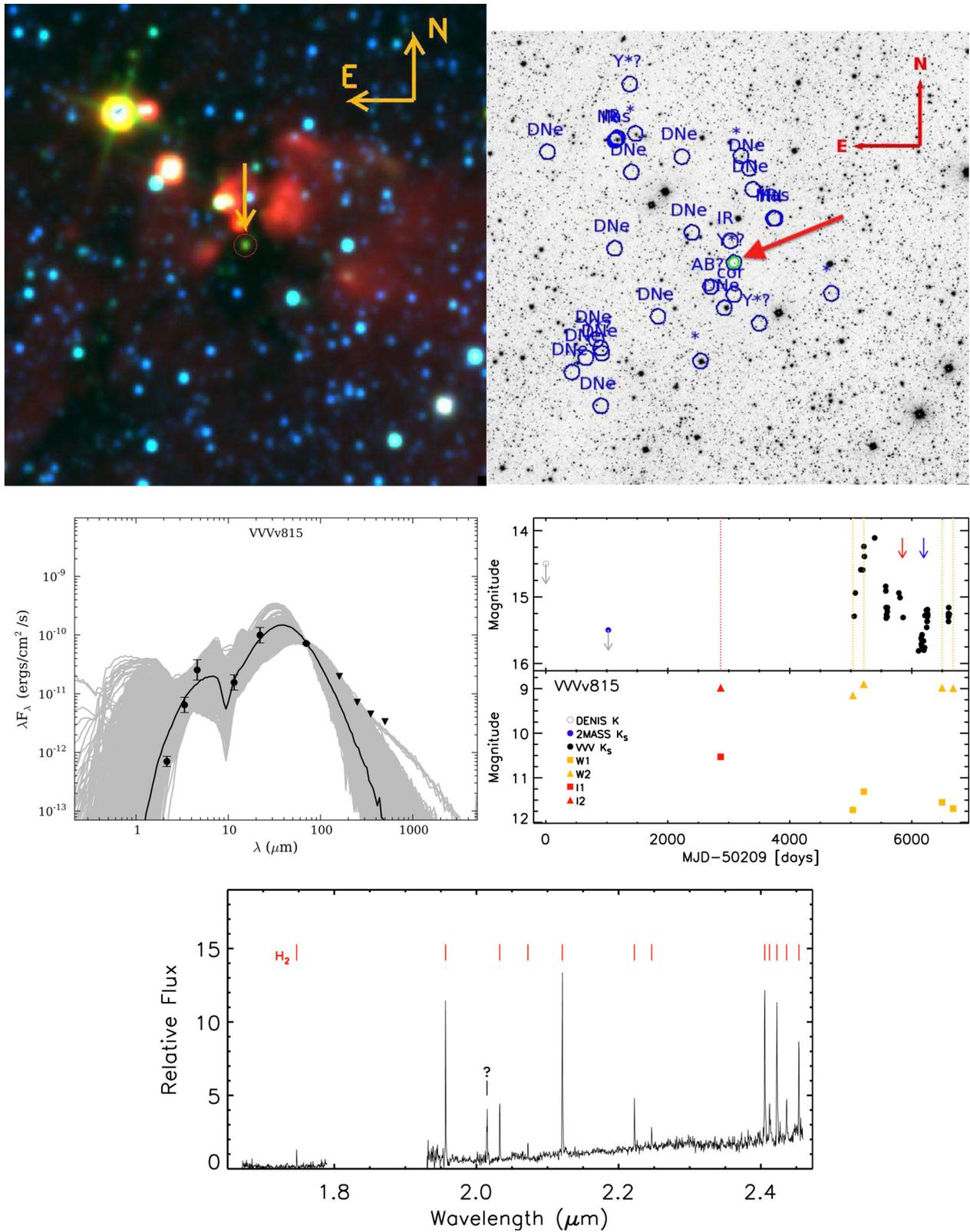
Figure B6. Same as Fig. B1. In the top left, we present a 10 arcmin × 10 arcmin *WISE* false colour image of the area near VVVv815.
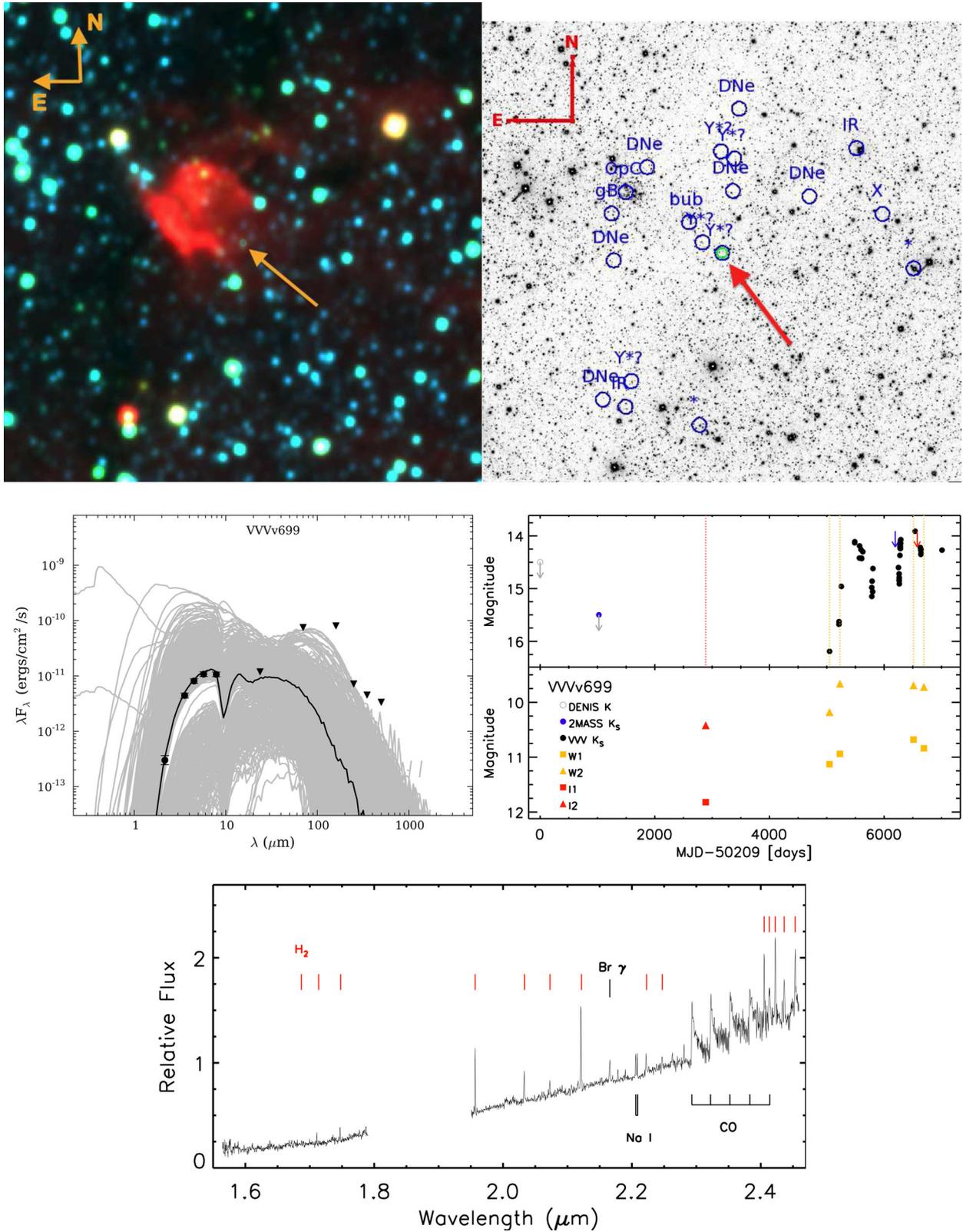
Figure B7. Same as Fig. B1. In the top left, we present a 10 arcmin × 10 arcmin *WISE* false colour image of the area near VVVv699.

APPENDIX C: EVOLVED OBJECTS

In this section, we analyse the objects that show characteristics of being from a different variable class, not related to YSOs. These are found to be likely contaminants of our YSO sample and were not included in the analysis in Section 4.

C1 Novae

Two objects are classified as likely novae. VVVv514 shows $Br\gamma$, Br10 (1.73 μm) and He I (2.058 μm) emission. This object shows a blue SED ($\alpha = -1.41$) and was classified as a fader from its LC in Paper I. Inspection of its LC in Fig. C1 shows that the object went into outburst prior to 2010 and a second peak is apparent at the end of the 2010 campaign. These spectroscopic and photometric characteristics are similar to nova V1493 Aql (Venturini et al. 2004).

The second object, VVVv240, is classified as an LPV (Mira-like) in Paper I. The poor sampling of the data probably led to this classification. The object has a rich emission-line spectrum (Fig. C1) which includes weak $Br\gamma$ and C I lines (2.10, 2.29 μm). The presence of these carbon lines are characteristics of Fe II novae (see e.g. V476 Scuti; Das et al. 2013).

We note that this classification is based entirely on some similarities of our objects with novae. We do not discard the possibility of these objects belonging to a different class of variable stars.

C2 AGB stars

We find that seven VVV objects are more likely AGB stars. Most of these display long-term periodic variability in Paper I, where five are classified as displaying Mira-like LC, whilst VVVv202 is classified as YSO-like. VVVv25 was originally given an eruptive LC classification. The spectra of these objects are dominated by strong CO absorption and in many cases, a lack of other photospheric absorption features, similar to FUors. These objects also show an apparent association with SFRs, e.g. VVVv42 and VVVv45 are located within the G305 star-forming complex (see Fig. C2 for other examples). These characteristics lead to an early idea of these objects being (eruptive) YSOs because the LC are in some cases not truly periodic. However, the recognition that the LC of dusty-AGB stars can have additional trends due to variable extinction on time-scales of years, superimposed on the periodic LC, revived our view that these sources can be dusty AGB stars. Also, sources with Mira-like LC tend to have SEDs that are less well fit by the YSO SED fitting tool (see Fig. C2 and Appendix D) which cast doubt on a YSO classification.

We study the AGB scenario following Contreras Peña et al. (2014), estimating whether an AGB star at the magnitudes of the VVV sources can be found within the Galactic disc. In Contreras Peña et al. (2014), we estimated this parameter by (1) Assuming the source is a Mira variable star with $M_K = -7.25$ (Whitelock, Feast & van Leeuwen 2008) and (2) from the observed $K_s - [9]$ colour of the star and following appendix A of Ishihara et al. (2011).
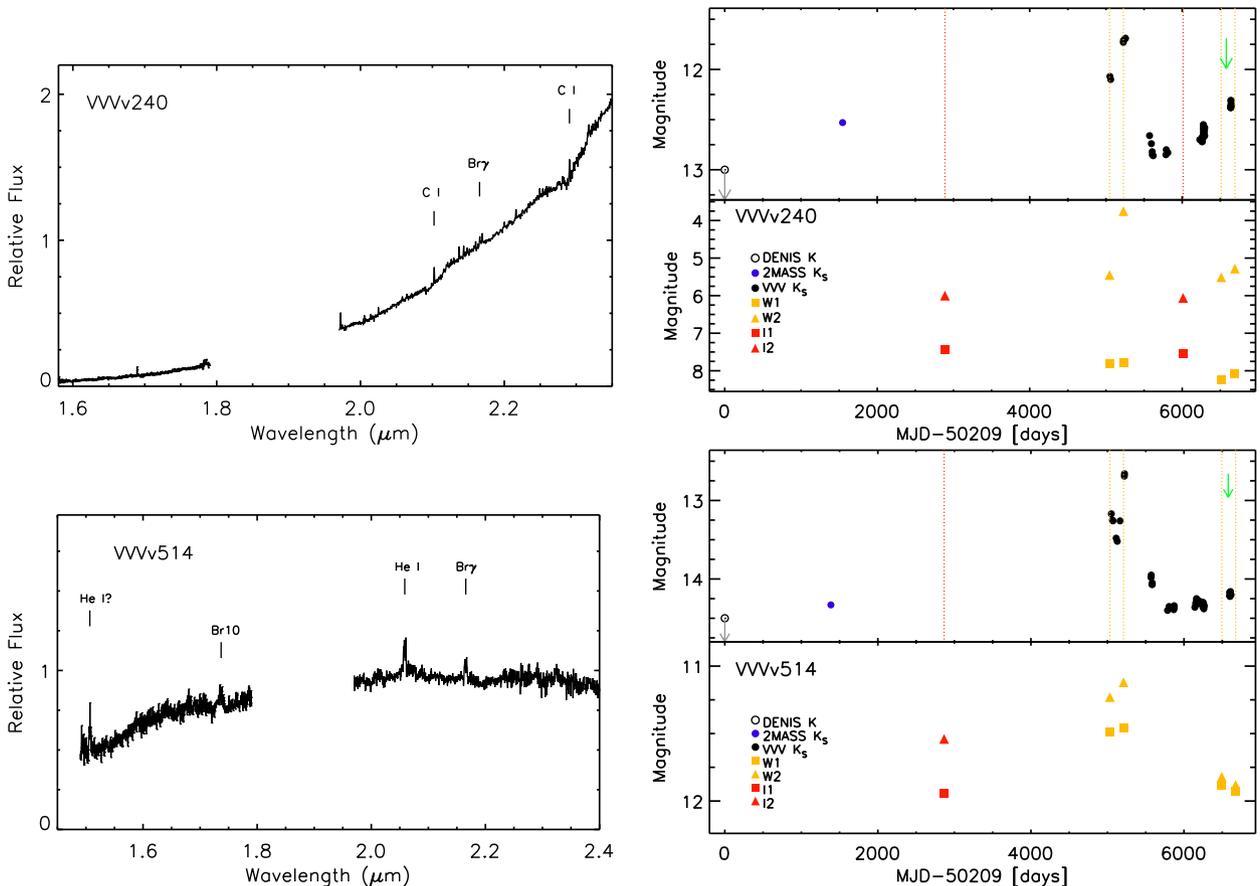

Figure C1. FIRE spectra (left), near- and mid-IR photometry (right) of likely novae VVVv240 (top) and VVVv514 (bottom).
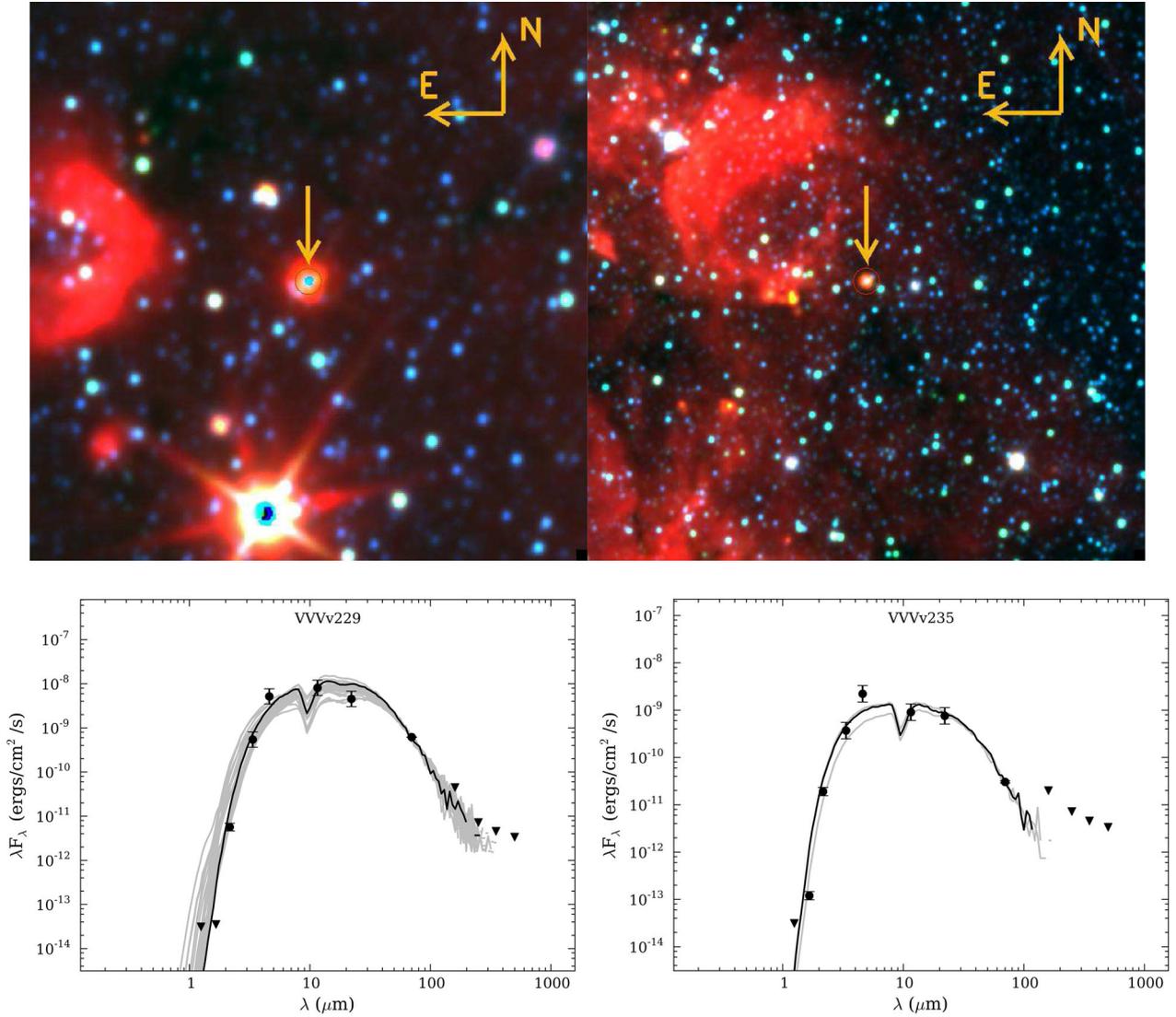
Figure C2. (top) *WISE* false colour images of 10 arcmin×10 arcmin areas centred on objects VVVv229 (left) and VVVv235 (right). (bottom) Robitaille et al. (2007) SED fits for the same objects.

We have shown in Paper I that Mira variable stars are very likely to saturate in VVV, even when considering large distances and extinctions towards the source. Then, evolved long period variables in the sample are very likely AGB stars with thick circum-stellar envelopes, which makes them fainter and thus able to appear at the magnitudes covered in VVV. Given this, method 1 above would not be applicable to our sub-sample of periodic variable stars. This is confirmed by the fact that the periods observed in this sub-sample are not found within 100–400 d, the typical period of Mira variable stars.

The distance estimate from method 2 is subject to several sources of error. The distance equation (A4 in Ishihara et al. 2011) depends on the observed 9 μm flux as well as the mass-loss rate of the object. The latter is derived from the $K - [9]$ colour of the star. Given the high variability on our sample, this value can have errors of about ±1 mag. In addition, the $\log \dot{M}$–$(K - [9])$ relation shows large scatter in fig. A2 of Ishihara et al. which is of the order of $\Delta[\log \dot{M}(M_{\odot} \ yr^{-1})] = \pm 0.5$ dex. These errors propagate into the distance estimate which, for typical values of mass-loss rates and $F_{9 \, \mu m}$ fluxes of our sample, yield $\Delta(\log d) \sim 0.2$ dex.

When discussing the AGB scenario in the following, we will only take into account the distance derived from $K_s - [9]$ colours and appendix A in Ishihara et al. (2011).

(i) VVVv202: the LC of this object was classified as LPV, but YSO-like in Paper I. We note that the latter classification might have been due to the star being saturated in some of the VVV epochs. The projected location of VVVv202 is found in an area of active star formation (see Fig. C2), being 96 arcsec from H II region [CH87] 327.759−0.351 ($v_{LSR} = -75 \ km \, s^{-1}$; Brown et al. 2014) and 202 arcsec from dense core [PLW2012] G327.721−00.383 −075.1 ($v_{LSR} = -95$ to $-55 \ km \, s^{-1}$; Purcell et al. 2012). The radial velocity of VVVv202 ($v_{LSR} = -84.2 \ km \, s^{-1}$, see Table 4) agrees with those of the star-forming regions. We are unable to compare its distance from radial velocity to that of an AGB star given that it is not detected in Akari nor GLIMPSE.

The spectrum of VVVv202 shows strong CO absorption, with Na I and Ca I also in absorption. In addition, this object shows absorption features from $^{12}CO \ v = 3$–0, 4–1 bandheads in its *H*-band spectrum, as well as strong absorption from $^{13}CO \ v = 2$–0, 3–1 at

2.3448 and 2.3739 µm. Absorption from ^{13}CO is usually observed in the spectrum of K–M giant and supergiant stars (see e.g. Wallace & Hinkle 1997). The ^{13}C/^{12}C ratio increases as a consequence of the first dredge up during the star's ascent through the giant branch. The appearance of this feature (in emission) has also been proposed to help distinguish evolved Be from Herbig Ae/Be stars by Kraus (2009). This is very likely an evolved star.

(ii) VVVv25: this object is optically invisible and shows a very similar SED and spectrum to object GPSV15 (Contreras Peña et al. 2014). *WISE* and VVV images with SIMBAD sources overlaid reveal possible association with SFRs.

It is unclear whether the LC is periodic: if so, then the period indicated by the Lomb–Scargle fit from Paper I is very long at ∼5100 d. However, and as noted in Section 4, our analysis of possible periods in Paper I shows that a period of 400–500 d (typical of a carbon star) is amongst the possibilities consistent with the sparsely sampled LC. VVVv25 brightened from 2010 to 2012 and remained stable in 2013. The 2014 photometry shows a small decline which appears to have continued into 2015, based on the K_s datum from the second epoch of VVV multicolour data. In addition, the DENIS ($K = 10.99 \pm 0.06$) and 2MASS ($K_s = 10.59 \pm 0.02$) photometry indicates that this object had been in a bright state previously. However, the LC of the object (until 2014) is consistent with that of an eruptive YSO.

The potential classification as an AGB star is discussed based on similar arguments used for the previous object. A carbon- or oxygen-rich AGB star losing mass at a rate of ∼$10^{-4.8}$ M$_\odot$ yr^{-1} (estimated from the $K - [9]$ colour of VVVv25) would be located at a heliocentric distance of 29^{+17}_{-11} kpc. The radial velocity of VVVv25 indicates $d \sim 10.9$ kpc.

The resemblance of the spectrum with likely eruptive variables from the GPS and its apparent strong association with an SFR would favour a YSO interpretation. However, the radial velocity distance is not far off from the lower end of the distance to an AGB star. In addition, the 2015 spectrum of the object reveals the presence of an absorption bandhead at 1.76 µm, which is more likely from C$_2$. This is generally observed in carbon stars, making VVVv25 more likely an evolved object.

(iii) VVVv42: the star is 1.5 arcsec from IRAS source IRAS 13063−6233 which is classified as a stellar object in SIMBAD. The object is located within 300 arcsec of five IRDCs and is in the vicinity of the G305 star-forming complex. The spectrum of the object is very red and does not show any features that could be associated with a stellar photosphere. The source resembles GPS variable GPSV3 as it is dominated by absorption of low temperature rotational transitions from CO (see Appendix E). However, doubts regarding a YSO classification arise given its periodic LC (see Appendix F) which led to a 'Mira-like' LC classification in Paper I.

The object is detected at 9 µm in the Akari mission with $F_{9\,µm} = 7.53$ Jy. The $K - [9]$ colour would correspond to a dust-enshrouded AGB star losing mass at a rate of $10^{-4.6}$ M$_\odot$ yr^{-1} in the work of Ishihara et al. (2011). A star with that observed flux and mass-loss rate would be located at a distance of ∼14^{+7}_{-4} kpc according to equation A3 of Ishihara et al. which would place VVVv42 within the Galactic disc. The distances estimated from the radial velocity of VVVv42 are $d_{\mathrm{near}} = 4.0$ and $d_{\mathrm{far}} = 6.1$ kpc. We see that d_{near} places this object within the G305 SFC, but d_{far} does not completely disagree with the distance from Akari.

This object is very likely an evolved star. However, some doubt remains given the near-IR spectrum of the object. To our knowledge, dust-enshrouded AGB stars have not previously been seen

with the cold CO signatures observed in VVVv42. However, this feature could be explained if we are observing the circum-stellar dust rather than the stellar photosphere, with CO arising within the circum-stellar envelope at $T \sim 1000$ K. AGB stars show acetylene absorption in the L band which can be explained by a similar effect (see e.g. van Loon et al. 2008).

(iv) VVVv235: the variable star is likely associated with OH maser OH 330.93−0.14 (Sevenster et al. 1997) which is located 1.4 arcsec from the VVV object. This source is also located 164 arcsec from several masers (see Fig. C2) that form the maser cluster OH 330.953−0.182 which is associated with massive star formation (Caswell et al. 2010).

The K_s LC of VVVv235 is also classified as Mira-like in Paper I, which is confirmed by the mid-IR information from *WISE* and NEOWISE. We used the phase dispersion minimization (PDM; Stellingwerf 1978) in IRAF to estimate a period in between 760–790 d. Given this, we have to consider the possibility that the maser emission is not related to star formation but rather to an evolved star. Galactic OH/IR stars are characterized by the presence of this type of maser emission. In addition, the SED of the object does not appear to be fit by the YSO models, having the largest χ^2 in the sample (Table D1).

We find that a dust-enshrouded AGB star with the measured 9 µm flux from the Akari survey could be located at $d \sim 24.7^{+14}_{-9}$ kpc, which is within the Galactic disc edge (located at ∼20.8 kpc at this longitude). However, this distance is much larger than the one estimated from radial velocities. The radial velocity of the object is found to be $v_{\mathrm{LSR}} = -92.8 \pm 0.3$ km s^{-1} ($d_{\mathrm{near}} = 4.8$ kpc, $d_{\mathrm{far}} = 10.6$ kpc). The radial velocity agrees with the velocities found for masers in the maser cluster OH 330.953−0.182 (-80 to -100 km s^{-1}; Caswell et al. 2010). However, the separation of VVVv235 with respect to the maser cluster is large (164 arcsec). In addition, the far kinematic distance is not too dissimilar to the lower limit of the distance from the Akari flux. Schlegel et al. (1998) maps show a large value of the extinction towards VVVv235, with $A_v = 178$ mag. This large value would have a strong effect even at 9 µm, bringing the distance into agreement with the kinematic distance and thus making an AGB classification more likely.

The classification of this object is very likely that of an evolved object.

(v) VVVv796: this star has been previously identified as a YSO in the area of H II region RCW 120 ($d \sim 1.4$ kpc) in the work of Deharveng et al. (2009). These authors identify it based on near- and mid-IR colour-colour selection and it is estimated to be a class I or class II object; our value of α identifies this star as a class I object. Images from VVV (with SIMBAD sources overlaid) and *WISE* show a concentration of YSOs around VVVv796. We note that these are likely YSOs associated with RCW120, classified as such based only on near- and mid-IR colours in the works of Zavagno et al. (2007) and Deharveng et al. (2009).

This is a deeply embedded, optically invisible star which is only detected at H and K_s in VVV. Accordingly, the spectrum of the object lacks any flux at J band. Some flux can be observed at wavelengths greater than 1.5 µm and some H$_2$O absorption could be present. The spectrum steeply rises beyond 2 µm showing deep ^{12}CO absorption. We note that ^{13}CO could also be present in the spectrum of the object.

The LC shows $\Delta K_s = 2.6$ mag and it is also a Mira-like LPV in Paper I. Near- and mid-IR photometry from other surveys proves the high variability of this object. VVVv796 is detected in 2MASS with $K_s = 9.69 \pm 0.02$ and in DENIS with $K = 11.47 \pm 0.11$.

The *WISE* and NEOWISE photometry is contemporary to VVV. The data show $\Delta W1 = 1.5$ and $\Delta W1 = 1.3$ mag, where changes in colours show that extinction might be involved. The variability data from *WISE* also seem to support the periodic variations.

We use PDM in IRAF to determine a period of $P \sim 780$–820 d, with some difficulties in phase folding the LC. The object is detected in the Akari survey and has $F_{9\mu m} = 3.1$ Jy. Using similar arguments as before, we find that a dust-enshrouded AGB star with that flux would be located at a distance of 18^{+10}_{-7} kpc, which puts it within the Galactic disc. The radial velocity yields $d_{near} = 5.1$ kpc, $d_{far} = 12.1$ kpc.

First, we can see that the radial velocity of the object shows that VVVv796 is not associated with RCW120. This was to be expected given the large separation from RCW120 (~ 30 arcmin). Inspection of the Hi-Gal 70 μm image shows some diffuse emission around the object, but does not conclusively prove an active area of star formation.

The far kinematic distance agrees within the errors with the distance estimated to a dust-enshrouded AGB star. The LC of VVVv796 and the possible ^{13}CO absorption also supports the latter interpretation.

The object seems more likely and evolved object.

(vi) VVVv45: this object is located within several star formation indicators associated with the G305 star-forming complex (see e.g. Faimali et al. 2012). VVVv45 is source 33941 in table 2 of the study of YSOs towards the G305 star-forming complex of Baume, Carraro & Momany (2009). This object is selected based on its near-IR colours, but no information can be found whether the authors consider this as a likely YSO and/or a member of the complex.

The SED of this star is consistent with a class I object, with $\alpha = 1.26$. This is an optically invisible object which is not detected at J nor H bands in VVV photometry. The spectrum of the object resembles that of deeply embedded FUor stars, with no flux at wavelengths shorter than 1.9 μm and steeply rising in the K band, with deep CO absorption at 2.29 μm. This object does not show any absorption from H_2O. We note that ^{13}CO at 2.34 μm might be present in the spectrum of the object.

The LC of VVVv45 looks clearly to be periodic resembling the LC of AGB variable stars and with an amplitude of $\Delta K_s = 2.2$ mag. This object had also been detected in 2MASS with $K_s = 13.53 \pm 0.04$ mag. The photometry from the *WISE* surveys also shows the object to be highly variable at mid-IR wavelengths, with $\Delta W1 = 1.4$ and $\Delta W2 = 1.6$ mag. The colour change does not seem consistent with variable extinction. The *WISE* data also support the periodic variability. We use PDM within IRAF to search for a period in the K_s LC of the object. We find $P \sim 520$–530 d, although with some difficulty in phase folding the data. This object has an LPV-Mira classification from paper I.

VVVv45 is detected at 9 μm in the Akari mission with $F_{9\mu m} = 0.52$ Jy. The $K - [9]$ colour would correspond to a dust-enshrouded AGB star losing mass at a rate of $\sim 10^{-4.6}$ $M_{\odot}$ yr^{-1} in the work of Ishihara et al. (2011). A star with that observed flux and mass-loss rate would be located at a distance of 44.6^{+26}_{-16} kpc according to equation A3 of Ishihara et al. The estimated distances to a dust-enshrouded AGB star are much larger than the distance to the Galactic disc edge. However, we note that the large extinction towards this source, with $A_v \sim 137$ mag from Schlegel et al. (1998) maps could put the object within the Galactic disc. The radial velocity of VVVv45 (see Table 6) places the object at $d \sim 11.6$ kpc

The spectrum of this object points to an embedded YSO classification. However, the distance derived from its radial velocity places it outside the G305 star-forming complex and if the ^{13}CO is present

in the spectrum, then this object is more likely to be an evolved object. The periodicity of the LC also supports an AGB interpretation. This object is more likely an evolved star.

(vii) VVVv229: the projected location of this star is within 300 arcsec from several indicators of active star formation. The star is not detected in both J and H bands in VVV and its spectrum shows the lack of flux at these wavelengths, rapidly rising towards 2 μm and only showing CO absorption at 2.29 μm. This is all in agreement with a FUor classification. However, there are several characteristics that point towards a different classification of the star. The LC is clearly periodic with an amplitude of $\Delta K_s = 3.7$ mag, making it the most extreme in the spectroscopic sample and the second most extreme in the whole VVV sample, with the first being VVVv360, an OH/IR star. Its $K - [12]$ colour (using *WISE* filter $W3$) is 14 mag (see Fig. 1), which is typical of dust-enshrouded AGB stars (see the discussion on these type of variable stars in Contreras Peña et al. 2014) and larger than any other object in the spectroscopic sample. The star is clearly not well fitted by the YSO models of Robitaille et al. (2007), having the second largest χ^2 of the spectroscopic sample (see Appendix D).

The observed 9 μm flux is also the largest of the sample, with $F_{9\mu m} = 37.8$ Jy. An OH/IR star with this flux can easily be found within the Galactic disc at a distance of 8.6^{+4}_{-3} kpc and show up in VVV. Distance which somewhat agrees with d_{far} of 11.4 kpc from the radial velocity of the source.

Thus, this object is much more likely an evolved star rather than a YSO.

APPENDIX D: SED FITS

We use the command-line version of the SED fitting tool of Robitaille et al. (2007) to provide a rough estimate of the physical properties of objects in the sample. We note that in our analysis, this tool is used as a measurement of how well the SED of our objects can be fitted by that of a YSO and we do not take the values of physical parameters as reliable estimates for our variable stars. Nevertheless, these results do allow us to make some general remarks about the likely characteristics of the sample.

For the SED fits, we use photometry arising from VVV (JHK_s; Paper I), *WISE* $W1 - W4$ (Wright et al. 2010) or (when necessary) *Spitzer* IRAC $I1 - I4$ and MIPS 24 μm data from the GLIMPSE and MIPSGAL surveys (Benjamin et al. 2003; Carey et al. 2009). We note that this process is unreliable given that the Robitaille et al. fits might not be able to describe these highly variable sources. In addition, the near- and mid-IR photometric measurements are not contemporaneous. To minimize the latter problem, we combine the contemporaneous VVV JHK_s data from 2010 with *WISE* data taken in the same year, in preference to *Spitzer* data from the earlier GLIMPSE survey. If a *WISE* detection is lacking due to source confusion which occurred for seven sources, *Spitzer* GLIMPSE photometry is fed to the fitting tool. The effect of using *Spitzer* data taken in 2003 and 2004 is discussed below. A 2 arcsec cross-match radius was used for *WISE* and MIPSGAL matches to each VVV source, whereas a 1 arcsec radius was used for GLIMPSE data. In an additional attempt to minimize the effect of using non-contemporanoues data, we also feed the tool with larger uncertainties for the data. Typically, we used 0.2 mag for near-IR (JHK_s) observations and 0.4 mag for mid-IR data from *WISE* or *Spitzer*. Far-IR fluxes are estimated from Hi-GAL PACS and/or SPIRE photometry (Molinari et al. 2010). Detections at 70 μm are given as data points to the tool, whilst detections at longer wavelengths are given as upper limits. If the objects are not detected at these wavelengths, then we provided

Table D1. Parameters derived from the Robitaille et al. models SED fitting as explained in the text.

Object	M_* (M$_\odot$)	log $\dot{M}_{env}$ (M$_\odot$ yr^{-1})	log $\dot{M}_{disc}$ (M$_\odot$ yr^{-1})	log Age (yr)	d (kpc)	log L_{bol} ($L_\odot$)	χ^2_{best}/N	N_{fits}	N_{fits2}
VVVv20	3.0 ± 2.7	-5.7 ± 0.7	-8.1 ± 1.5	5.2 ± 0.6	$2.5^{+3.6}_{-2.4}$	1.5 ± 1.2	0.09	10 000	9715
VVVv32	2.5 ± 2.2	-5.7 ± 0.8	-8.3 ± 1.4	5.3 ± 0.7	$3.1^{+3.6}_{-3.0}$	1.3 ± 1.1	0.01	10 000	8169
VVVv63	2.2 ± 1.6	-6.6 ± 1.0	-8.7 ± 1.6	6.3 ± 0.5	3.4 ± 3.3	1.0 ± 1.2	0.01	10 000	4572
VVVv65	1.8 ± 1.7	-6.3 ± 1.0	-9.0 ± 1.4	6.0 ± 0.6	$2.1^{+2.9}_{-2.0}$	0.7 ± 1.2	0.01	10 000	5152
VVVv94	2.4 ± 1.5	-7.3 ± 0.8	-8.4 ± 1.4	6.3 ± 0.4	$0.9^{+1.3}_{-0.8}$	1.1 ± 0.9	0.01	6200	3303
VVVv118	2.5 ± 2.1	-7.2 ± 0.9	-9.0 ± 1.6	6.2 ± 0.4	$1.5^{+2.7}_{-1.4}$	1.1 ± 1.2	0.04	10 000	3647
VVVv193	1.7 ± 1.5	-6.7 ± 0.9	-9.1 ± 1.3	6.0 ± 0.5	$1.1^{+1.9}_{-1.0}$	0.5 ± 0.9	0.01	10 000	6563
VVVv270	2.3 ± 1.8	-5.4 ± 0.9	-8.0 ± 1.4	5.3 ± 1.0	3.5 ± 3.3	1.3 ± 0.8	0.01	10 000	8190
VVVv322	$1.5^{+1.6}_{-1.4}$	-5.2 ± 0.7	-8.1 ± 1.4	5.0 ± 0.8	3.6 ± 3.2	0.9 ± 0.9	0.01	10 000	8613
VVVv374	4.2 ± 2.1	-7.7 ± 0.4	-8.6 ± 1.4	6.6 ± 0.3	$1.2^{+1.5}_{-1.1}$	2.3 ± 0.6	0.35	610	26
VVVv405	4.8 ± 4.1	-5.3 ± 0.9	-6.9 ± 1.6	4.7 ± 1.3	$3.7^{+4.4}_{-3.6}$	2.3 ± 1.2	0.05	2154	1846
VVVv406	2.8 ± 2.6	-5.2 ± 0.6	-8.0 ± 1.7	5.0 ± 0.7	$2.2^{+3.0}_{-2.1}$	1.6 ± 1.0	0.01	10 000	9300
VVVv452	2.1 ± 1.8	-5.6 ± 0.9	-8.5 ± 1.5	5.5 ± 0.9	2.8 ± 2.7	1.2 ± 1.0	0.02	10 000	8171
VVVv473	$1.5^{+2.0}_{-1.4}$	-5.8 ± 0.6	-8.7 ± 1.3	5.2 ± 1.0	$0.5^{+0.7}_{-0.4}$	0.7 ± 1.1	1.17	4222	3053
VVVv480	1.4 ± 1.3	-6.5 ± 1.1	-9.0 ± 1.5	6.1 ± 0.7	4.2 ± 3.9	0.5 ± 1.1	0.04	10 000	5324
VVVv562	2.8 ± 2.0	-6.3 ± 1.0	-8.7 ± 1.4	6.1 ± 0.7	$2.8^{+3.1}_{-2.7}$	1.4 ± 1.2	0.01	10 000	5946
VVVv625	$0.8^{+1.0}_{-0.7}$	-7.4 ± 0.9	-10.2 ± 1.4	6.1 ± 0.4	$0.3^{+0.9}_{-0.2}$	0.0 ± 0.7	0.08	10 000	4348
VVVv628	$0.7^{+1.1}_{-0.6}$	-7.3 ± 1.0	-10.3 ± 1.7	6.2 ± 0.5	$1.0^{+1.8}_{-0.9}$	-0.4 ± 1.0	0.11	10 000	3456
VVVv630	$0.7^{+0.9}_{-0.6}$	-7.3 ± 1.1	-11.1 ± 2.2	6.2 ± 0.5	$0.4^{+1.1}_{-0.3}$	-0.4 ± 0.8	0.01	10 000	2742
VVVv631	1.8 ± 1.7	-5.4 ± 0.6	-8.3 ± 1.4	5.1 ± 0.6	$2.5^{+2.8}_{-2.4}$	1.0 ± 0.9	0.01	10 000	8986
VVVv632	2.7 ± 2.1	-5.6 ± 0.8	-8.1 ± 1.5	5.4 ± 1.0	2.5 ± 2.4	1.5 ± 0.9	0.22	4769	3667
VVVv662	$0.3^{+0.5}_{-0.2}$	-5.9 ± 0.4	-9.1 ± 1.3	5.1 ± 0.4	0.3 ± 0.2	-0.2 ± 0.4	0.03	2934	2890
VVVv665	1.8 ± 1.1	-7.6 ± 0.7	-8.8 ± 1.4	6.2 ± 0.5	0.4 ± 0.3	0.8 ± 0.7	0.20	1230	539
VVVv699	5.6 ± 2.4	-7.8 ± 0.7	-7.3 ± 1.1	6.5 ± 0.3	5.1 ± 3.5	2.7 ± 0.7	0.02	1960	50
VVVv717	2.9 ± 2.2	-7.6 ± 0.8	-8.4 ± 1.5	6.3 ± 0.4	$1.8^{+2.6}_{-1.7}$	1.4 ± 1.2	0.03	9474	2988
VVVv721	2.4 ± 2.1	-5.4 ± 0.8	-8.0 ± 1.5	5.2 ± 0.9	2.9 ± 2.8	1.4 ± 1.0	0.03	10 000	8186
VVVv800	4.5 ± 3.9	-5.4 ± 0.9	-7.0 ± 1.5	4.7 ± 1.1	$3.8^{+4.4}_{-3.7}$	2.2 ± 1.2	0.18	1573	1389
VVVv815	2.8 ± 2.5	-5.4 ± 0.9	-7.1 ± 1.5	4.5 ± 1.1	$3.0^{+3.1}_{-3.0}$	1.6 ± 1.0	0.48	4336	4011
Non-YSOs									
VVVv25	7.7 ± 4.9	-7.5 ± 0.8	-7.2 ± 1.5	6.4 ± 0.3	$2.7^{+3.1}_{-2.6}$	3.1 ± 0.9	0.60	1214	2
VVVv42	8.4 ± 5.1	–	-8.0 ± 1.9	6.4 ± 0.3	2.0 ± 1.9	3.2 ± 0.9	1.59	139	0
VVVv45	6.6 ± 3.7	-7.5 ± 1.1	-7.9 ± 1.4	6.5 ± 0.3	2.4 ± 2.3	2.9 ± 0.8	2.48	3464	39
VVVv202	2.8 ± 2.3	-6.8 ± 1.0	-9.4 ± 1.5	6.2 ± 0.4	$1.0^{+2.2}_{-0.9}$	1.2 ± 1.1	0.38	6090	2879
VVVv229	7.5 ± 2.4	–	-8.1 ± 0.9	6.4 ± 0.2	0.5 ± 0.4	3.3 ± 0.4	3.01	62	0
VVVv235	10.0 ± 1.8	–	-8.4 ± 0.3	6.4 ± 0.1	1.3 ± 0.5	3.7 ± 0.3	3.61	3	0
VVVv240	6.8 ± 3.2	–	-7.4 ± 1.2	6.4 ± 0.3	1.6 ± 1.5	3.0 ± 0.7	0.40	1180	0
VVVv514	$0.4^{+0.5}_{-0.3}$	-7.7 ± 0.9	-12.7 ± 1.9	6.4 ± 0.4	0.3 ± 0.2	-0.7 ± 0.6	0.01	10 000	2319
VVVv796	9.5 ± 4.1	–	-7.5 ± 1.6	6.3 ± 0.2	2.7 ± 2.0	3.5 ± 0.7	0.15	430	0

the fitting tool with upper limit fluxes from Elia et al. (2013). The interstellar extinction and distance to the objects where left as free parameters, with $A_v = 1$–50 mag and $d = 0.1$–13 kpc.

Table D1 shows the weighted mean values for different parameters of the spectroscopic sample. The weights are taken as the inverse of χ^2, so results from the best fits are given greater weights when estimating the mean value. The values are determined using the models for which $\chi^2 - \chi^2_{best} < 3N$ (as suggested in Robitaille et al. 2007), where N is the number of data points used for the fits. These physical parameters include the stellar age, mass, M_*, envelope infall rate, $\dot{M}_{env}$, disc mass accretion rate, $\dot{M}_{disc}$, luminosity of the system, L_{tot}, and distance to the system, d. We also provide information regarding the χ^2 per data point of the best-fitting model,

χ^2_{best}/N and the number of fits used to derive the weighted mean values, N_{fits}. We note that the envelope infall rate is derived only using those models which had a non-zero value for this parameter. The number of models which fulfil this condition are given by N_{fits2} in the table. In this table, we have divided objects according to the final classification given in this work, i.e. between objects with characteristics of YSOs and those that are more likely evolved objects, such as AGB stars and Novae.

The values of χ^2/N provided in Table D1 are small in many cases. This might suggest that the error bars are overestimated (which is a result of our attempt to minimize the effect of using non-contemporaneous data), or alternatively that the fitting tool has so many free parameters and such a large library of model results that
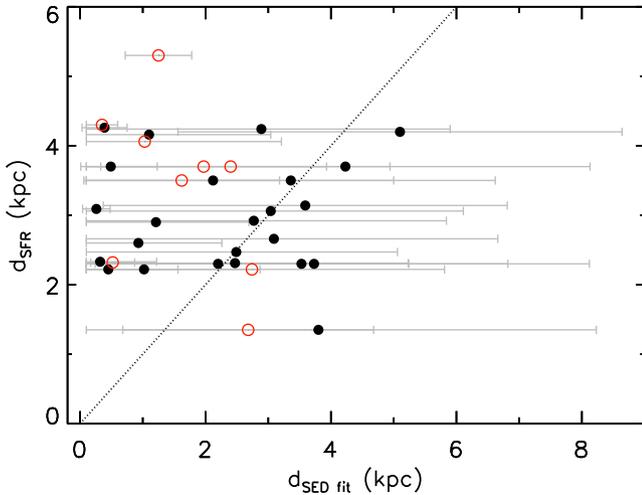
Figure D1. Comparison of the distances from SFRs taken from literature sources, d_{SFR} and those provided by the results from SED fits. Objects later classified as more likely non-YSOs are marked by red circles. The dotted line marks the identity line. For the sake of simplicity, we do not give errors on d_{SFR} because this is difficult to do accurately.

it can often find a perfect fit between YSO data and a given YSO model, with suitable reddening and inclination of the system. Given this, and as mentioned before, the values obtained from SED fits are only used to make general remarks regarding the likely properties of the spectroscopic sample.

We studied the effect that using photometry from a different survey or giving a narrow range in distance had on the final values of physical parameters presented in Table D1. In both cases, we find that although the weighted means suffer a change, these variations are always smaller than the errors on the estimation of the physical parameter. Thus, we always prefer the use of *WISE* photometry given that these observations overlap with VVV (or at least occur a few months apart). Due to the possibility of misassociation with an SFR due to chance projection, we prefer the use of a range 0.1–13 kpc for all the fits.

From Table D1, we first see that objects which are classified as Mira-like from their LC in Paper I, and also have other characteristics that support an AGB classification as discussed later on this work, tend to have poor fits to the model grid. In fact, we see that 26/28 YSOs show $\chi^2/N < 0.4$, whilst the majority of non-YSOs (6/9) show $\chi^2/N > 0.4$. The three non-YSOs with $\chi^2/N < 0.4$, VVVv202, VVVv514 and VVVv796 are classified as non-YSOs based on their spectroscopic and photometric properties (see Appendix C).

The use of a large range in distance allows us to check whether the distance provided by the fitting tool, d_{fit}, agrees with that of the SFR to which the object appears to be associated with. Fig. D1 shows the comparison of d_{fit} with the literature based estimate d_{SFR}, for objects where d_{SFR} is available. It is hard to see a correlation between the two measurements, even considering only the likely YSOs (black circles in Fig. D1). However, in most cases, the distances agree within the (large) errors estimated from the SED fits, so the apparent lack of correlation may well be due to the large uncertainties. The d_{SFR} values will also be uncertain or simply wrong in cases of chance projection. Fortunately, both methods agree that distances for most of the YSOs are larger than 2 kpc. The stellar masses and luminosities of most of the objects are also found to be larger than the ones observed in the UKIDSS GPS sample of Contreras Peña

et al. (2014). This agrees well with our suggestion in Paper I that the VVV is detecting a larger number of more distant, higher luminosity YSOs than UGPS due to the mid-plane location of the VVV sample. The fitted masses typically correspond to intermediate-mass YSOs but they span a wide range. The possibility that some of the highly variable YSOs in the full VVV photometric sample may be high-mass objects is the subject of a separate paper (Kumar et al. 2016).

The disc accretion rates indicated by the SED fits are typically a few $\times 10^{-9}$ $M_{\odot}$ yr^{-1}. This is lower than the expected level for low-mass EXors during outburst (e.g. Audard et al. 2014) and lower than the 10^{-3} to 10^{-6} $M_{\odot}$ yr^{-1} seen in the accretion events of FUors. As we have shown, the sample is dominated by emission-line objects with EXor-like spectra rather than FUors, but these accretion rates still appear low for relatively luminous YSOs at distances of a few kiloparsecs. However, we use 2010 photometry for the SED fits, an epoch in which the majority of the objects, from the inspection of their LC, appears to be at quiescent states (with the exception of some objects that show fading LC such as VVVv562, see Section 4.3). In Section 5.2, we estimate accretion luminosities, L_{acc}, using the Brγ emission line observed in most of the YSOs. The accretion rates derived from L_{acc} for these objects show higher values than those from SED fits and more in line with the values expected in eruptive variables. The spectra were typically taken when the sources were brighter.

APPENDIX E: CO MODEL

In this section, we present a first attempt to determine the temperature of the region responsible for the CO emission/absorption in some of our objects. This is based on the modelling of the CO band emission from MCW 349 (a peculiar B[e] star) done by Kraus et al. (2000). A brief explanation of the basics of the model is presented below.

The energy of the rovibrational states (v, J) of a diatomic molecule are expanded in the following way (from Dunham 1932)

$$E(v, J) = \sum_{k,l} Y_{k,l} \left(v + \frac{1}{2} \right)^k \left(J^2 + J \right)^l, \tag{E1}$$

with $Y_{k,l}$ the Dunham coefficients which, for CO, are taken from Farrenq et al. (1991). Now, assuming that the gas is in local thermodynamic equilibrium, then the levels are populated according to

$$n_{v,J} = \frac{n}{Z}(2J+1)e^{\frac{-E(v,J)}{kT}}, \tag{E2}$$

where n and T are the total number density and temperature of CO molecules and Z corresponds to the partition function. The latter has been derived by summing over vibrational levels up to $v = 15$ and rotational levels up to $J = 110$, where the states with larger quantum number contribute little to the partition function due to their low-level populations.

The absorption coefficient is calculated from

$$\kappa_v = \frac{c^2 n_{v,J} A_{vJ;v'J'}}{8\pi v^2} \left(\frac{2J+1}{2J'+1} \frac{n_{v',J'}}{n_{v,J}} - 1 \right) \phi(v), \tag{E3}$$

with v and J the indices for the upper energy level, whilst v' and J' are for the lower energy level. $\phi(v)$ is the line profile function and $A_{vJ;v'J'}$ the Einstein A coefficient which are taken from Chandra, Maheshwari & Sharma (1996).

The absorption coefficient is assumed to be constant along the line of sight; in this way, the optical depth is simply the product of

Table E1. Temperature, T, and column density, N_{CO}, estimated from fitting the CO model to the observed spectrum of VVV objects.

Object	T (K)	N_{CO} (cm^{-2})
Emission		
VVVv32	2500	3×10^{20}
VVVv193	2500	1×10^{20}
VVVv270	2700	1×10^{20}
VVVv665	2900	6×10^{20}
VVVv699	2900	5×10^{20}
Absorption		
VVVv25	1800	2×10^{20}
VVVv42	1100	9×10^{19}
VVVv45	2100	5×10^{20}
VVVv229	1600	3×10^{20}
VVVv235	2100	5×10^{20}
VVVv322	2700	2×10^{20}
VVVv628	3200	1×10^{20}
VVVv630	3100	1×10^{20}
VVVv717	1600	2.5×10^{20}
VVVv721	2200	1×10^{20}
VVVv796	2800	2×10^{20}

the absorption coefficient per CO molecule times the CO column density, i.e.

$$\tau_\nu = N_{CO} \times \sum_{\text{lines}} \frac{\kappa_\nu}{n}. \tag{E4}$$

The line profile function is assumed to be Gaussian (neglecting disc rotation) of the form

$$\phi(\nu) = \frac{c}{\sqrt{\pi}\nu_0 v_g} \exp\left[-\frac{c^2}{v_g^2}\left(\frac{\nu - \nu_0}{\nu_0} \right)^2 \right], \tag{E5}$$

with v_g the width of the Gaussian profile, where the dominant broadening mechanism corresponds to the instrumental resolution. In these preliminary calculations, we assume $v_g = 50 \, \text{km s}^{-1}$, the instrumental resolution of the FIRE spectrograph.

Finally, the flux of the absorbing CO gas will be given by

$$I_\nu = B(\lambda, T)e^{-\tau_\nu}, \tag{E6}$$

and

$$I_\nu = B(\lambda, T)(1 - e^{-\tau_\nu}), \tag{E7}$$

for the emitting gas.

In these preliminary calculations, we assume that this is the emission/absorption arising from a non-moving cloud of gas. We intend to include the effect of rotation and inclination of an accretion disc as well as the varying of the temperature and density profiles with distance to the central star (following e.g. Najita et al. 1996). In addition, in these preliminary attempts the best models are obtained by manually varying the temperature and column density of the gas until obtaining a model that best described the observations.

In the case of CO emission, we find that objects that show this characteristic can be fitted by models with temperatures between 2500 and 3500 K and column densities in between 9×10^{19} and 6×10^{20} cm^{-2} (see Table E1). The range in temperatures agrees with those expected to give rise to CO emission in gaseous discs of YSOs. Fig. E1 shows the results of applying the model ($T = 2900$ K, $N_{CO} = 6 \times 10^{20}$ cm^{-2}) to VVVv665. Here, we observe that the observed profile of the $\nu = 2$–0 bandhead seems to be broader than
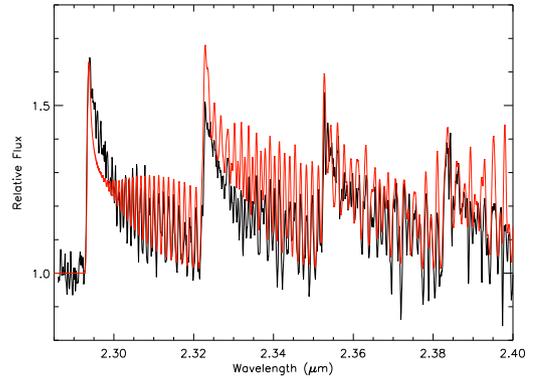
Figure E1. Observed spectrum (black line) and CO model (red line) for VVVv665. The model is derived using $T = 2500$ K and $N_{CO} = 6 \times 10^{20}$ cm^{-2}.
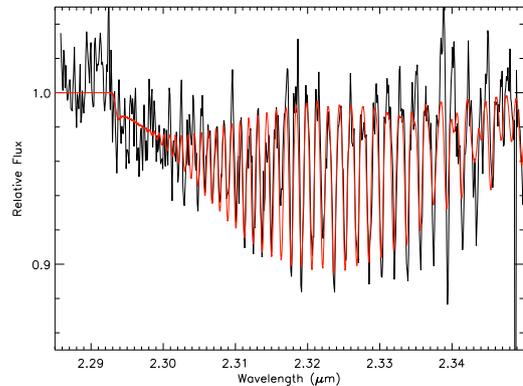
Figure E2. Observed spectrum (black line) and CO model (red line) for VVVv42. The model is derived using $T = 1100$ K and $N_{CO} = 9 \times 10^{19}$ cm^{-2}.

the one produced by the model. Increasing the values of the column densities produces a broadening of the bandhead profile (Kraus et al. 2000). However, even with high values of N_{CO}, the broad CO profile of VVVv665 cannot be reproduced. Rotation in Keplerian discs have been shown to produce broadened CO bandhead profiles (see e.g. Najita et al. 1996; Davies et al. 2010). Although this needs a more detailed investigation, the observed broadened profile might give the evidence of the presence of an accretion disc in VVVv665.

We also estimate temperatures for objects showing CO absorption, a sample mainly composed of the FUor candidates that were shown in previous sections. One particularity interesting case is VVVv42. Here the absorption seems to arise from cooler CO gas given the lack of prominent bandhead absorption and stronger absorption from low-J transitions of the CO $\nu = 2$–0 state. The observations are best fitted by models with $T \sim 1100$ K. The object resembles likely eruptive variables GPSV3 and GPSV15 in Contreras Peña et al. (2014). Applying the model to these objects yield similar results ($T \sim 1100$–1800 K). Contreras Peña et al. (2014) have argued that absorption in these objects might be arising from an ejecta (as in GPSV15) or from outer parts of the disc. Davies et al. (2010) shows that the CO absorption observed in W33A is due to cool gas ($\sim$30 K) in the envelope of the massive YSO. Then it is possible that we are observing a similar effect in our VVV object. Fig. E2 shows the results of applying the model to VVVv42.

APPENDIX F: SPECTRA AND LC OF VVV HIGH-AMPLITUDE VARIABLES

Here we show the 37 Magellan/FIRE spectra and the 2010–2015 VVV LC for all the high-amplitude variables discussed in this paper. We mark some of the most prominent features observed in the spectra. The preliminary LC classifications from Paper I are indicated for each source. Note that these were based on the 2010–2014 photometry only, not including the final datum from 2015, and a few of these initial classifications were found to be incorrect after consideration of the spectra and other data; see the main text. The final classifications for the objects are also indicated in each figure. In the LC plots, the date of spectroscopic follow-up is marked with a blue dashed line.
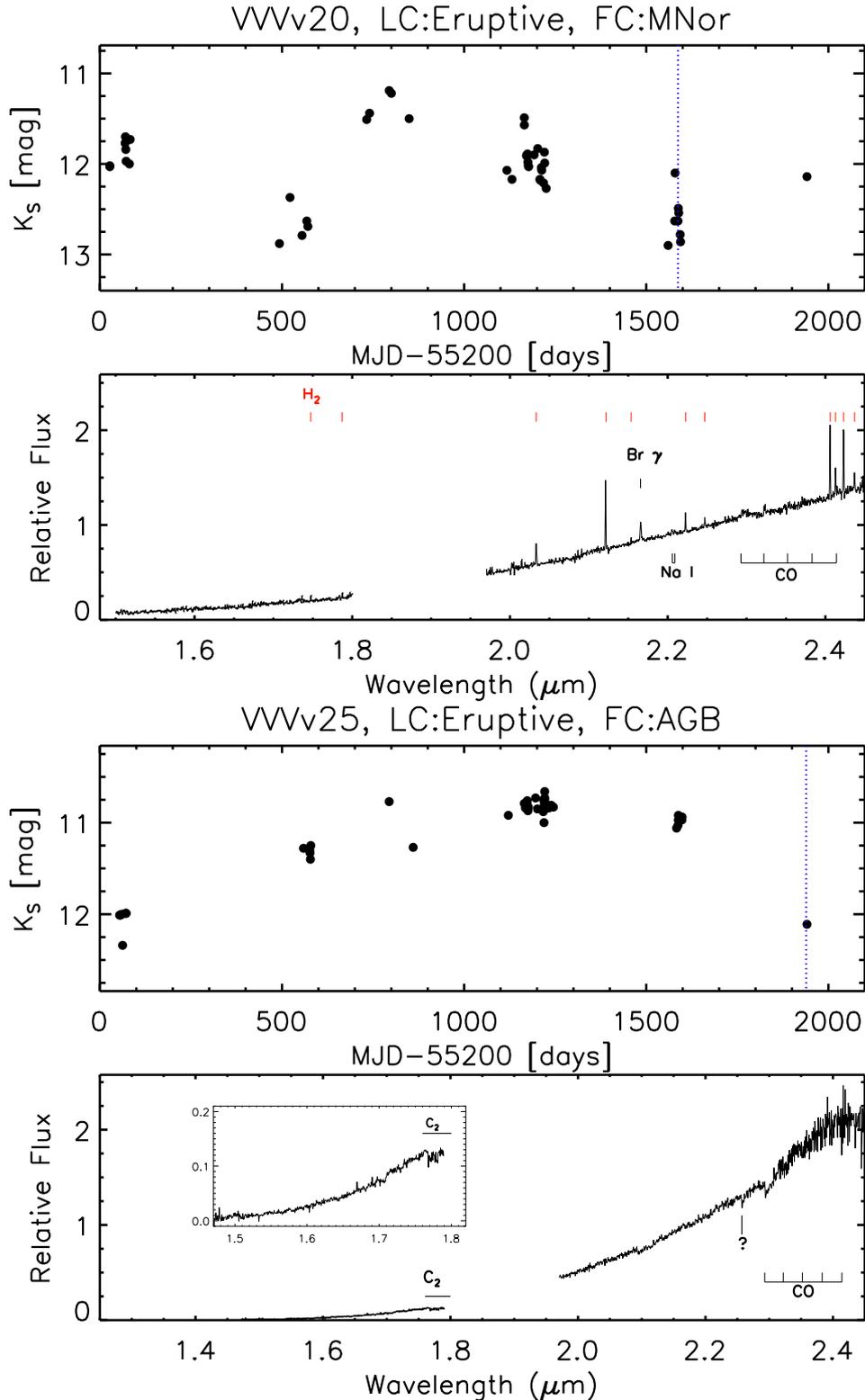

Figure F1. FIRE spectra and K_s LC.
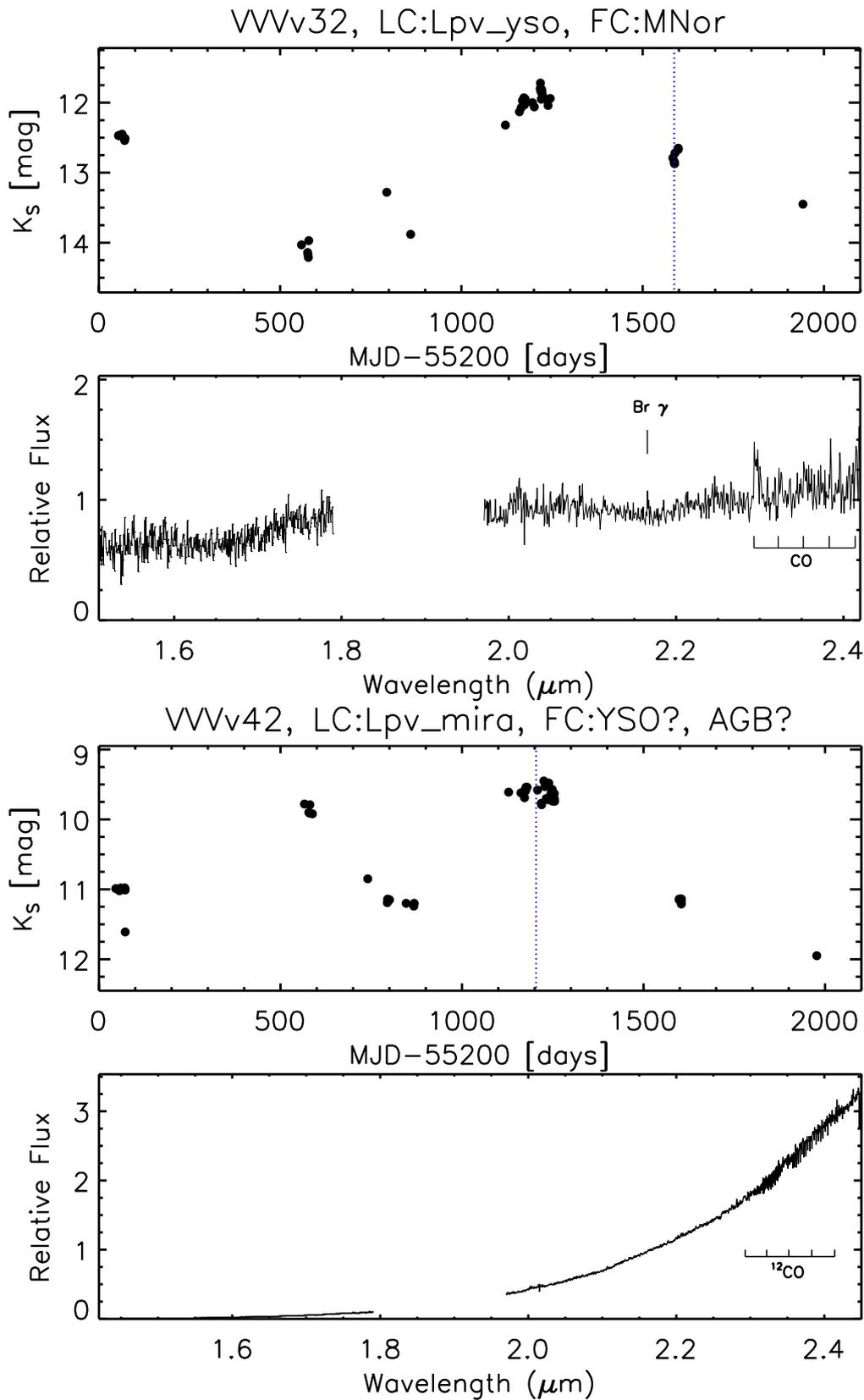
Figure F2. FIRE spectra and K_s LC.

VVVv45, LC:Lpv_mira, FC:AGB

## VVVv63, LC:Eruptive, FC:YSO, non−er?

Figure F3. FIRE spectra and K_S LC.

Figure F4. FIRE spectra and K_s LC.
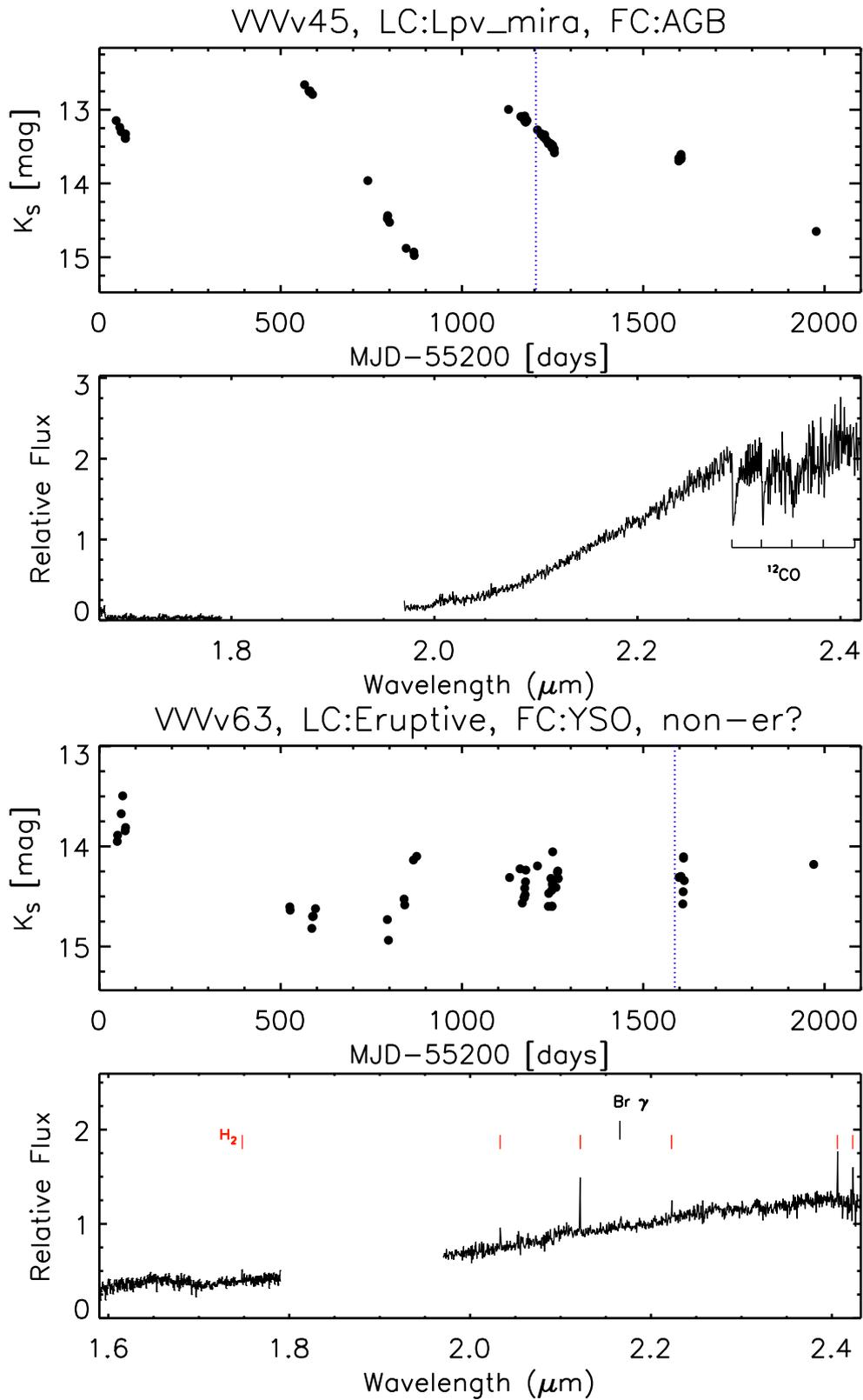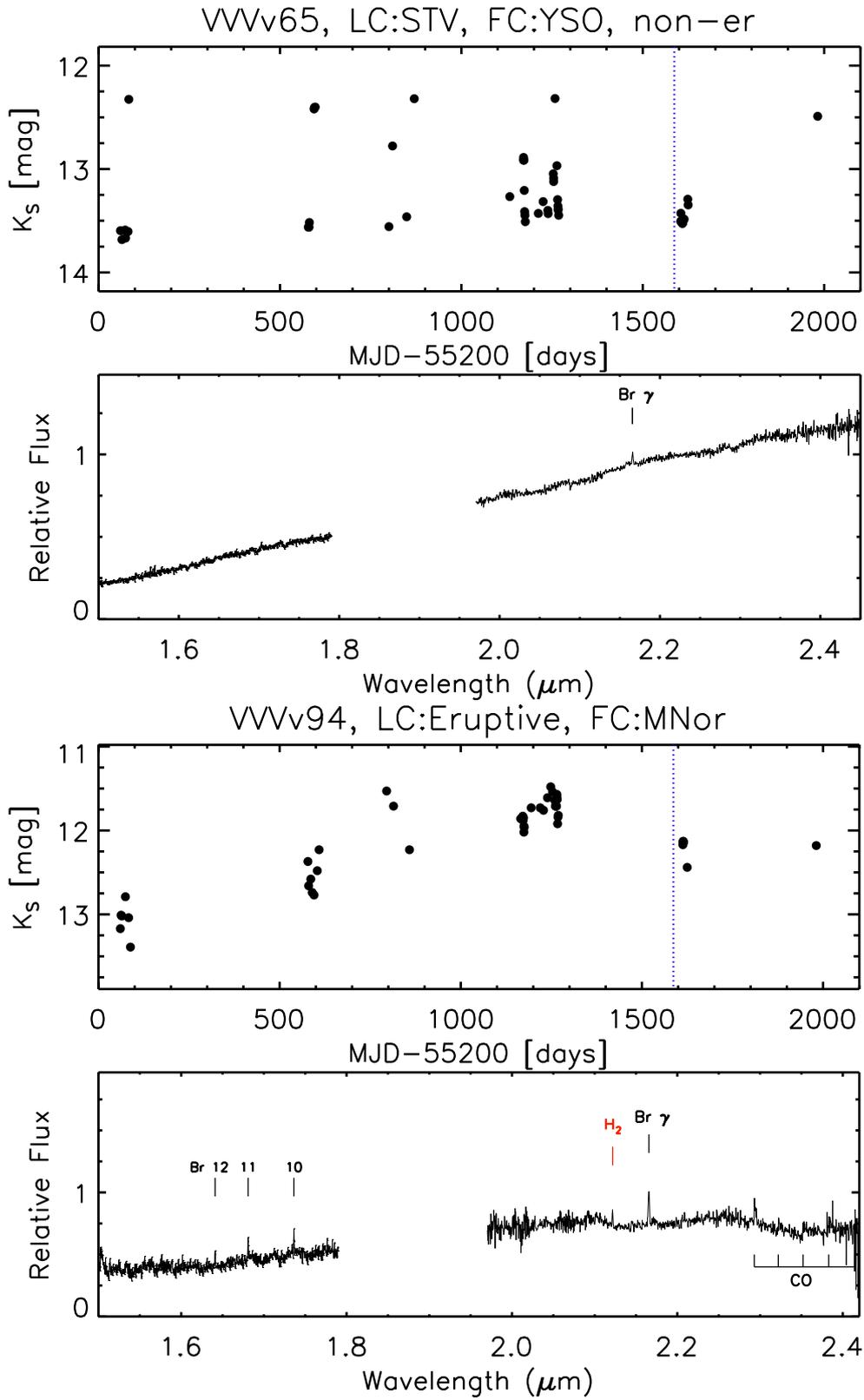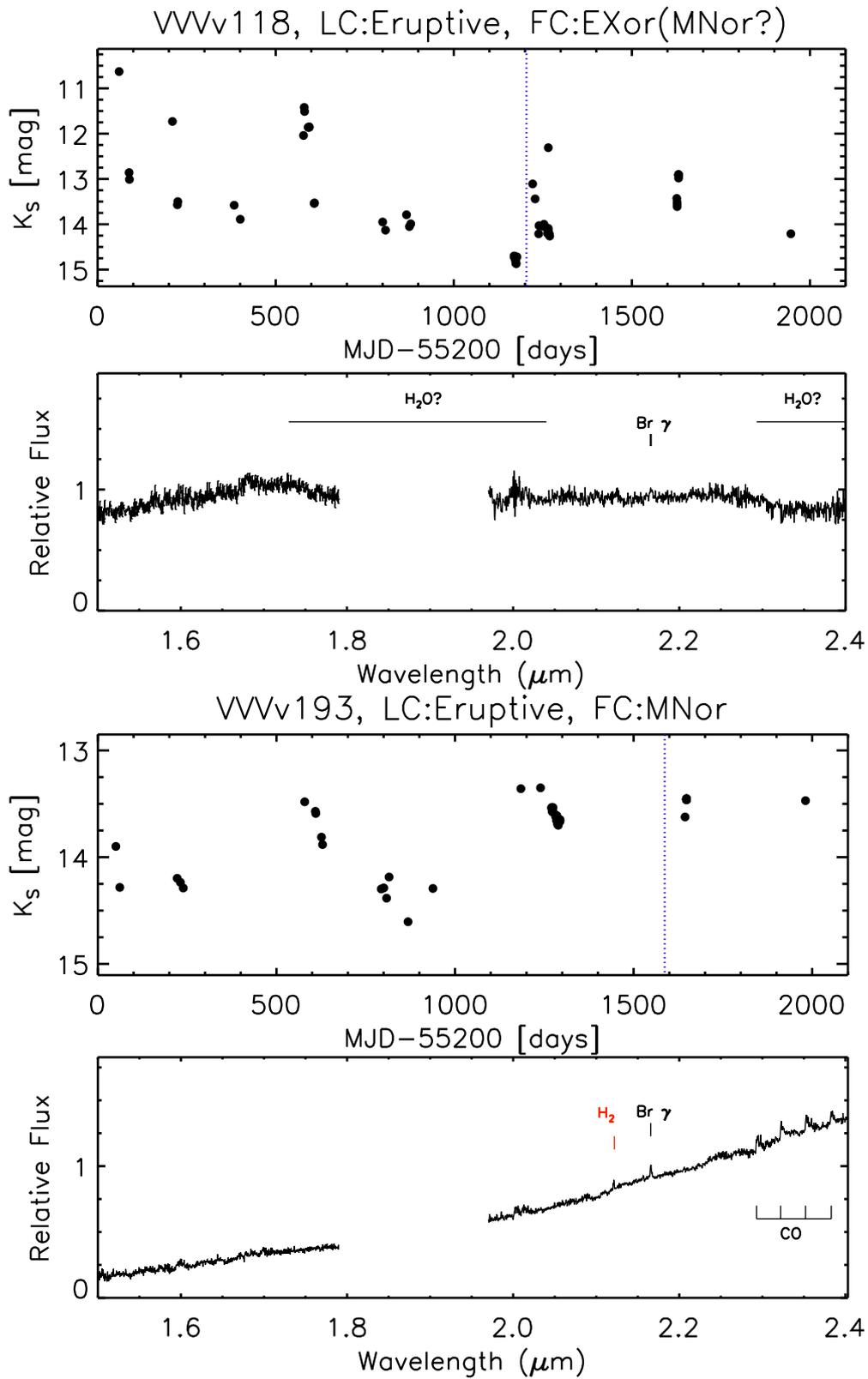
Figure F5. FIRE spectra and K_s LC.
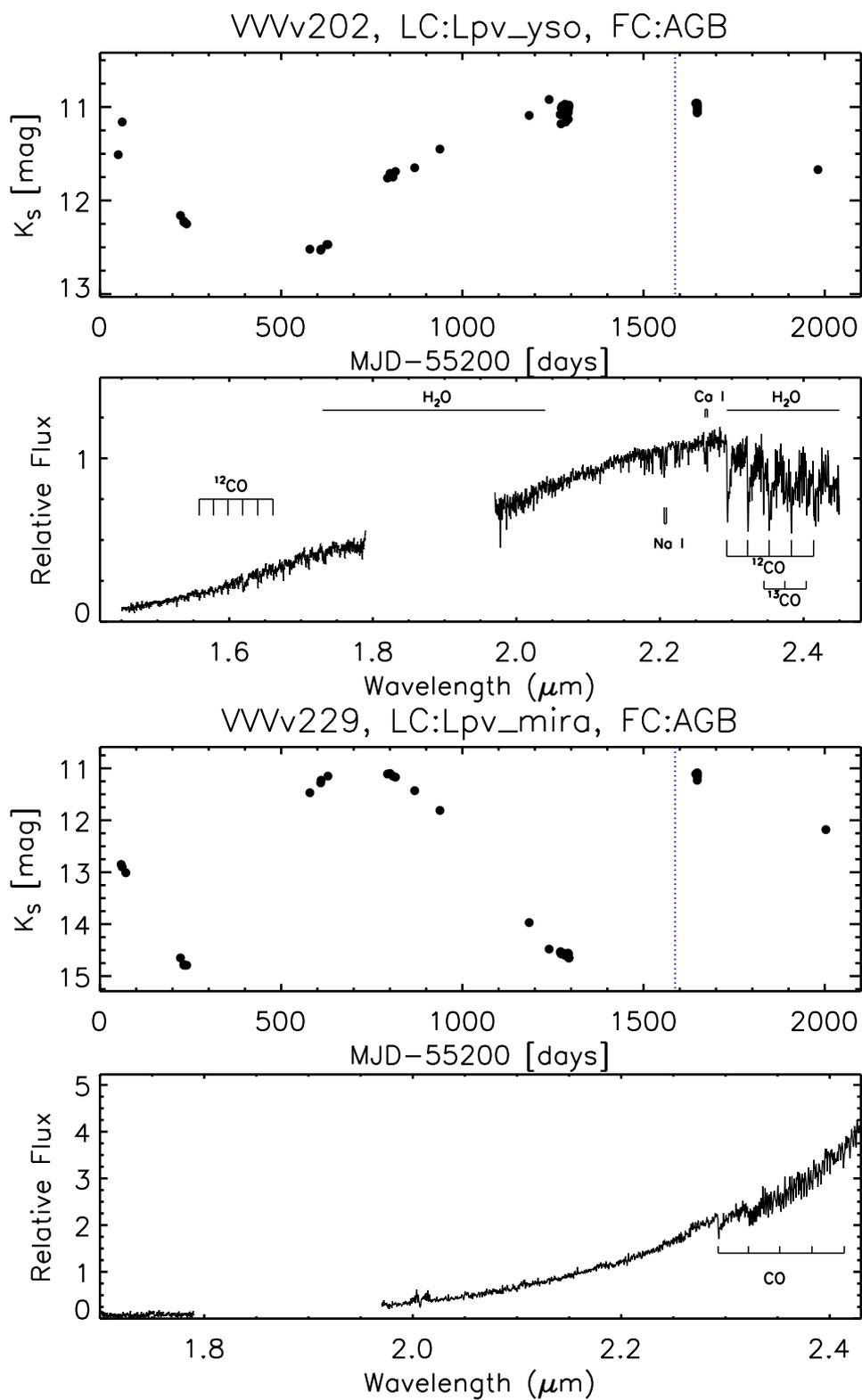
Figure F6. FIRE spectra and K_s LC.

Figure F7. FIRE spectra and K_S LC.

Figure F8. FIRE spectra and K_s LC.

Figure F9. FIRE spectra and K_S LC.

**Figure F10.** FIRE spectra and K_s LC.
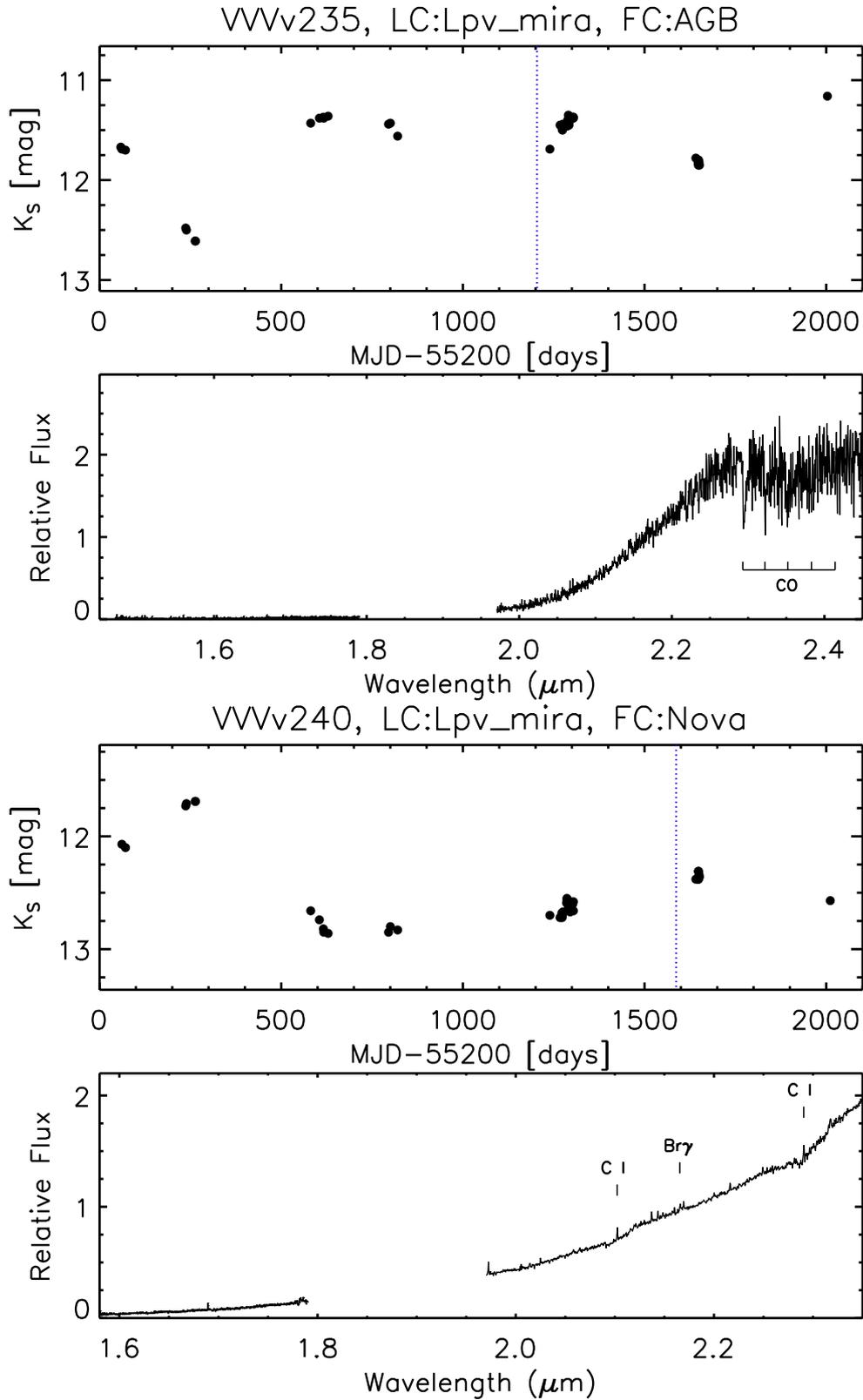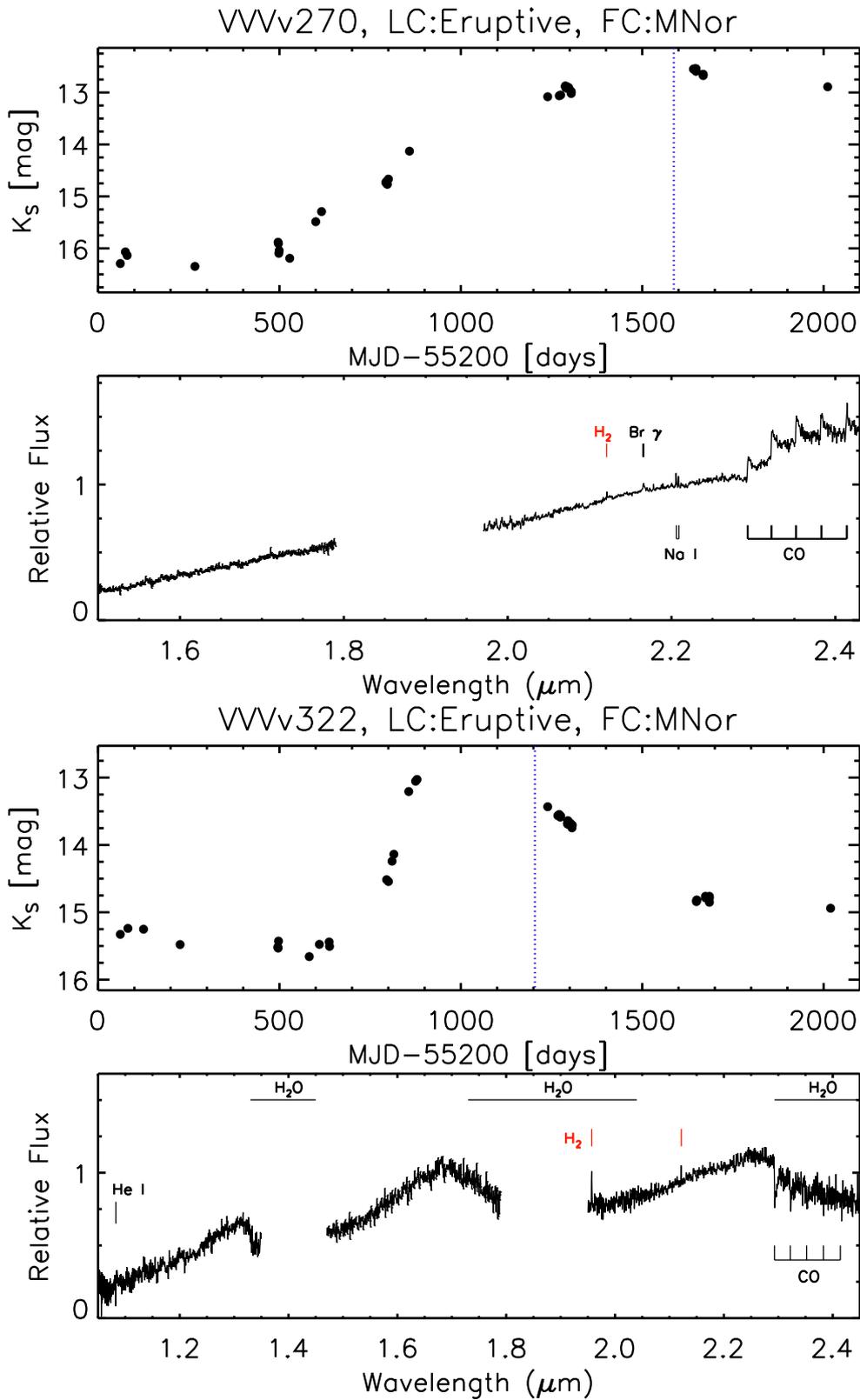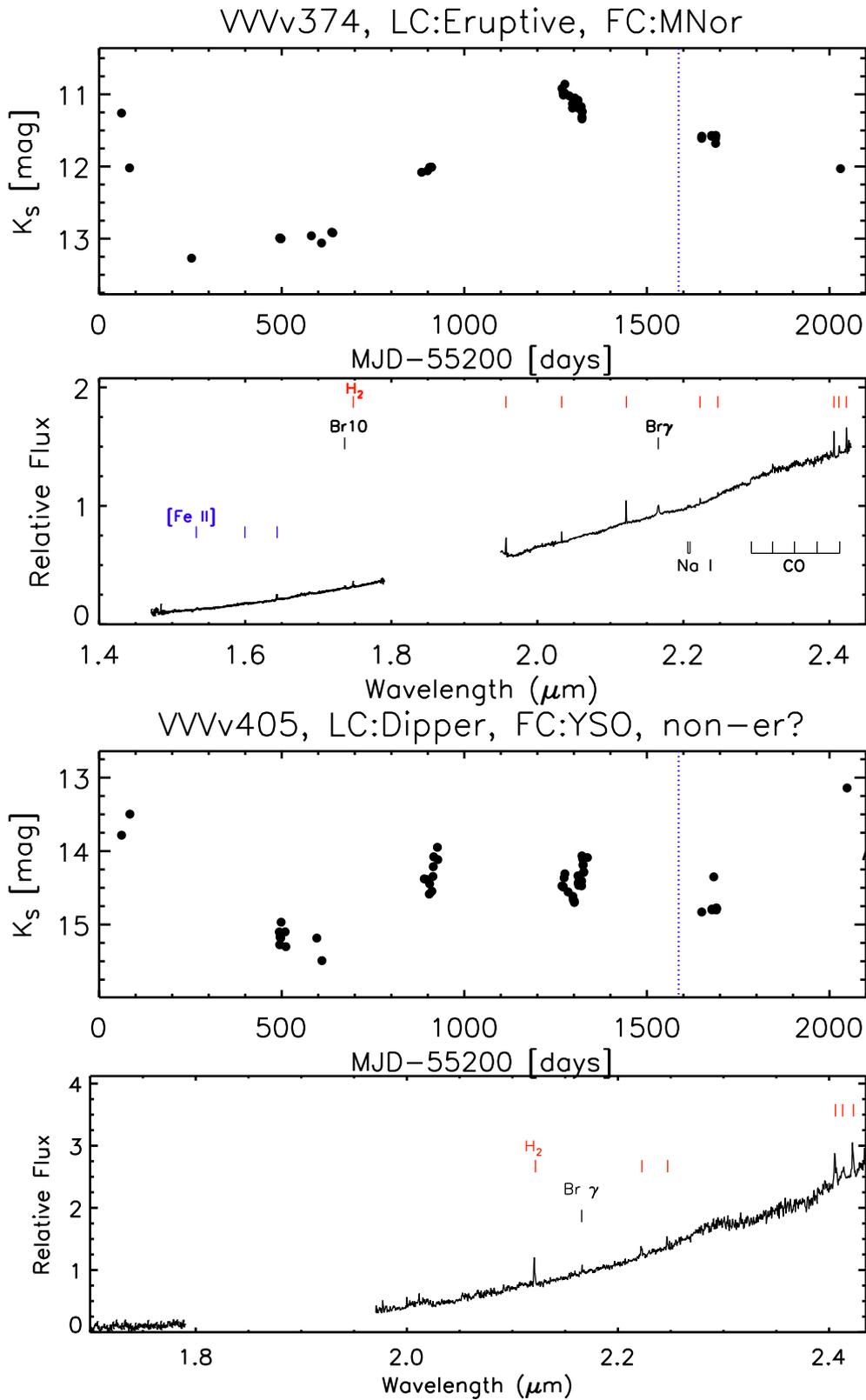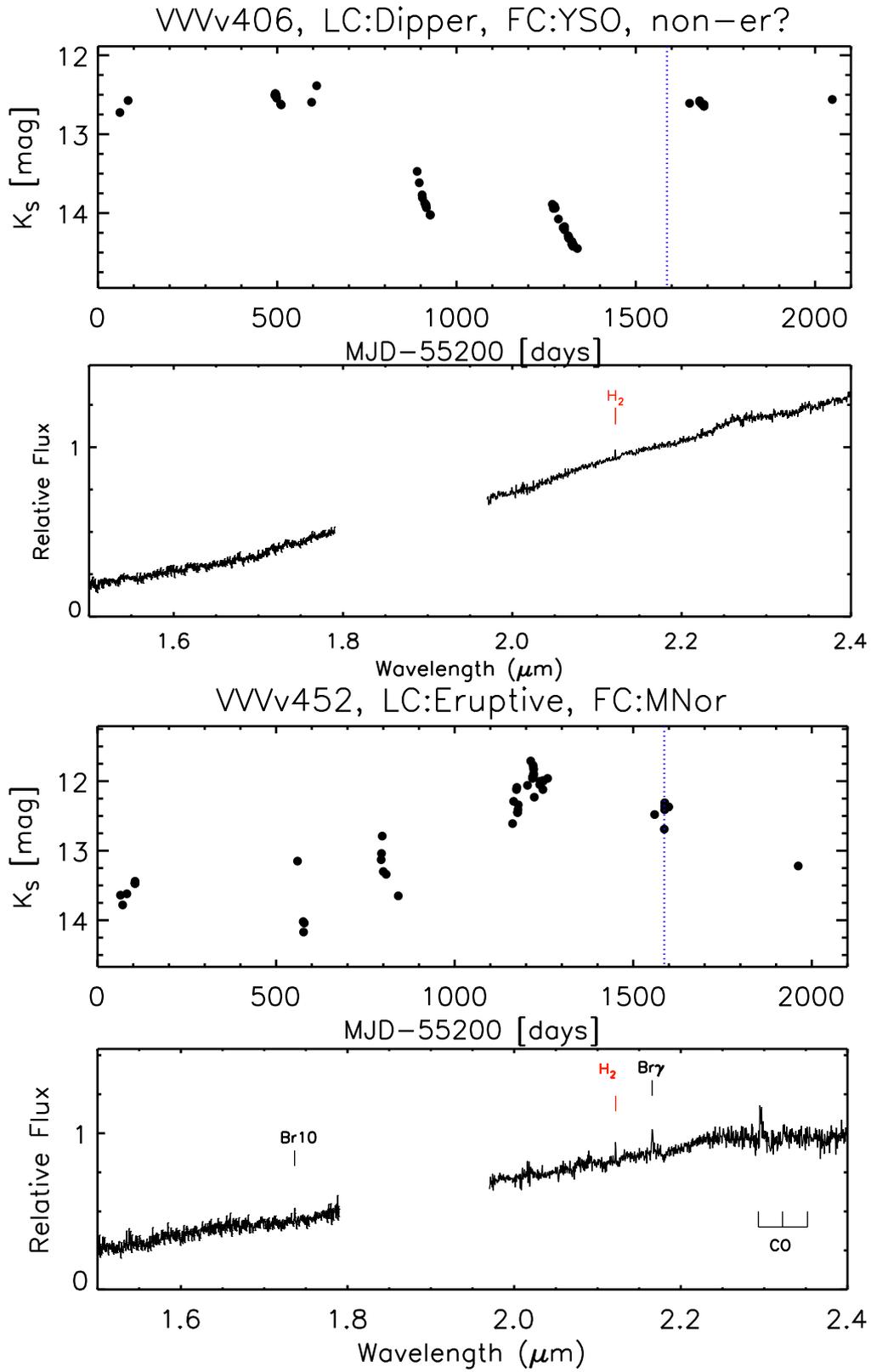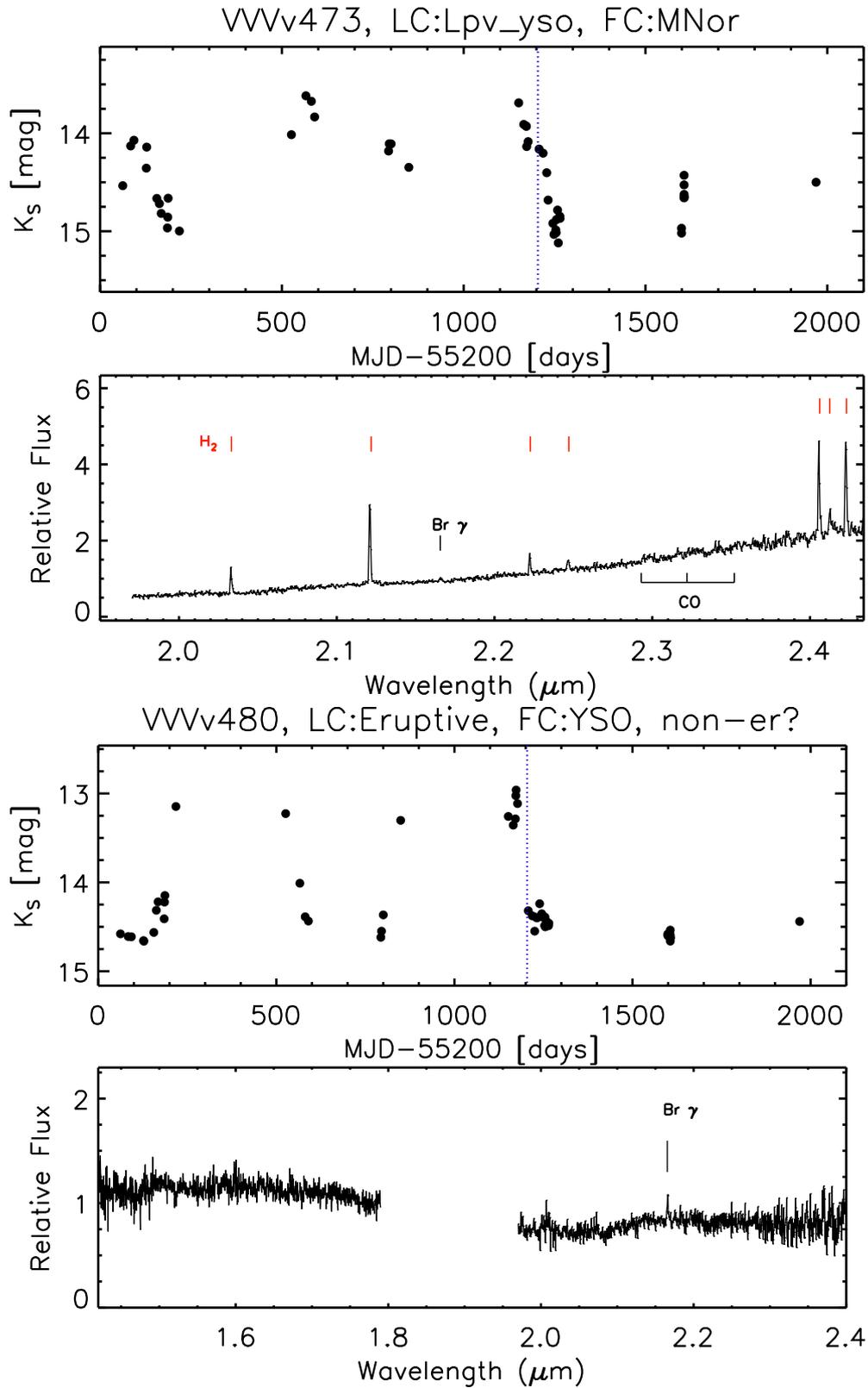
Figure F11. FIRE spectra and K_s LC.

Figure F12. FIRE spectra and K_s LC.

Figure F13. FIRE spectra and K_s LC.

Figure F14. FIRE spectra and K_s LC.

Figure F15. FIRE spectra and K_s LC.
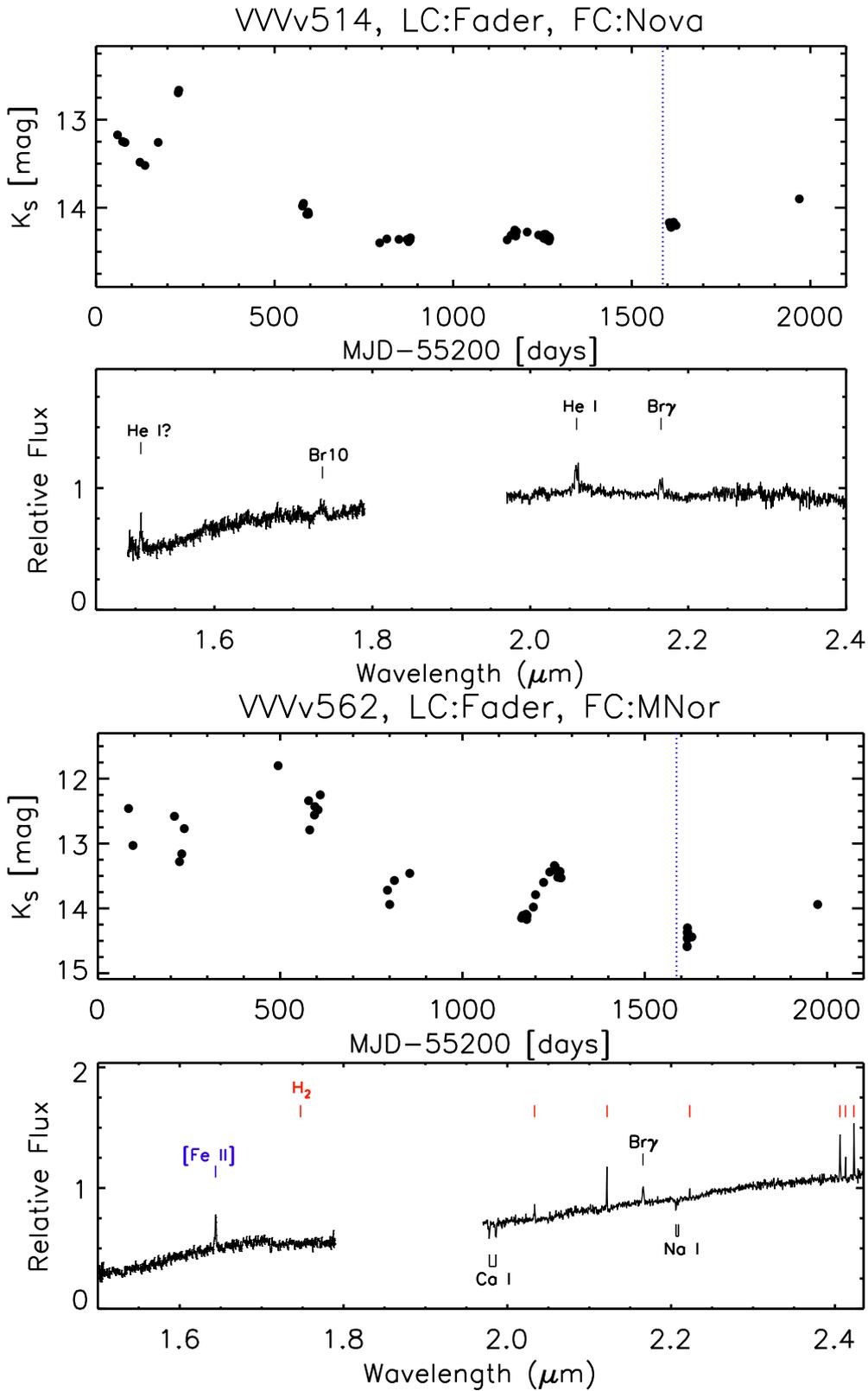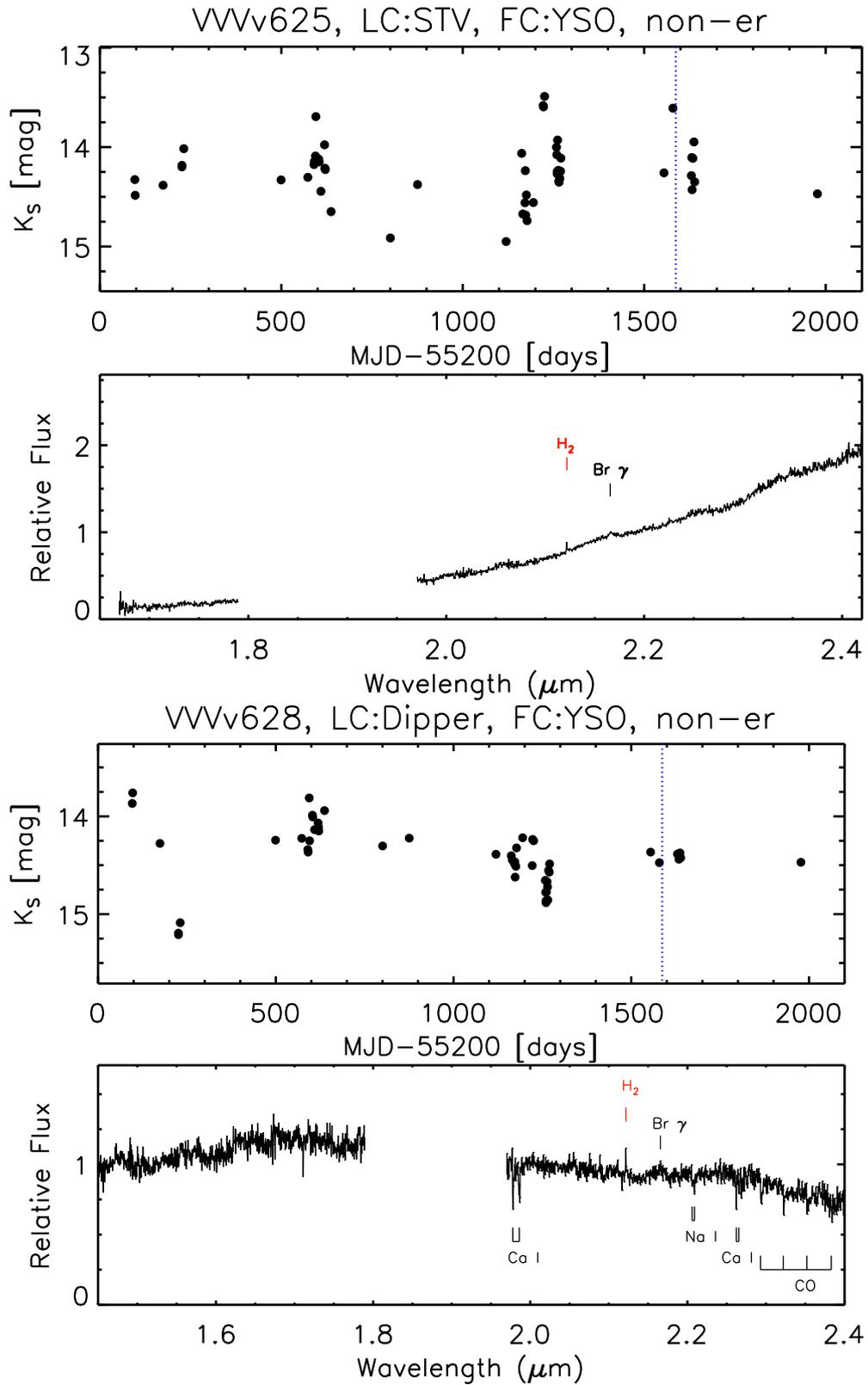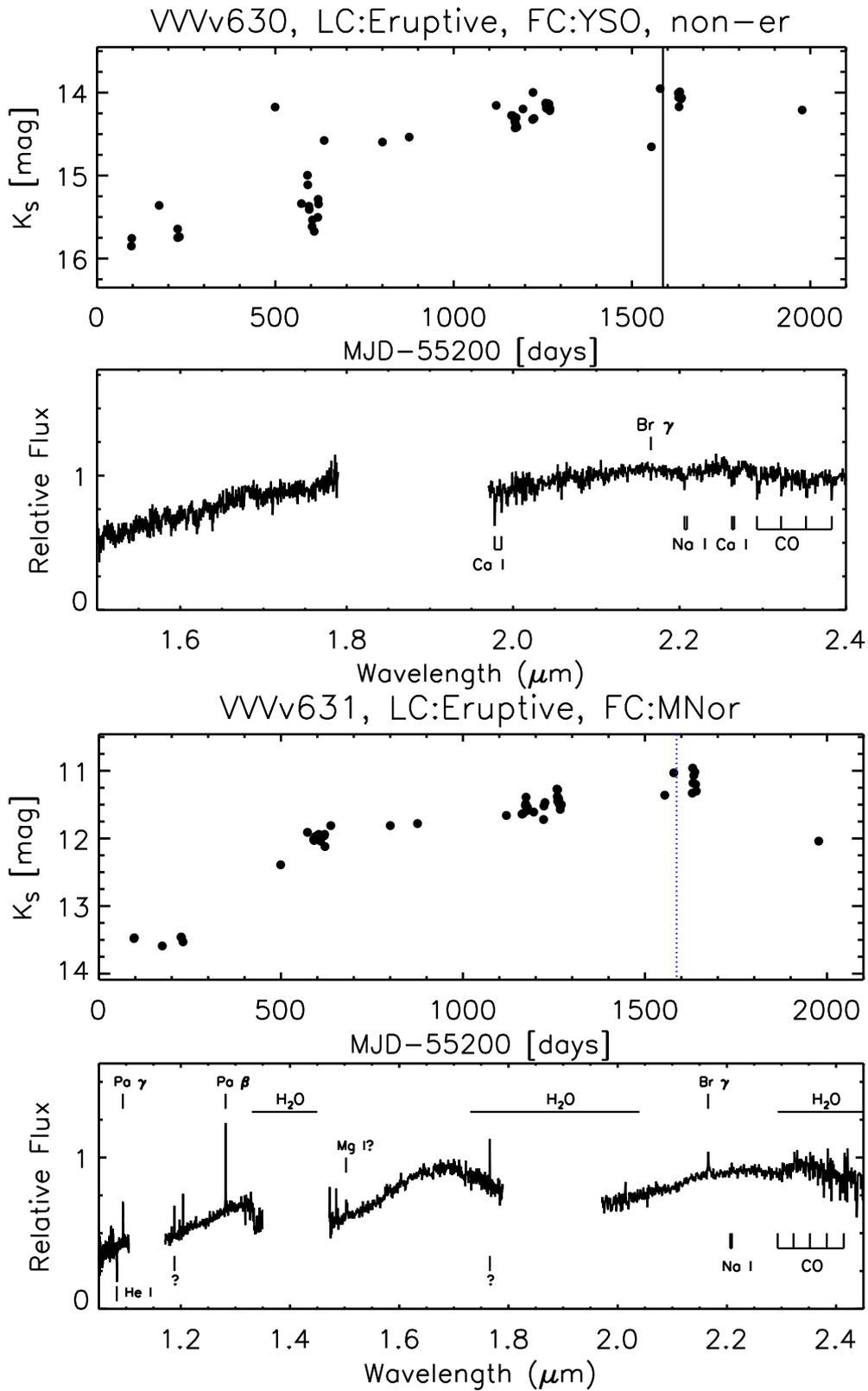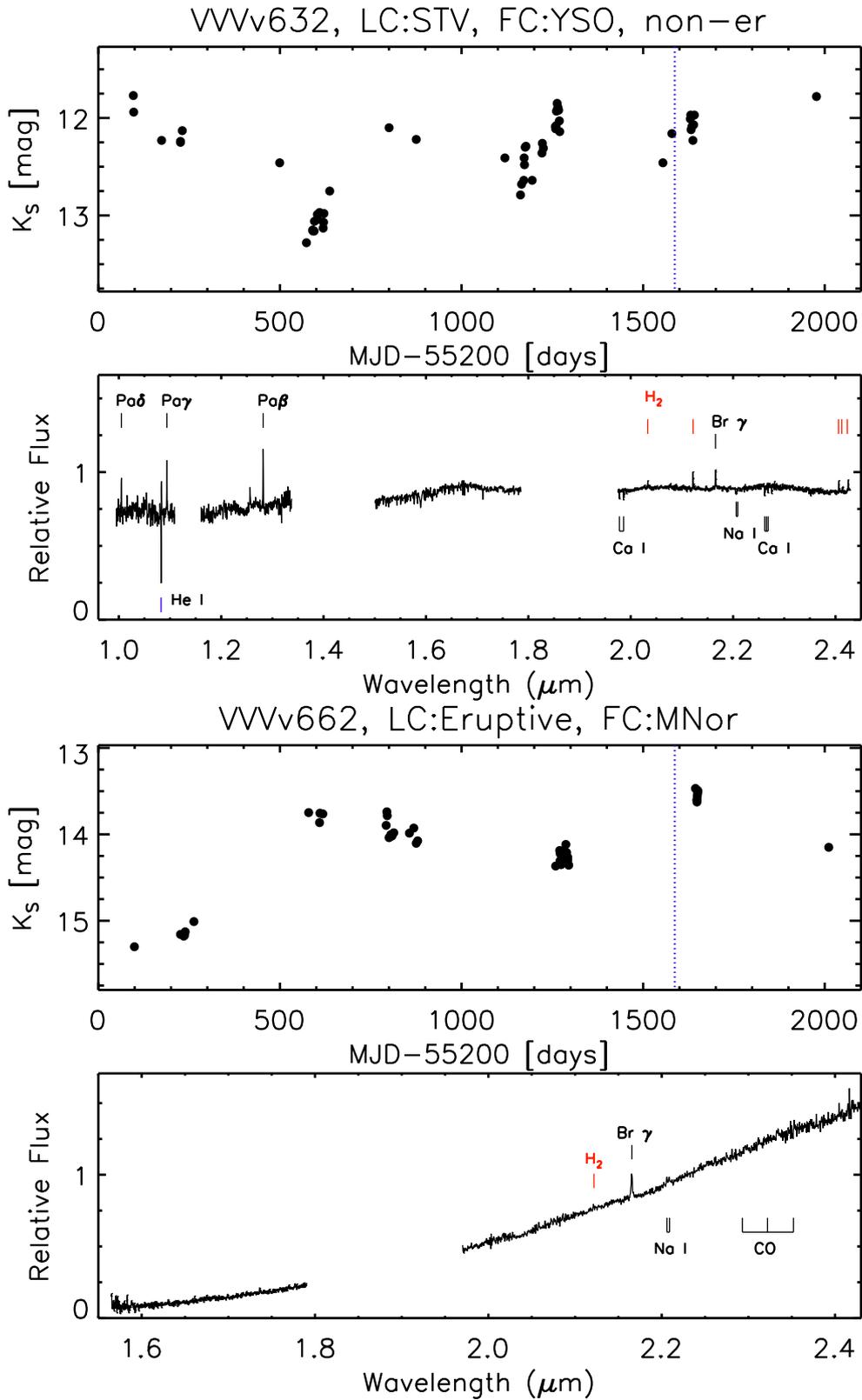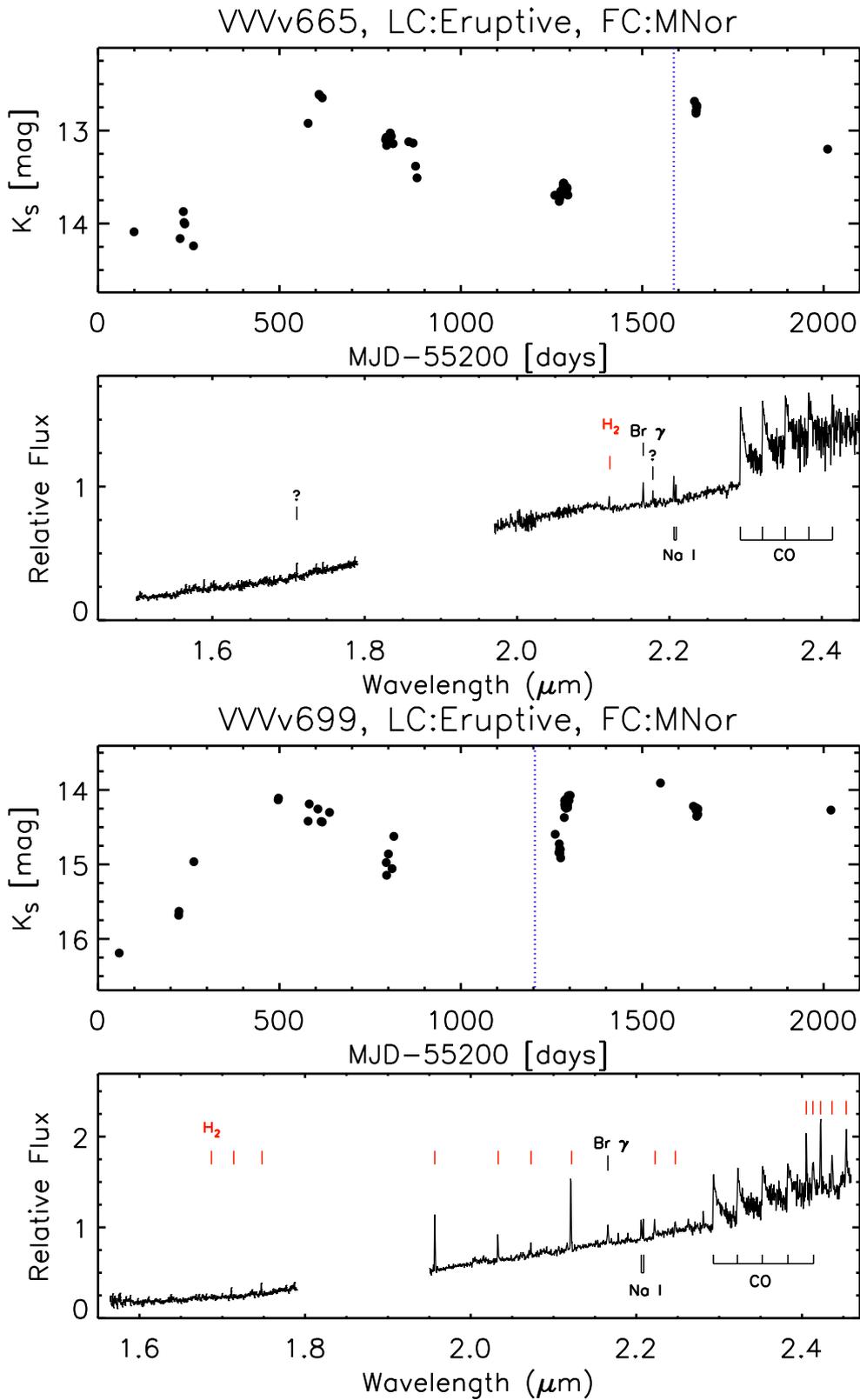
Figure F16. FIRE spectra and K_s LC.

VVVv717, LC:Lpv_yso, FC:MNor

VVVv721, LC:Eruptive, FC:FUor

Figure F17. FIRE spectra and K_s LC.
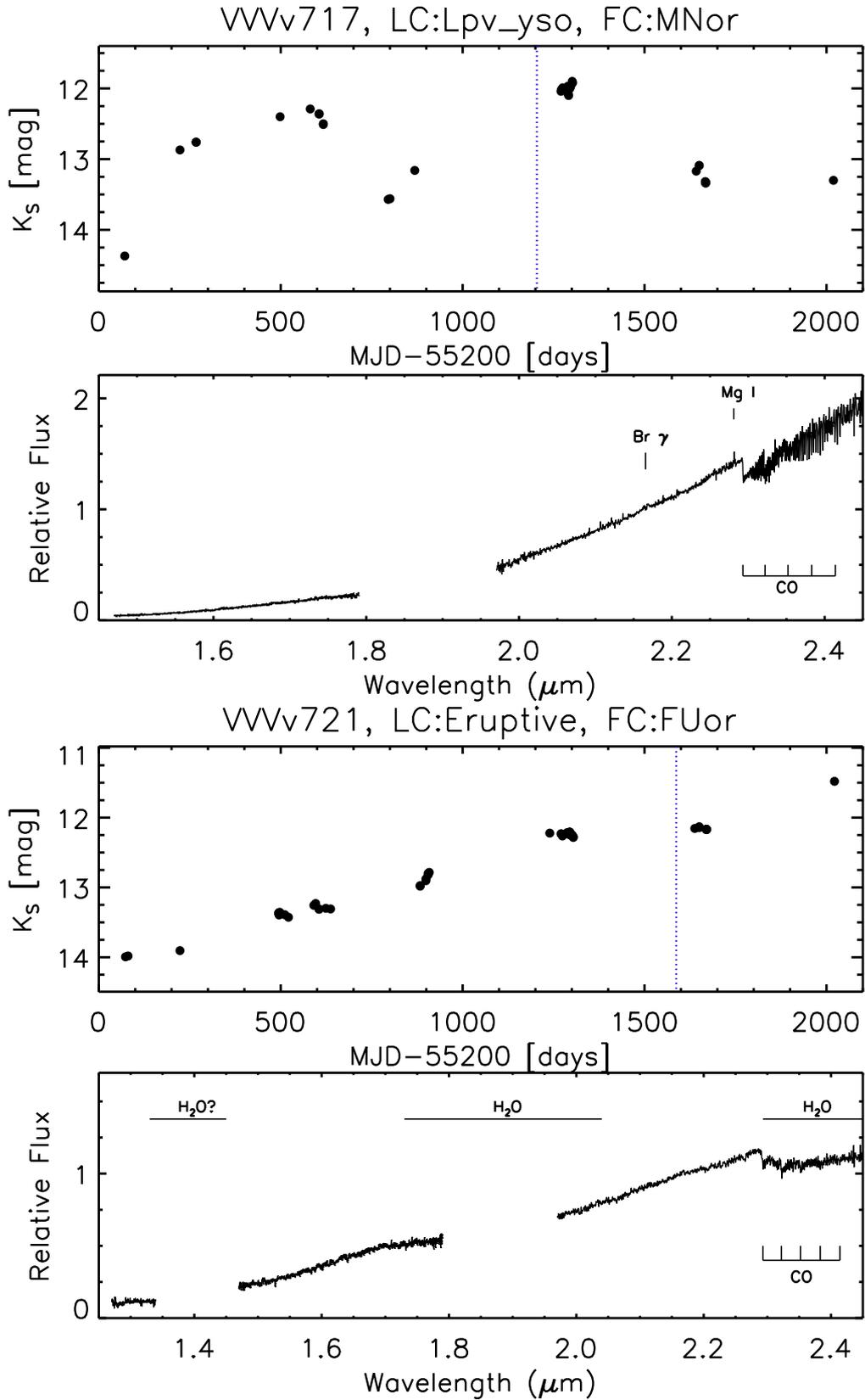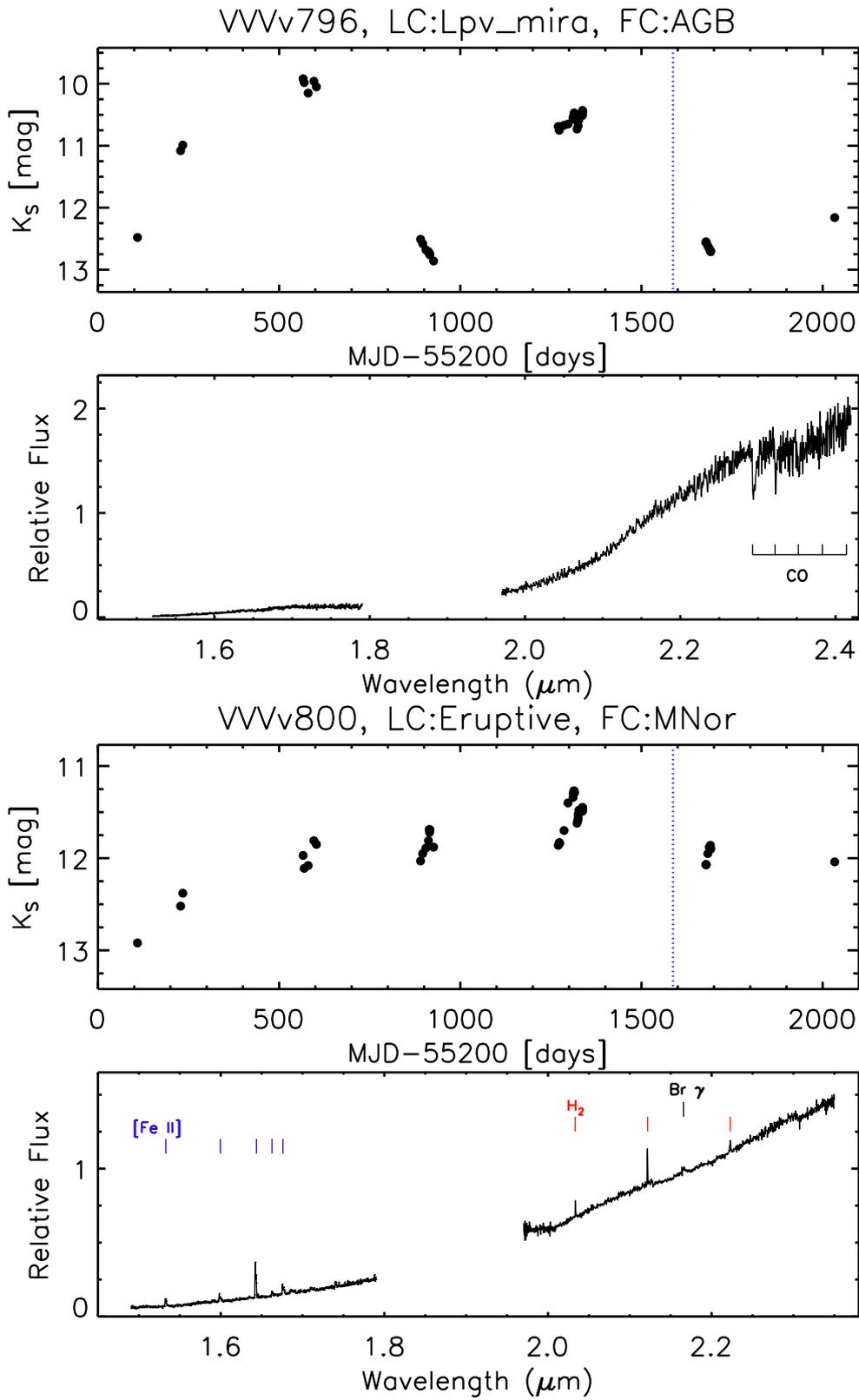
**Figure F18.** FIRE spectra and K_s LC.
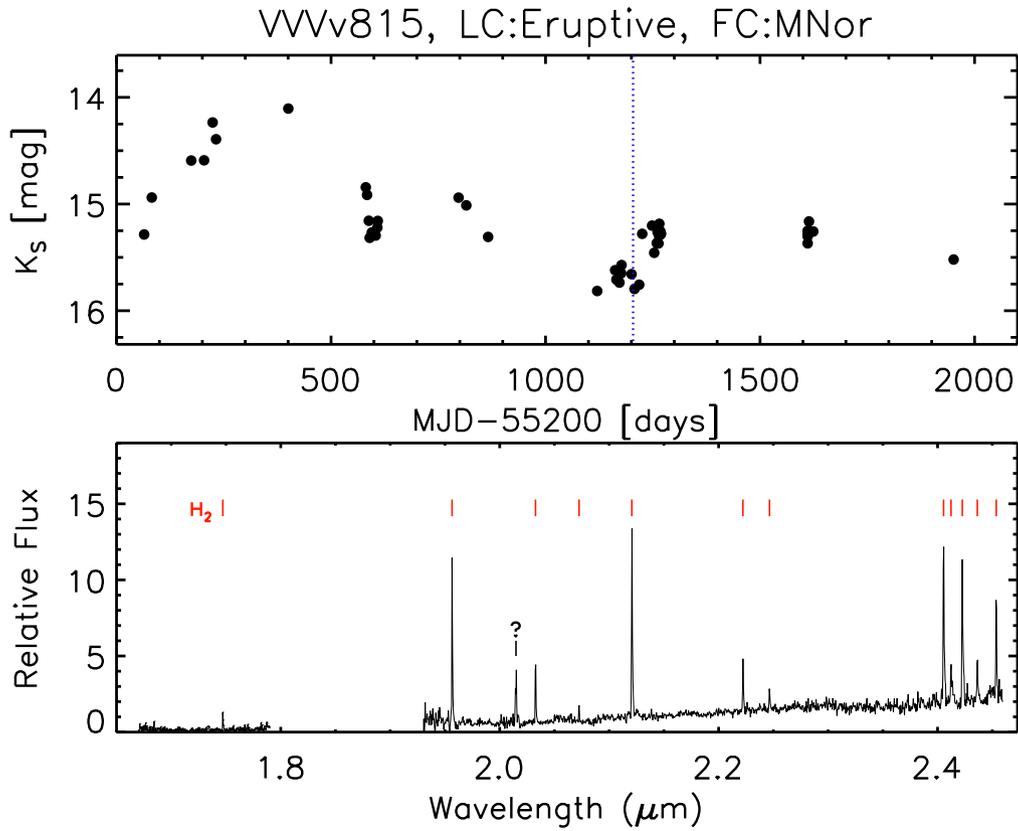
Figure F19. FIRE spectra and $K_{\rm s}$ LC.

APPENDIX G: FINDING CHARTS

In this section, we present finding charts for the 37 objects analysed in this work. The images are 1 arcmin×1 arcmin $K_{\rm s}$ cutouts which were downloaded from the Vista Science Archive and correspond to images from the first epoch of contemporaneous colour photometry in 2010. The designation of each object is shown at the top left corner of the images.
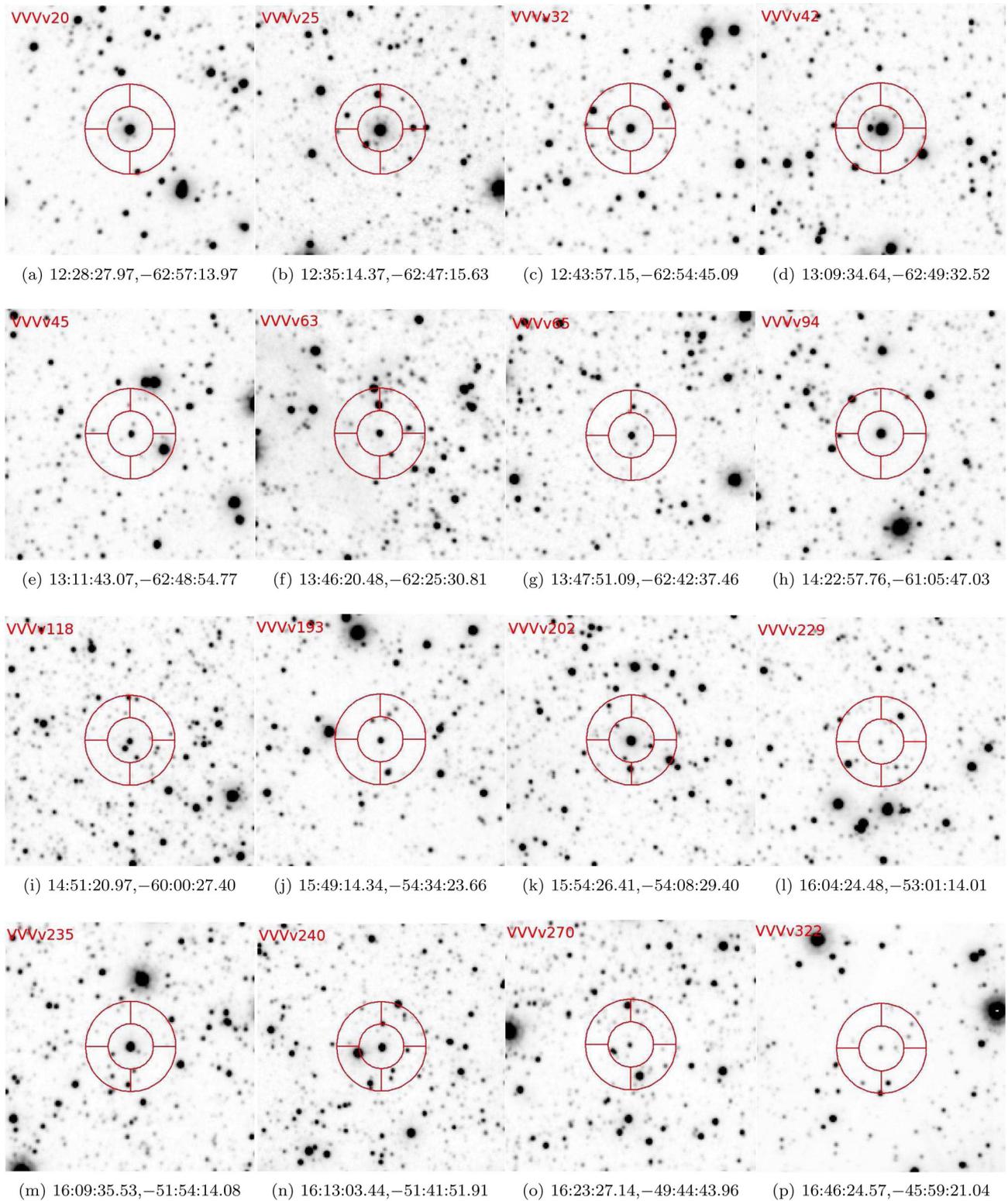
Figure G1. 1 arcmin×1 arcmin K_s images of VVV high-amplitude variables analysed in this work. The object designation is shown in the top left corner of the images, whist the right ascension and declination of the object is shown in the individual subcaptions. In the images, north is up and east is to the left.
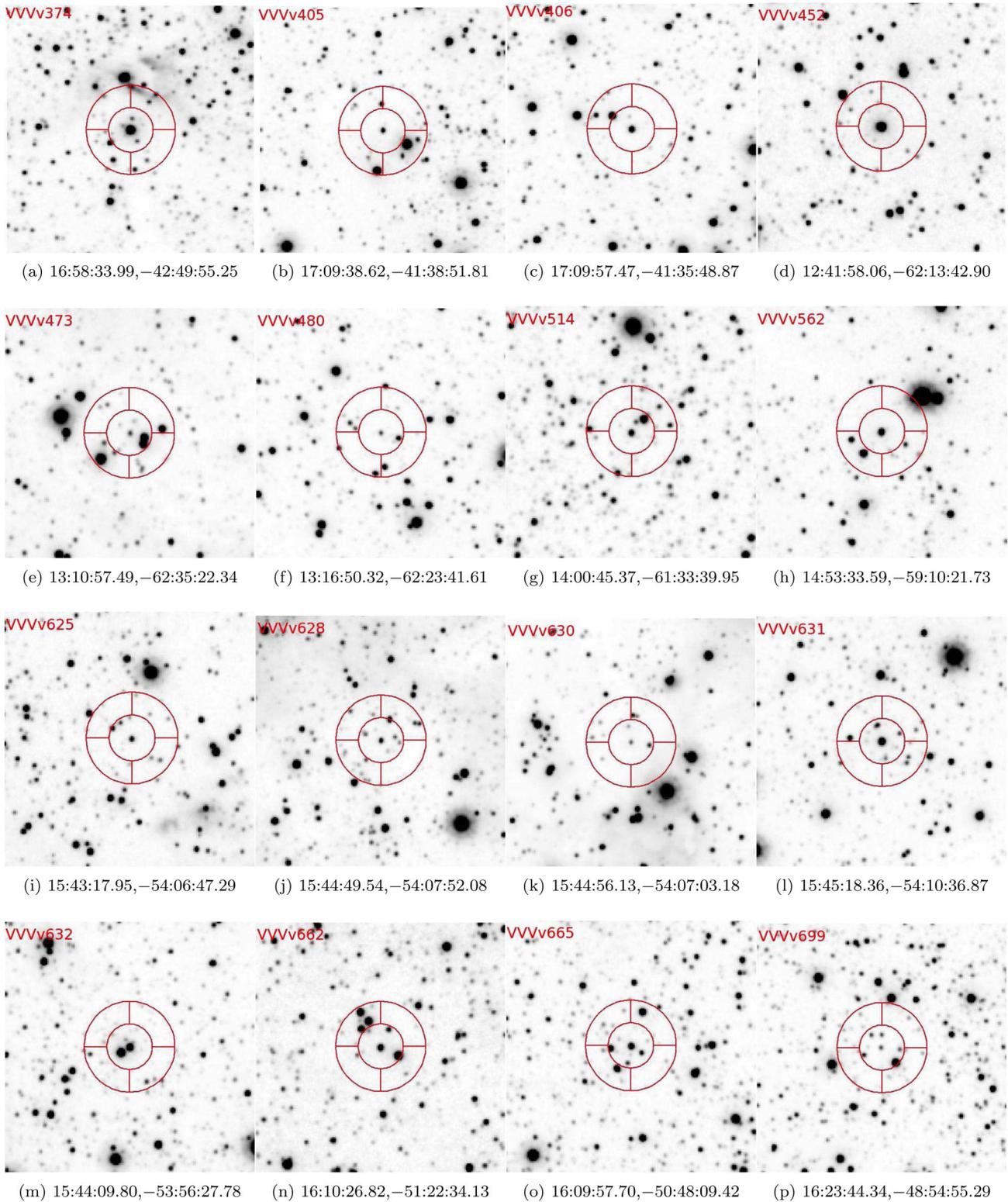
Figure G2. 1 arcmin×1 arcmin K_s images of VVV high-amplitude variables analysed in this work. The object designation is shown in the top left corner of the images, whist the right ascension and declination of the object is shown in the individual subcaptions. In the images, north is up and east is to the left.

(a) 16:58:33.99,−42:49:55.25   (b) 17:09:38.62,−41:38:51.81   (c) 17:09:57.47,−41:35:48.87   (d) 12:41:58.06,−62:13:42.90

(e) 13:10:57.49,−62:35:22.34   (f) 13:16:50.32,−62:23:41.61   (g) 14:00:45.37,−61:33:39.95   (h) 14:53:33.59,−59:10:21.73

(i) 15:43:17.95,−54:06:47.29   (j) 15:44:49.54,−54:07:52.08   (k) 15:44:56.13,−54:07:03.18   (l) 15:45:18.36,−54:10:36.87

(m) 15:44:09.80,−53:56:27.78   (n) 16:10:26.82,−51:22:34.13   (o) 16:09:57.70,−50:48:09.42   (p) 16:23:44.34,−48:54:55.29

(a) 16:36:05.56,−46:40:40.61   (b) 16:39:48.77,−45:48:47.96   (c) 17:12:07.43,−38:41:26.86   (d) 17:12:46.04,−38:25:24.63

(e) 14:26:04.95,−60:41:16.81
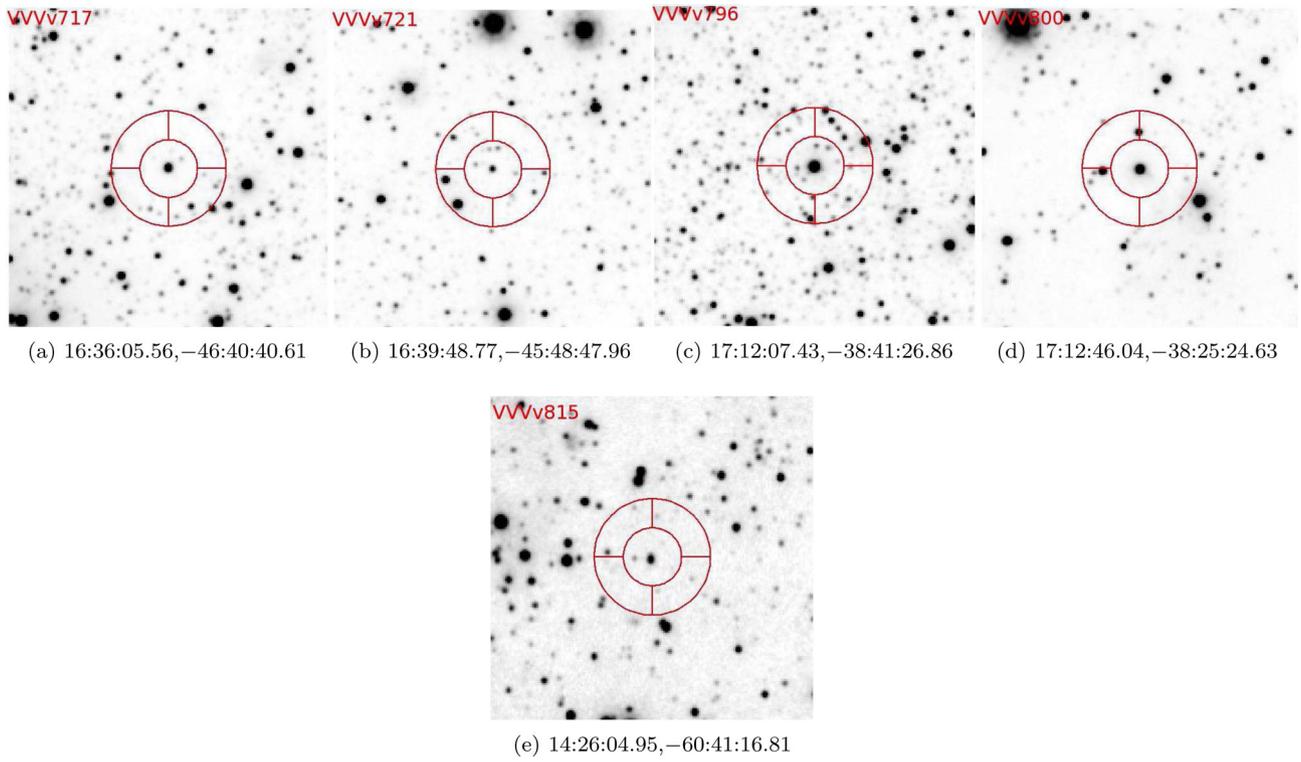
Figure G3. 1 arcmin×1 arcmin K_s images of VVV high-amplitude variables analysed in this work. The object designation is shown in the top left corner of the images, whist the right ascension and declination of the object is shown in the individual subcaptions. In the images, north is up and east is to the left.

This paper has been typeset from a TEX/LATEX file prepared by the author.